2006

# Cellular Magnetic Resonance Imaging at 1.5T: Application to Imaging Neuroinflammation in Experimental Models of Multiple Sclerosis

Ayman J. Oweida
*Western University*

# Cellular Magnetic Resonance Imaging at 1.5T: Application to Imaging Neuroinflammation in Experimental Models of Multiple Sclerosis

(Spine title: Cellular Imaging of Neuroinflammation in Multiple Sclerosis)

(Thesis format: Integrated-Article)

by

**Ayman J. Oweida**

Graduate Program in Medical Biophysics

A thesis submitted in partial fulfillment
of the requirements for the degree of
Master of Science

Faculty of Graduate Studies
The University of Western Ontario
London, Ontario, Canada

THE UNIVERSITY OF WESTERN ONTARIO
FACULTY OF GRADUATE STUDIES

# CERTIFICATE OF EXAMINATION

| Supervisor | Examiners |
|---|---|
| Dr. Paula Foster | Dr. Tamie Poepping |
| Supervisory Committee | Dr. Gill Strejan |
| Dr. Greg Dekaban | Dr. Savita Dhanvantari |
| Dr. Steve Karlik | Dr. Robert Bartha |

The thesis by

**Ayman Jafar Oweida**

entitled:

Cellular Magnetic Resonance Imaging at 1.5T: Application to Imaging Neuro-inflammation in Experimental Models of Multiple Sclerosis

is accepted in partial fulfillment of the
requirements for the degree of
Master of Science

Date_____ _____
Chair of the Thesis Examination Board

# Abstract

The thesis herein addresses an important, yet unresolved, problem in the field of cellular MRI. The natural ability of macrophages to engulf foreign particles has made them ideal candidates for taking up cellular MR labels in vivo. In multiple sclerosis, macrophage populations in the circulation increase substantially as they home to the CNS where they cause a massive and destructive inflammatory response. Labeling macrophages in the circulation and being able detect and track them in the CNS can significantly improve the prognosis of MS and thus aid in the correct identification of a treatment plan. However, it remains unknown whether it is indeed labeled macrophages from the circulation that are detected on MR images or whether they are different cell populations actively involved in MS. In the present thesis, two novel methods are used to determine the source of the MR label in the CNS. One study utilizes a transgenic mouse where peripheral macrophages express the green fluorescent protein while other cell populations do not. Another study utilizes clodronate liposomes to deplete the macrophage population in the circulation prior to injection of the MR label. By using the mentioned two approaches it was determined that the source of label on MR images is largely attributed to peripheral macrophages from the circulation. The findings illustrated in this thesis will have a major impact on our understanding of neuroinflammation in multiple sclerosis and on the development of disease-modifying therapies.

# Keywords

Multiple sclerosis, experimental autoimmune encephalomyelitis, magnetic resonance imaging, superparamagnetic iron oxide, macrophages, inflammation, central nervous system.

# Co-Authorship

The following thesis contains text and figures extracted from a published manuscript and from a manuscript submitted for publication. The introduction (Chapter 1) contains selected data from the paper "Cellular Imaging at 1.5T: Detecting Cells in Neuroinflammation using Active Labeling with Superparamagnetic Iron Oxide" published in 2004 in *Molecular Imaging* and which was the fruit of Mr. Oweida's fourth year project. The paper was coauthored by Ayman J. Oweida, Elizabeth A. Dunn and Paula J. Foster. The full paper is presented in the appendix section of this thesis.

Chapter 2 involves slight modifications to the paper "Iron Oxide Labeling of Hematogenous Macrophages in a Model of Experimental Autoimmune Encephalomyelitis and the Contribution to Signal Loss in FIESTA Images" submitted to JMRI and coauthored by Ayman J. Oweida, Elizabeth A. Dunn, Greg A. Dekaban, Steve J. Karlik and Paula J. Foster. As principal author Ayman Oweida performed the experiments, analyzed the data, interpreted the results and

wrote the manuscript. Dr. Foster, as Mr. Oweida's supervisor, reviewed the results, provided guidance and editorial assistance for the project. Dr. Dekaban provided the transgenic mouse model, helped with fluorescence microscopy and provided editorial assistance for the project. Dr. Karlik provided expert advice on development of the animal model and provided editorial assistance as well. Ms. Dunn and Mrs. Simdrea performed much of the histology work needed for the project.

Chapter 3 summarizes a pilot study that involved a number of imaging and biology experiments. As principal author Ayman Oweida performed the experiments, analyzed the data and interpreted the results. Dr. Foster reviewed the results, provided guidance and editorial assistance for the project. Ms. Dunn performed the bulk of the histology work needed for the project.

# Acknowledgements

The work presented in this thesis would not have been possible without the help and encouragement of many individuals who I am truly indebted to. I will not do justice to these individuals by merely mentioning their names, but I hope my humble words will attest to their invaluable contributions towards my thesis. I am truly thankful to my supervisor, mentor and friend, Dr. Paula Foster for giving me the opportunity to drive my research in the direction I wanted, while offering me full support and guidance. I am thankful to Dr. Greg Dekaban and Dr. Steve Karlik for the many insightful and informative discussions I had with them and for their expert advice on various experiments. I am thankful to Dr. Brian Rutt and Mr. Andrew Alejski for providing me with guidance, support and training on the use of MRI hardware. I am grateful to Ms. Elizabeth Dunn for her enormous help in many of my experiments. Her final touches always paved the way to a successful experiment. I am thankful to Mrs. Carmen Simdrea and Mr. Dennis Gris for providing expert help on histology and flow cytometry respectively. I am thankful to the lab members for offering their time and energy at times when life was just overwhelming. I am thankful to my numerous friends who have provided me with support and encouragement during my graduate years. Finally, I am very grateful to all of my family members who have always been an invaluable source of guidance, support and encouragement during my life and in particular during my graduate years. In particular, my parents, Jafar and Fawzyah, who have helped make everyday of my graduate years a day of success and happiness. I thank my siblings Ehab, Areej, Reem and Mustafa for keeping up with me during

stressful times. I thank my wife, Fatimah, who has been an invaluable source of encouragement and support during my graduate study and who sacrificed her time to take care of our newborn daughter, Huda, during all those sleepless nights for the sake of finishing my degree.

*Dedicated to my parents*

# Table of Contents

# List of Tables

# List of Figures

# List of Appendices

# List of Abbreviations and Symbols

| | |
|---|---|
| $B_0$ | external magnetic field |
| $h$ | Planck's constant |
| $\gamma$ | gyromagneic ratio |
| $M_0$ | magnetization |
| $\rho_0$ | spin density |
| $\omega$ | Larmour frequency |
| APC | antigen presenting cell |
| BBB | blood brain barrier |
| CFA | complete Freund's adjuvant |
| CL | clodronate liposomes |
| $CL_2MDP$ | dichloromethylene diphosphonate |
| CNS | central nervous system |
| CSF | cerebrospinal fluid |
| EAE | experimental autoimmune encephalomyelitis |
| EAN | experimental autoimmune neuritis |
| EGFP | enhanced green fluorescent protein |
| FIESTA | fast imaging employing stead state acquisition |
| FSE | fast spin echo |
| Gd | Gadolinium |
| hMac | hematogenous blood-derived macrophage |
| HRP | horseradish peroxidase |
| IFA | incomplete Freund's adjuvent |
| IFN | interferon |
| Il | interleukin |
| MBP | myelin basic protein |
| MHC | major histocompatibility complex |
| MION | monocrystalline iron oxide nanoparticle |
| MOG | myelin oligodendrocyte glycoprotein |

| | |
|---|---|
| MPIO | micron-sized iron oxide nanoparticles |
| MRI | magnetic resonance imaging |
| MS | multiple sclerosis |
| MTB | mycobacterium tuberculosis |
| PR-MS | progressive relapsing multiple sclerosis |
| PP-MS | primary progressive multiple sclerosis |
| SP-MS | secondary progressive multiple sclerosis |
| SPGR | spoiled gradient echo |
| SPIO | superparamagnetic iron oxide |
| SC | subcutaneous |
| RR-MS | relapsing remitting multiple sclerosis |
| $T_1w$ | $T_1$ weighted imaging |
| $T_2w$ | $T_2$ weighted imaging |
| TMEV | Theiler's murine encephalomyelitis virus |
| USPIO | ultra small paramagnetic iron oxide |

# Chapter 1

# General Introduction

This thesis describes a series of studies using cellular magnetic resonance imaging (MRI) to image inflammation associated with experimental autoimmune encephalomyelitis (EAE), a commonly used animal model for multiple sclerosis (MS).

## *1.1 Multiple Sclerosis*

*"The one who sent down the disease sent down the remedy."*
-Prophet Muhammad

### 1.1.1 Etiology and Prevalence

Multiple Sclerosis is an autoimmune disease of the central nervous system (CNS) characterized by focal areas of inflammation and demyelination in the brain and spinal cord. MS affects mainly young individuals between the ages of 15-45 and is 2-3 times more prevalent in females. Currently MS affects over 2.5 million individuals worldwide and is considered the most common debilitating disease affecting young adults (1). MS exhibits enormous heterogeneity in the clinical course, lesion pathology and response to therapy. The clinical courses of MS are typically categorized as: relapsing-remitting (RR-MS), secondary progressive (SP-MS), primary progressive (PP-MS) and progressive relapsing (PR-MS) (2). Common clinical symptoms of MS include fatigue, loss of balance, impaired vision, bowel irritation, slurred speech, and paralysis. The type and severity of the symptoms depends on the location and type of lesions in the CNS.

The etiology of the MS lesion is unknown, although is widely considered to involve organ-specific autoimmune destruction of CNS myelin (3). Various environmental (4) and genetic factors (5) have also been suggested as potential contributors in the development of MS. The environmental factor is clearly visible in the world-wide distribution of MS. High frequency areas include those with a temperate climate including Canada, northern parts of the united states (US) and the northern part of Europe.

### 1.1.2 Animal Model

Two main animal models are often utilized for the study of MS: Experimental autoimmune encephalomyelitis (EAE) and Theiler's murine encephalomyelitis virus (TMEV). EAE is an autoimmune disease induced following immunization with neural auto-antigens or by adoptive transfer of neural-antigen specific T cells in susceptible animals. TMEV disease is induced following intracerebral inoculation of the TME virus in susceptible animals. Both diseases involve the infiltration of inflammatory cells into the CNS and the subsequent destruction of myelin sheath leading to varying degrees of paralysis in the animals. Although, EAE and TMEV involve similar disease processes, the mechanism of pathogenesis leading to myelin destruction and the clinical manifestation of the disease is different in each model. Further discussion of the different disease mechanisms is beyond the scope of this thesis and the reader is referred to alternate review articles (6-9). All experiments in the present thesis utilize the EAE animal model.

Various forms of EAE can be induced in animals depending on the animal strain, the method of inoculation and the antigen used. EAE is typically induced with a subcutaneous (sc) injection of the CNS antigen that has been homogenized with complete freund's adjuvant (CFA) containing mycobacterium tuberculosis (MTB). Common CNS antigens used for EAE induction include myelin basic protein (MBP) (10,11), myelin oligodendrocyte glycoprotein (MOG) (12,13) and proteolipid protein (PLP) (14). Depending on the EAE model required, a booster injection can be used to modify the clinical course of the disease and produce a chronic or relapsing form of EAE. In mice, an intra-peritoneal (ip) injection of pertussis toxin is often administered to the animals on days 0 and 2 post EAE induction. Pertussis toxin is thought to increase vascular permeability of the CNS resulting in a greater influx of inflammatory cells (15), although this hypothesis has recently been challenged with a number of alternative mechanisms (16).

### 1.1.3 Disease Mechanism and Lesion Development

Multiple sclerosis involves an attack on myelin in the CNS initiated by autoreactive T and B cells (17,18). The underlying cellular mechanism behind MS is summarized in figure 1.1. Autoreactive cells constantly circulate in the blood-stream in pursuit of their respective antigen, which is displayed by major histocompatibility molecules (MHC) and co-stimulatory molecules by antigen-presenting cells such as dendritic cells. Once activated, T cells elicit a cascade of inflammatory events that are initiated with the secretion of various cytokines (19) and matrix metalloproteases (20), which act on the endothelial lining of the

vasculature allowing the T cells to bind to adhesion molecules and subsequently infiltrate into the CNS parenchyma past the endothelial layer and the blood brain barrier (BBB).

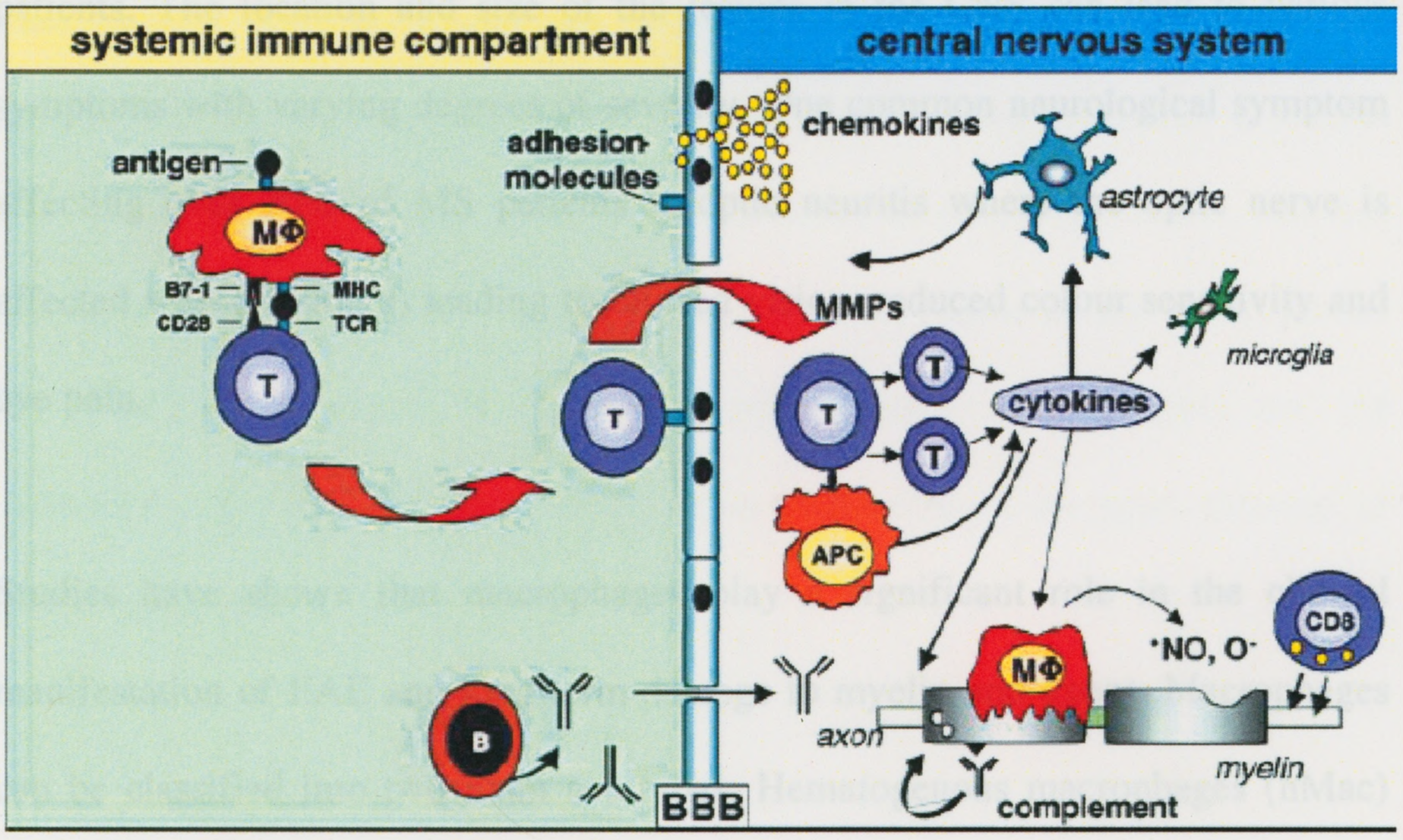


**Figure 1.1:** Cartoon illustration of the disease mechanism in MS (33).

Inside the CNS various resident APCs including microglia, pericytes and dendritic cells stimulate the T cells by displaying their respective autoantigen (21-23). The T cells release further cytokines that initiate a local inflammatory response resulting in the subsequent recruitment of additional macrophages from the circulation which participate in the destruction of the myelin sheath. B cells are also thought to infiltrate vessels near the site of inflammation resulting in perivascular cuffs and the release of antibodies that contribute to myelin destruction (24). Furthermore, toxic substances discharged from T cells cause further damage to the axons of neurons that have been demyelinated. Through this complex disease mechanism a focal lesion is formed in the CNS that consists of

varying degrees of demyelination and axonal damage and may persist after the acute inflammatory event is over. The accumulation of these lesions most probably leads to the clinical manifestation of the neurological symptoms in MS patients. The location and size of the lesions in the CNS can lead to various symptoms with varying degrees of severity. One common neurological symptom affecting over 70% of MS patients is optic neuritis where the optic nerve is affected with a lesion(s) leading to blurred vision, reduced colour sensitivity and eye pain.

Studies have shown that macrophages play a significant role in the clinical manifestation of EAE and long-term damage to myelin and axons. Macrophages can be classified into two main sub-types: Hematogenous macrophages (hMac) derived from the peripheral circulation and microglial macrophages that reside in the CNS parenchyma. Both hMac and microglia are involved in the inflammatory response in EAE. Both cell types exhibit similar phenotypic markers when activated and thus are indistinguishable (32). Berger *et al* showed disease severity in EAE correlates with the absolute number of macrophages invading the CNS parenchyma, but not with the number of infiltrating T cells (25). Huitinga *et al* showed that depletion of hMac prior to initiation of clinical symptoms in EAE rats resulted in the complete suppression of EAE and a drastic reduction of infiltrating macrophages to the brain parenchyma (26). Similar findings were reported by Tran *et al* in macrophage-depleted EAE mice (27). Furthermore, numerous studies have clearly illustrated the involvement of macrophages in the

destruction of myelin around axons which results in demyelination and therefore loss of efficient signal conduction (28-30). Activated macrophages have been demonstrated to secrete numerous products which can play multiple roles in inflammatory reactions underlying breakdown of the BBB, the activation and attraction of immunocompetent cells into the CNS and the generation of edema and degradation of myelin (31). These results allude to a crucial role for macrophages in the clinical outcome of the disease. Methods that would permit the tracking of hMac in particular will provide new insights on the pathophysiology of EAE and the effective evaluation of therapies directed at blocking the entry of hMac into the CNS.

### 1.1.4 Diagnosis and Treatment

Multiple sclerosis is diagnosed based on the existence of two clinical episodes involving two or more areas of the CNS over time. A number of criteria exist for diagnosis of MS, the most common one is the McDonald criteria which incorporates magnetic resonance imaging (MRI) in addition to clinical and laboratory elements (34). MS patients are classified into one of 4 main subtypes as defined in section 1.1.1. Approximately 85% of patients with MS have the RR form, comprising episodic relapses and remissions. After many years, most of these patients will enter into a SP form of MS. About 15% of MS patients present with the PP form that is characterized by a slowly progressive pattern. If these patients enter into a relapse they are characterized under the PR form of MS. Each MS category comprises a unique set of pathological and clinical elements.

Classification of MS is important as different disease-modifying drugs maybe needed to effectively control or halt the different forms of MS (35). Most MS treatments that exist today are aimed at preventing relapses, plaque development and disease progression. Since the mid-1990s clinical trials of new drugs have shown reductions in the number and severity of relapses, the number of new lesions appearing on MRI and long term progression of MS (36). Current disease modifying drugs for MS include beta-interferon and glatiramer acetate. Both beta-interferon and glatiramer acetate have been shown to modulate many of the biological processes responsible for the occurrence of relapses (37,38) through various mechanisms. However, neither beta-interferon nor glatrimir acetate comprise a cure for MS. The effect of both drugs has been limited to only reducing the activity and severity of the underlying illness, and even then not in all individuals.

Current therapeutic approaches to MS at the experimental level include: blockade of leukocyte infiltration using antibodies directed against specific cell integrins/adhesion molecules (39,40), stem cell therapy whether by whole bone marrow transplant or by stromal cell treatment (41), and more recently modulating the function of matrix metalloproteases which facilitate the passage of leukocytes across matrix barriers (42).

## *1.2 Magnetic Resonance Imaging*

Magnetic resonance imaging is increasingly used as a paraclinical measure for the diagnosis of MS and for monitoring disease activity and progression in patients with established disease (43,44). MRI is also an integral tool for assessing the efficacy of various therapies in clinical trials (45-47). The exquisite soft-tissue contrast provided by MRI and the ability to acquire clinically relevant information using non-invasive and non-destructive methods gives MRI great superiority for contrast generation over other imaging modalities. This section introduces the principle and mechanism upon which MRI operates, starting with the principle of nuclear spin and its behaviour in a magnetic field. The section concludes with a detailed discussion of the use of MRI in detection and tracking of MS lesions and the correlation of MR to MS pathology.

### 1.2.1 Principle and Mechanism

#### 1.2.1.1 Spin Physics

Nuclear angular momentum is a fundamental principle of MRI. All atoms in nature are assigned a spin number, which represents the net angular momentum of nuclear elements in the atom (neutrons, protons). MRI is able to detect nuclei with an odd number of protons and neutrons when the nuclei are in a magnetic field. The most common nucleus used in MRI is the proton in hydrogen due to its high prevalence in the body and its sensitivity to magnetic fields. The presence of hydrogen in water makes MRI a very powerful tool that is able to detect small changes in tissue pathology and even detect changes in water diffusion through

tissues. Imaging of humans relies on the ability to manipulate the bulk precession of hydrogen spins in water, fat and other organic molecules when the spins are made to interact with an external magnetic field. When a nucleus is placed in a magnetic field, it precesses at a characteristic frequency. This frequency is termed the Larmor frequency and for hydrogen atoms has a value of 42.6 MHz for an external magnetic field of strength 1.0 Tesla. The relationship between the Larmor frequency ($\omega_0$) and the external magnetic field is given by equation 1.2.1:

$$\omega_0 = \gamma B_0 \qquad \textit{Equation 1.2.1}$$

Gamma ( $\gamma$ ) is a constant called the gyromagnetic ratio and has a characteristic value for each atom. The precession of spins in a magnetic field is a result of a positive difference in energy which allows the protons to precess in a clockwise direction. This difference in energy is given by equation 1.2.2:

$$\Delta E = \gamma \hbar B_0 \qquad \textit{Equation 1.2.2}$$

Where $\hbar$ is Planck's constant divided by $2\pi$. As long as the protons are under the influence of $B_0$, there is a natural tendency for an excess of spins to align in the direction of $B_0$, the lower energy state. The ratio of spins aligned against the field to those with the field is given by the Boltzmann probability distribution given by equation 1.2.3.

$$\frac{n_-}{n_+} = e^{-\Delta E / kT} \qquad \textit{Equation 1.2.3}$$

Where $n$- represents spins aligned against the field, $n$+ represents spins aligned with the field, $k$ is Boltzmann's constant and T is the temperature in degrees Kelvin. Under the influence of any magnetic field, there will be a slightly higher

number of spins aligned with $B_0$. At 1.5T, an excess of approximately 5 per million protons are aligned with $B_0$. Given the large quantity of hydrogen atoms in the body, this net number of spins is sufficient to produce a net magnetic moment described by the Magnetization (equation 1.2.4):

$$M_0 = \frac{\rho_0 \gamma \hbar^2}{4kT} B_0 \qquad \textit{Equation 1.2.4}$$

Where $M_0$ represents the net magnetic moment or so called 'magnetization', and $\rho_0$ is the proton spin density.

When protons are excited with a radio-frequency (rf) pulse at the Larmor frequency, the protons begin to precess at a frequency equal to the Larmor frequency. The precession of any particular proton is influenced by its surrounding environment and the neighbouring protons. These internal and external factors control the rate at which the precession of the proton dies off; this is referred to as relaxation. The rate of relaxation is an important parameter in determining image contrast.

### 1.2.1.2 Signal Relaxation and Contrast Generation

The MRI signal is a result of the net response of the excited spins in a tissue to a specified set of rf pulses. This set of rf pulses is called a pulse sequence and can be altered in various ways depending on the information required from the tissue. One of the simplest and most common type of MR pulse sequences is the spin echo (SE) sequence. Spin echo sequences typically include a slice selective 90-degree rf pulse to excite the magnetization and one or more 180 degree pulses to

refocus the spins and generate signal echoes. The two variables of interest in a SE pulse sequence are the repetition time (TR), which is the time interval between each 90-degree pulse, and the echo time (TE), which is the time between the application of the 90-degree pulse and the peak of the echo signal. Another type of pulse sequence is the gradient echo (GRE) sequence generated by using a pair of bipolar gradient pulses. There is no refocusing of the 180-degree pulse and the magnetization is tilted by a flip angle, which is typically between 0-90 degrees. A variation of the GRE pulse sequence is the steady state free precession (SSFP) pulse sequence where TR and flip angle maintain a steady state and the value of TR is shorter than the $T_1$ and $T_2$ values of the tissue.

Immediately after the target tissue is excited using the specified pulse sequence, the signal begins to relax. The relaxation of spins in the tissue occurs by different mechanisms characterized by the time constants $T_1$, $T_2$ and $T_2$*. Spin-lattice or longitudinal relaxation (characterized by the time constant $T_1$) represents the characteristic time for $M_o$ to return to the direction of the main magnetic field ($B_0$). Spin-spin or transverse relaxation (characterized by the time constant $T_2$) represents the time for spins to dephase in the transverse plane. In the presence of $B_0$ inhomogeneities the transverse relaxation is characterized by the time constant $T_2$*. Generally, $T_1$ values are longer than $T_2$ values, and this difference is greater in tissues with low water content. By varying MR acquisition parameters, such as TR or the TE , one can generate contrast that highlights differences in $T_1$, $T_2$ or $T_2$*. Tissues with higher water content (and longer relaxation times) appear

hypointense on $T_1$-weighted ($T_1$w) images and hyperintense on $T_2$-weighted ($T_2$w) images. Tissues with low water content (shorter relaxation times) appear hyperintense on $T_1$w images and hypointense on $T_2$w images (48). Such contrast is generated by the intrinsic properties of the tissue ($T_1$ and $T_2$ values) and the set of rf pulses and gradient waveforms used to excite and manipulate the MR signal. Additional contrast can be generated by the administration of paramagnetic or superparamagnetic contrast agents. This contrast is particularly advantageous when assessing changes between normal and pathologic tissues where relaxation times are often similar. The interaction of such administered contrast agent molecules with adjacent water molecules leads to a local reduction in $T_1$ and/or $T_2$ relaxation times of water. Paramagnetic contrast agents, such as gadopentetate dimeglumine, otherwise known as Gadolinium (Gad), shorten the $T_1$ relaxation times resulting in increased signal on $T_1$w images, while superparamagnetic contrast agents, such as iron oxide nanoparticles, predominantly shorten $T_2$ relaxation times resulting in a reduction of signal on $T_2$w or $T_2$*w images.

### 1.2.2 Correlation to MS Pathology

The conventional MRI methods used to detect focal tissue changes in the CNS of MS patients include SE-$T_1$w, SE-$T_2$w and Gad-enhanced SE-$T_1$w techniques. Often, these multiple contrasts complement each other when diagnosing or assessing an MS patient. The appearance of hyperintense lesions on $T_2$w images is indicative of non-specific pathologic changes in the tissue. These pathologic changes may include inflammation, demyelination, edema and axonal loss (49).

The lesions often appear in peri-ventricular regions of the white matter, the corpus callosum, the juxtacortical gray-white junction and the infratenorial brain regions (50). Hypointense lesions on $T_1$w images (often called black holes) are predictive of active regions of severe axonal loss (51).

### 1.2.3 Gadolinium Enhancement

Gadolinium-enhanced MRI is considered to be the most sensitive tool for the clinical diagnosis and assessment of MS patients and for assessing treatment efficacy in clinical trials (52). Brain inflammation in MS is associated with local increase in BBB permeability, which can be imaged *in vivo* with MRI after an iv injection of Gad. The presence of a leaky BBB is thought to allow differentiation between active inflammatory lesions and lesions with less active inflammation or chronic inactive lesions (53). In normal humans the endothelial cells that line the BBB are tightly bound preventing entry of foreign bodies and/or immune cells.

Gad-enhanced MRI has been shown to correlate with the initial phase of lesion development (53,54) which is comprised of macrophage infiltration and an astroglial response, both leading to active demyelination. After 2-6 weeks enhancement subsides, however myelin breakdown products may persist for up to 9 months (55). Gad enhancement is therefore a sensitive indicator of the initial inflammatory phase of lesion development. However, demyelination probably progresses after breakdown of the BBB has subsided and therefore Gad enhancement is not a sensitive indicator of ongoing demyelination or chronic

inflammation (56). Furthermore, Gad-enhanced MRI is not able to identify the various cell components of the immune system trafficking across the damaged BBB (57).

Recent animal studies employing the use of superparamagnetic iron oxide (SPIO), an MR contrast agent that can be used to label inflammatory cells, have pointed to a clear difference between regions displaying Gad enhancement and regions showing SPIO uptake (58,59). This difference alludes to two distinct pathological processes that occur in the CNS of EAE animals: a transient state of BBB breakdown and a chronic state of inflammation and demyelination.

## *1.3 Cellular Magnetic Resonance Imaging*

Cellular MRI is a rapidly evolving field that combines the technology of high-resolution MRI and cellular MR markers to visualize targeted cells and cellular processes in living organisms. For cellular MRI, cells need to be labelled with MR contrast agents in order to make them stand out from the surrounding tissues and render them distinctly visible on MRI. Ideally, it will be possible to target a particular population of cells in a living organism for cellular MRI to study their tissue distribution, differentiation, proliferation, regeneration, survival and death (93). The development of a wide range of paramagnetic and superparamagnetic contrast agents, in addition to the techniques for incorporating these labels into cells has stimulated numerous applications for cellular MRI. In particular, superparamagnetic iron oxide contrast agents are especially effective in reducing the $T_2$* relaxation time of targeted tissues due to the induction of strong field inhomogeneities resulting in the creation of signal hypointensity on MR images.

Superparamagnetic iron oxide contrast agents are comprised of an iron-oxide core and a carbohydrate coating with a diameter of 50-100nm. SPIO particles first appeared in the late 1980s as MR contrast agents for detection of liver and spleen tumors (64,65). Upon systemic injection of the SPIO agent, macrophages in the liver and spleen naturally engulf the SPIO particles causing a large region of signal hypo-intensity on $T_2$w and $T_2$*w MR images. Regions where there is no signal loss correspond to tumor cells which are unable to engulf SPIO particles. The signal loss that results from the presence of SPIO particles in a specific

region is a consequence of a significant reduction in the $T_2$ relaxation time of the tissue (87). The $T_2$ shortening arises from the interactions between the unpaired electrons of SPIO and the hydrogen nuclei of water molecules. The size of the signal loss can span an area up to 50-100 times larger than the actual size of the SPIO particle.

Shortly after the introduction of SPIO to image liver and spleen tumors, a smaller agent was proposed for applications requiring a longer half-life. Ultrasmall superparamagnetic iron oxide (USPIO) has a blood half-life that is more than 12 times longer than that of SPIO (66). USPIO is also small enough to migrate across the capillary wall (mean particle size of 20nm). One of the first applications of USPIO imaging was in assessing lymph nodes and detecting nodal metastasis (67). Further applications included bone marrow imaging (68), brain imaging (69) and angiography where USPIO was used as a blood pool agent (70).

Other variations of SPIOs include micron-sized iron oxide nanoparticles (MPIOs) and magnetodendrimers. MPIOs span a wide array of sizes ranging from 0.96um-10um and contain varying concentrations of iron oxide. MPIOs have mainly been used in imaging organ rejection/transplantation (89) and following tumor progression from the initial cancerous lesion through to metastasis (92). The main advantage of MPIOs is their inert nature which allows them to remain incorporated in cells over multiple cell divisions as opposed to dextran-coated iron oxide particles which are biodegradable. In addition, MPIOs contain up to 3

times more iron per particle than SPIOs, allowing for increased detection sensitivity on MR images (90). Magnetodendrimers are dendrimer-encapsulated SPIOs. Bulte *et al* showed that magnetodendrimers are efficiently taken up by a wide variety of mammalian cells, including human neural and mesenchymal stem cells and can easily be detected *in vivo,* with a good agreement between the achieved MR contrast and a traditional marker gene (91).

In the late 1990s the application of SPIO contrast agents to image inflammation was first introduced. During an inflammatory response the population of macrophages in the circulation increases substantially (71). The natural ability of macrophages to engulf foreign bodies through the process of phagocytosis meant that upon injection of SPIO/USPIO into the circulation, during a period of active inflammation, the macrophages would presumably be labeled in the circulation before reaching the site of inflammation. Hence, iron-oxide based MR imaging could be used to detect and monitor specific site(s) of inflammation. One of the first applications of this theory was in animal models of MS (78,79,81). Other applications included imaging inflammation in spinal cord injury (72), transplant rejection (73), cerebral ischemia (74), atherosclerotic plaques (75) and amyloid plaques in Alzheimer's (76).

The choice of contrast agent (USPIO vs. SPIO) for applications of inflammation is important. The majority of cellular MRI studies utilize USPIOs since they have a longer half-life and therefore increased contact of the particles with macrophages in the circulation (66). However, a number of studies have shown that larger size particles tend to be phagocytosed much more efficiently (77,78).

The studies in this thesis utilize the contrast agent Feridex®, an SPIO comprised of dextran-coated iron oxide with a mean diameter of approximately 100nm (Figure 1.2). Feridex® is approved by the food and drug administration in the US and has been shown to be readily phagocytosed by macrophages (77,78).

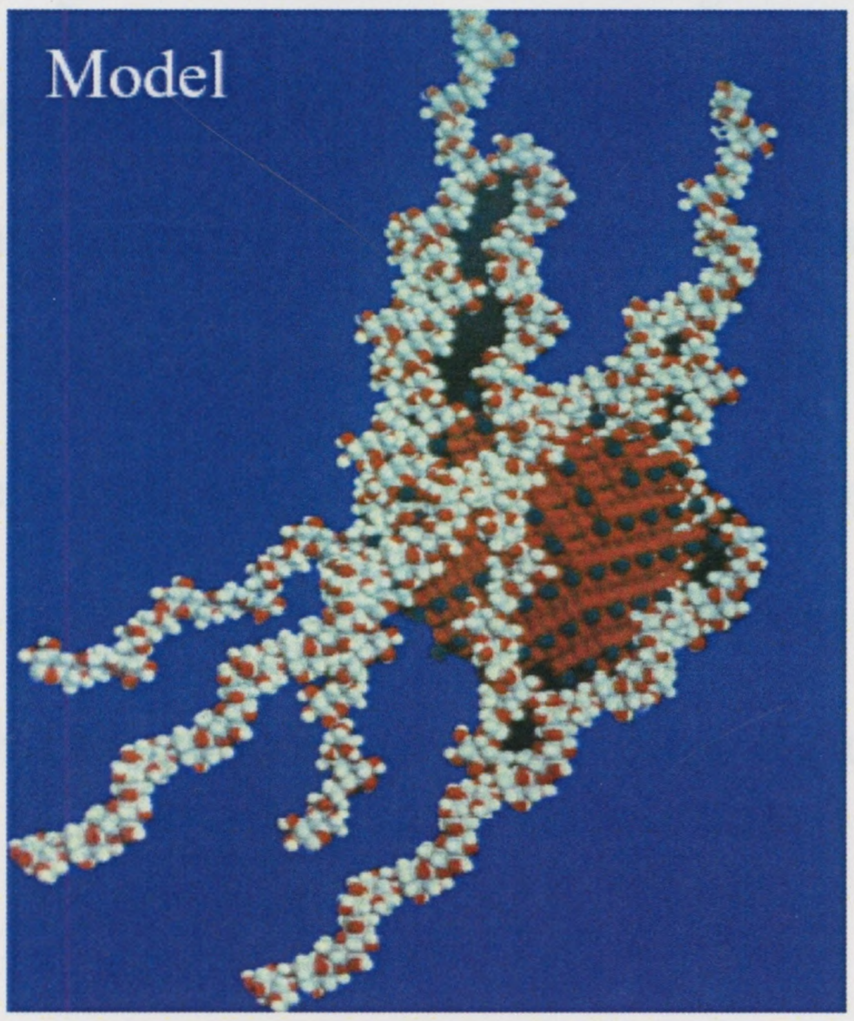


**Figure 1.2:** Chemical model showing the structure of an SPIO particle. Iron molecules make up the core of the SPIO particle (brown sphere). Dextran sugar molecules coat the SPIO particle.

An integral component of most cellular MRI experiments is the ability to acquire high-resolution images. In recent years the strength of MR magnets has grown substantially reaching up to 17.6T for small animal imaging (60) and 8T for human imaging (61). This increase in the main magnetic field ($B_0$) increases signal-to-noise ratio (SNR), contrast-to-noise ratio (CNR), and spectral resolution. In many cases, these benefits translate to higher spatial and/or temporal resolution compared to lower field strengths. However, the increase in $B_0$ does not come without an expense. A number of technological, physical and safety considerations must be taken into account when imaging at high-field strengths. Technology issues include maintaining the homogeneity of the static and rf magnetic fields, the design of efficient rf coils for signal reception, and the high cost of the main magnet. Physical considerations include changes in the relaxation mechanisms, increased susceptibility effects and other changes in contrast mechanisms. Safety considerations include higher power rf pulses and the potential for tissue heating and coil burns, and physiologic effects associated with motion at high-field strengths. Clearly, methods of performing high-resolution MRI which can overcome some of these disadvantages are highly desirable.

In the work presented in this thesis, high-resolution MRI was performed using a clinical 1.5T MR scanner, a high-strength custom-built gradient coil insert and a steady state free precession (SSFP) imaging sequence. The gradient coil insert had the following hardware specifications which were approximately 10 times

greater than those of a clinical 1.5T scanner: peak slew rate 2000 T/m/s and maximum gradient strength 1200mT. This unique method of acquiring high-resolution MR images for cellular MRI has a number of advantages. At the low field strength used in this study chemical shift artifacts and field inhomogeneities are minor, as compared with what is typically observed in SSFP images acquired at high magnetic field strengths. The gradient coil insert permits very high-resolution image acquisitions with very short scan times (short TR/TE). The time it takes to transform a clinical scanner to a high-resolution MRI scanner is approximately 15 minutes. Figure 1.3a shows the typical setup for incorporating the gradient coil insert into the MR scanner. The rf coil is equipped with tubes that carry warm water to maintain the animal's temperature and isoflurane to keep the animal anaesthetized during the scan (Figure 1.3b). In addition to the gradient coil insert, the fast imaging employing stead state acquisition (FIESTA) pulse sequence, which is a variation of the SSFP sequence has certain additional advantageous features over other imaging sequences for cellular imaging with SPIO. The FIESTA sequence provides better SNR, relative to GRE and SE sequences, as a result of the multiple signal refocusing paths available for tissues with $T_2$ much greater than TR (62). The significant improvement in SNR efficiency allows for acquisition of images at high spatial resolution with relatively short scan times and allows cellular imaging at lower field strengths than is typically possible. Using the customized hardware and the FIESTA pulse sequence, our lab has demonstrated the ability to perform cellular MRI at 1.5T in experimental models of spinal cord injury (72) and multiple sclerosis (89).

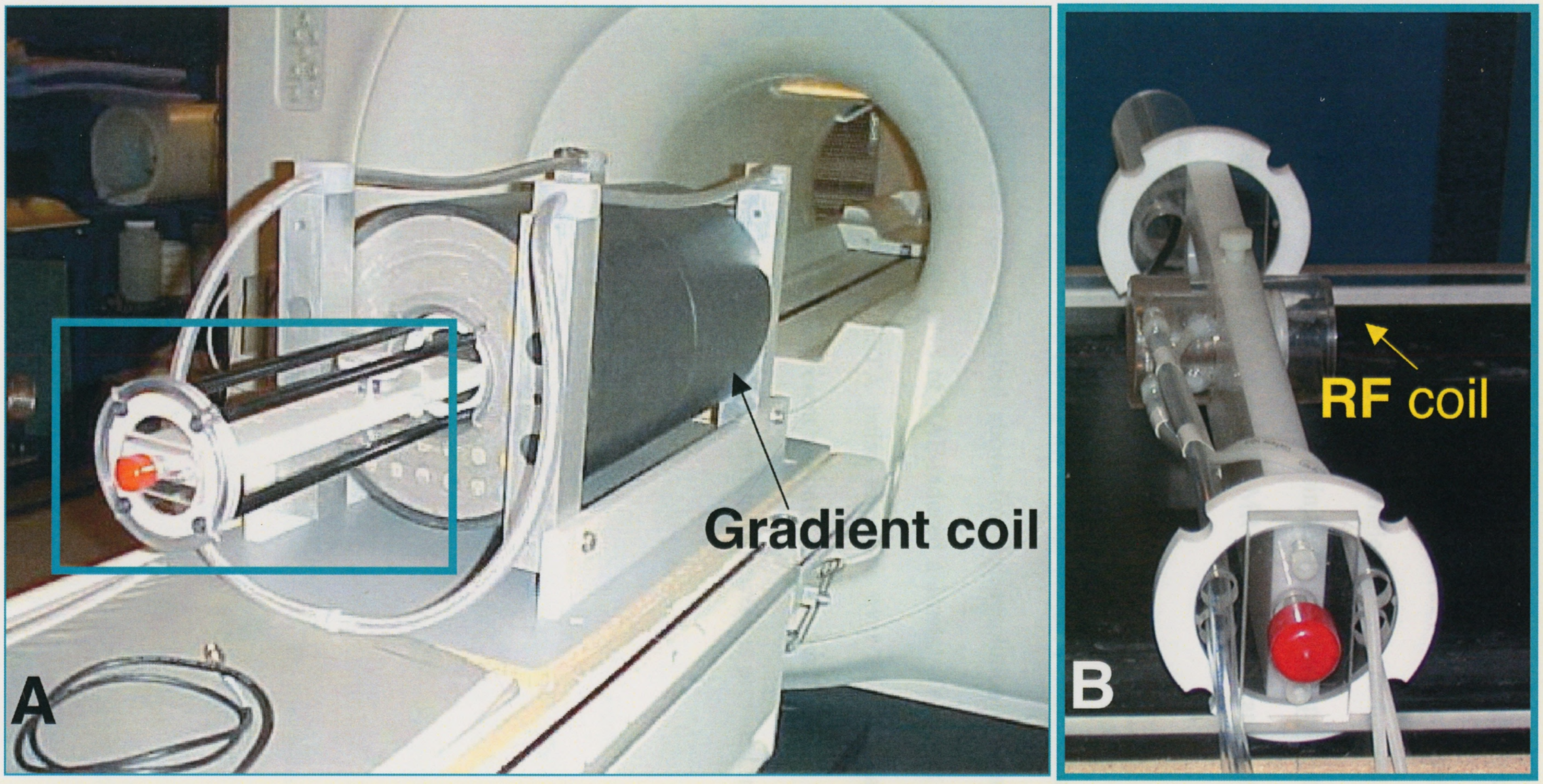


**Figure 1.3:** Transforming a 1.5T clinical MR scanner into a high-resolution small animal imaging system. (A) Gradient coil insert is shown lying on the patient bed of a clinical scanner. Blue box shows the tray in which the rf coil lies. (B) Close up on the tray showing the rf coil where a living mouse is placed. Tubes connected to the rf coil carry gas anesthetic to keep the animal anesthetized and warm water to keep the animal warm during the scan.

More recently Heyn *et al* showed, for the first time, that single cells labeled with SPIO particles, can be detected in mouse brain *in vivo* (63). The only comparable study to Heyn's *in vivo* detection of single cells was performed by Shapiro *et al* who showed indirect evidence that single liver cells (hepatocytes) labelled with SPIO can be detected *in vivo* on a 7T MR scanner after transplantation of the cells into the host animal (89).

In prior work performed during my 4$^{th}$ year project I demonstrated the capability of using the tools described above for high-resolution cellular MRI to detect inflammation in the CNS of EAE-induced animals. The work also showed the superiority of the FIESTA pulse sequence over FSE-$T_2$w and SPGR pulse sequences in resolving different regions of inflammation within the CNS of EAE animals. The resulting publication from this work is provided in the appendix of this thesis.

## *1.4 Cellular MRI of Inflammation in EAE: A Literature Review*

In 1998 Xu *et al* published the first report of detecting inflammatory lesions after an iv injection of SPIO (79). The experiments were performed *in vivo* in EAE-induced mice on a 4.7T animal MR scanner. Results showed the presence of regions of signal hypointensity on MR images, which corresponded to areas of dense perivascular mononuclear cell infiltration. In 1999 Dousset *et al* published a similar study using a USPIO contrast agent in EAE-induced rats on a 4.7T animal MR scanner (80). Dousset's results showed that the regions of signal loss on MR images corresponded to areas of macrophage accumulation as evidenced by ED1 immunohistochemistry (a common marker for macrophages in rats) and electron microscopy. Within the same year, Dousset *et al* reported the importance of USPIO dose and time delay before scanning in determining the sensitivity of cellular MRI to detecting inflammatory lesions in EAE (81). To conclude the year, Dousset *et al* performed a comparative study between USPIO-enhanced MRI, conventional $T_2$w MRI and Gad-enhanced $T_1$w MRI in EAE rats to determine the most sensitive technique for detecting EAE lesions. Dousset showed that USPIO-enhanced MRI was the most sensitive method for detecting MS lesions and attributed the cause of this to the intracellular uptake of USPIO and its transport to the CNS (82). With the above set of reports, cellular MRI of inflammation in EAE became well established, albeit with a number of unresolved questions. In 2003, Rausch *et al* studied disease burden during the acute phase and the first relapse phase of EAE in Lewis rats by using different

MRI techniques. Rausch *et al* showed that regions of USPIO accumulation coincided only in part with areas of BBB breakdown and suggested that monocyte infiltration and BBB breakdown may be two independent processes (83). Shortly after, Floris *et al* published a study that specifically addressed differences in the timing of BBB breakdown and monocyte infiltration in EAE rats (84). Floris *et al* demonstrated that BBB breakdown preceded cellular infiltration and peaked at the onset of the disease whereas cellular infiltration as demonstrated by SPIO-enhanced MRI peaked at later stages of EAE. Most recently, Dousset *et al* showed the application of USPIO-enhanced MRI as a prognostic measure for determining potentially severe forms of EAE (85). By injecting USPIO into rats induced with the severe protracted-relapsing EAE model, which is predominately characterized by axonal loss, Dousset *et al* showed that animals with SPIO-enhancing lesions at the onset of EAE later developed severe forms of the disease. On the other hand, EAE animals with no SPIO-enhancing lesions at the onset of the disease developed mild forms of EAE during later stages.

Eight years after the first application of cellular MRI to detecting inflammation in EAE the first reported study in humans was recently published by Dousset *et al* in the American Journal of Neuroradiology (86). Dousset *et al* demonstrated the potential advantages of using USPIO-enhanced MRI to detect and monitor lesion evolution in MS patients. The study also showed the heterogeneity of inflammatory MS lesions by comparing the different information provided from images with USPIO and Gad contrast agents.

## *1.5 Summary and Rationale*

Multiple sclerosis is the most common disabling neurological disease in young adults. The application of conventional MRI to the study of MS has greatly improved our ability to diagnose the disease and monitor its evolution. Nevertheless, the information provided by conventional MRI methods is limited in both accuracy and specificity. Recent work in the area of cellular imaging has improved our understanding of how the cellular aspects of inflammation evolve over the course of EAE. The correlation between macrophage accumulation and axonal loss in the CNS hints to the capability of using iron oxide-enhanced MRI as a prognostic tool for evaluating patients at higher risk of developing severe forms of MS and thus starting them on a suitable treatment. The latest work by Dousset *et al* demonstrates how SPIO-enhanced MRI can be used to complement Gad-enhanced MRI as both methods provide different information on the nature and pathology of the MS lesion. However, it remains unknown whether SPIO-enhancing lesions on MRI are attributed to the uptake of SPIO by hematogenous macrophages in the circulation or CNS-resident microglia. The specific objective of the present thesis is to determine the cell type involved in the uptake of SPIO in cellular imaging experiments. Having established the importance of hematogenous macrophages in EAE/MS in earlier sections of this chapter and the critical role they play throughout the disease course, the remainder of this thesis focuses on experiments aimed at detecting and tracking hematogenous macrophages in EAE.

## *1.6 Thesis Organization*

In this thesis I use customized high-resolution cellular MRI technology along with a SPIO contrast agent to study the inflammatory response in EAE and to address a fundamental research question related to cellular MRI.

The major work of this thesis is described in Chapter 2. This chapter has been submitted as a manuscript to the Journal of Magnetic Resonance Imaging. A novel EAE mouse model was used to study the contribution of hematogenous macrophages to the iron induced signal loss observed in EAE brains. My hypothesis was that hematogenous macrophages originating from the circulation are the primary cell type responsible for SPIO uptake. Through these experiments I have produced direct evidence that shows that SPIO labeled hematogenous macrophages can be identified in the brain after iv administration of Feridex® and that these cells contribute to the regions of signal loss observed in MR images of EAE brain.

To further examine the role of hematogenous macrophages a depletion experiment was designed. In chapter 3 a pilot study is described where macrophage depletion was performed using clodronate-loaded liposomes in EAE-induced rats. My hypothesis was that macrophage depletion in EAE animals would decrease the degree of signal loss typically observed in images of the brains of EAE animals. Macrophages were depleted just prior to the systemic

administration of SPIO to determine the contribution of SPIO to regions of signal loss on MR images in the absence of macrophages.

Chapter 4 summarizes the major results of this thesis and discusses potential future work in the field of cellular MRI for investigating EAE.

## *1.7 References*


1. Multiple Sclerosis Society of Canada
2. Noseworthy JH, Lucchinetti C, Rodriguez M, Weinshenker BG. Multiple Sclerosis. *N Engl J Med* 2000; 343:938-952
3. Sun, J. B., T. Olsson, W. Z. Wang, B. G. Xiao, V. Kostulas, S. Fredrikson, H. P. Ekre, H. Link. Autoreactive T and B cells responding to myelin proteolipid protein in multiple sclerosis and controls. *Eur J Immunol* 1991; 21:1461-1468
4. Kurtzke JF. Multiple sclerosis in time and space-geographic clues to cause. *J Neuroviro* 2000; 6 Suppl 2:S134-40.
5. Sawcer S. A new era in the genetic analysis of multiple sclerosis. *Curr Opin Neurol* 2006; 19:237-41.
6. Ercolini AM, Miller SD. Mechanisms of immunopathology in murine models of central nervous system demyelinating disease. *J Immun* 2006; 176:3293-98.
7. Barbano RL, Dal Canto MC. Serum and cells from Theiler's virus-infected mice fail to injure myelinating cultures or to produce in vivo transfer of disease. The pathogenesis of Theiler's virus-induced demyelination appears to differ from that of EAE. *J Neuro Sci* 1984; 66:283-93.
8. Dal Canto MC, Melvold RW, Kim BS, Miller SD. Two models of multiple sclerosis: experimental allergic encephalomyelitis (EAE) and Theiler's murine encephalomyelitis virus (TMEV) infection. A pathological and immunological comparison. *Microsc Res Tech* 1995; 32:215-29.
9. Tsunoda I, Fujinami RS. Two models for multiple sclerosis: experimental allergic encephalomyelitis and Theiler's murine encephalomyelitis virus. *J Neuropathol Exp Neurol* 1996; 55:673-86.
10. Pettinelli CB, Fritz RB, Chou CH, McFarlin DE. Encephalitogenic activity of guinea pig myelin basic protein in the SJL mouse. *J Immunol* 1982; 129:1209-11.
11. Chou CH, Shapira R, Fritz RB. Encephalitogenic activity of the small form of mouse myelin basic protein in the SJL/J mouse. *J Immunol* 1983; 130:2183-6.
12. Kerlero de Rosbo N, Mendel I, Ben-Nun A. Chronic relapsing experimental autoimmune encephalomyelitis with a delayed onset and an atypical clinical course, induced in PL/J mice by myelin oligodendrocyte glycoprotein (MOG)-derived peptide: preliminary analysis of MOG T-cell epitopes. *Eur J Immunol* 1995; 25:985-93.
13. Slavin A, Ewing C, Liu J, Ichikawa M, Slavin J, Bernard CC. Induction of multiple sclerosis-like disease in mice with an immunodominant epitope of myelin oligodendrocyte glycoprotein. *Autoimmunity* 1998; 28:109-20.
14. Tuohy VK, Sobel RA, Lees MB. Myelin proteolipid protein-induced experimental allergic encephalomyelitis. Variations of disease expression in different strains of mice. *J Immunol* 1988; 140:1868-73.
15. Linthicum DS, Munoz JJ, Blaskett A. Acute experimental autoimmune encephalomyelitis in mic: Adjuvant action of Bordetella pertussis is due to vasoactive amine sensitization and increased vascular permeability of the central nervous system. *Cell Immunol* 1982; 73:299-310.

16. Racke MK, Hu W, Lovett-Racke AE. PTX cruiser: driving autoimmunity via TLR4. *Trends Immunol* 2005; 26:289-91.
17. Lennon VA, Byrd WJ. Role of T lymphocytes in the pathogenesis of experimental autoimmune encephalomyelitis. *Eur J Immunol* 1973;3:243-5.
18. Traugott U, Raine CS. T and B cell distribution in multiple sclerosis (MS) lesions. *J Neuropathol Exp Neurol* 1982; 42:425.
19. Frohman EM, Racke MK, Raine CS. Multiple sclerosis – The plaque and its pathogenesis. *N Engl J Med* 2006; 354:942-55.
20. Yong VW, Power C, Forsyth P, Edwards DR. Metalloprotei-nases in biology and pathology of the nervous system. *Nat Rev Neurosci* 2001; 2:502-11.
21. Knight SC, Stagg AJ. Antigen-presenting cell types. *Curr Opin Immunol* 1993; 5:374–382.
22. Thomas WE. Brain macrophages: on the role of pericytes and perivascular cells. *Brain Res Rev* 1999; 31:42-57.
23. Banchereau J, Steinman RM. Dendritic cells and the control of immunity. *Nature* 1998; 392:245–252.
24. Archelos JJ, Storch MK, Hartung HP. The role of B cells and autoantibodies in multiple sclerosis. *Ann Neurol* 2000; 47:694–706.
25. Berger T, Weerth S, Kojima K, Linington C, Wekerle H, Lassmann H. Experimental autoimmune encephalomyelitis: the antigen specificity of T lymphocytes determines the topography of lesions in the central and peripheral nervous system. *Lab Invest* 1997; 76:355-64.
26. Huitinga I, van Rooijen N, De Groot CG, Uitdehaag BM, Dijkstra CD, Suppression of experimental allergic encephalomyelitis in Lewis rats after elimination of macrophages. *J Exp Med* 1990;172:1025–1033.
27. Tran EH, Hoekstra K, van Rooijen N, Dijkstra CD, Owens T. Immune invasion of the central nervous system parenchyma and experimental allergic encephalomyelitis, but not leukocyte extravasation from blood, are prevented in macrophage-depleted mice. *J Immunol* 1991;161:3767-75.
28. Lampert PW. Demylination and remyelination in experimental allergic encephalomyelitis – further electron microscopal observations. *J Neuropath Exp Neurol* 1965;24:371.
29. Epstein LG, Prineas JW, Raine CS. Attachement of myelin to coated pits on macrophages in experimental allergic encephalomyelitis. *J Neurol Sci* 1983;61:341.
30. Bruck W, Friede RL. Anti-macrophage CR3 antibody blocks myelin phagocytosis by macrophages *in vitro*. *Acta Neuropathol* 1990; 80:415-8.
31. Hartung HP, Keiniger K. Non-specific mechanisms of inflammation and tissue damage in MS. *Res in Immunol* 1989; 140:226.
32. Williams K, Bar-Or A, Ulvestad E, Olivier A, Antel JP, Yong VW. Biology of adult human microglia in culture: comparisons with peripheral blood monocytes and astrocytes. *J Neuropathol Exp Neurol* 1992; 51:538–49.
33. Hartung HP, Kisseier BC, Hemmer B. Purely Systemically Active Anti-Inflammatory Treatments are Adequate to Control Multiple Sclerosis. *J Neurol* 2005; 252 [Suppl 5]:30-37

34. McDonald WI, Compston A, Edan G, Goodkin D, Hartung HP, Lublin FD, McFarland HF, Paty DW, Polman CH, Reingold SC, Sandberg-Wollheim M, Sibley W, Thompson A, van den Noort S, Weinshenker BY, Wolinsky JS. Recommended diagnostic criteria for multiple sclerosis: guidelines from the International Panel on the diagnosis of multiple sclerosis. *Ann Neurol* 2001; 50:121-7.
35. Murray TJ. Diagnosis and treatment of multiple sclerosis. *BMJ* 2006; 332:525-7.
36. Goodin DS, Frohman EM, Garmany GP, Halper J, Likosky WH, Lublin FD, Silberberg DH, Stuart WH, van den Noort S. Disease modifying therapies in multiple sclerosis: report of the American academy of neurology and the MS council for clinical practice guidelines. *Neurology* 2002; 58:169-78.
37. Goodin DS. Treatment of Multiple Sclerosis with Human Beta Inteferon. *The Int MS Journal* 2005; 12:96-108.
38. Dhib-Jalbut S. Glatiramer acetate (Copaxone) therapy for multiple sclerosis. *Pharmacol Ther* 2003; 98:245-55.
39. Kanwar JR, Kanwar RK, Krissansen GW. Simultaneous neuroprotection and blockade of inflammation reverses autoimmune encephalomyelitis. *Brain* 2004; 127:1313-31.
40. Kent SJ, Karlik SJ, Cannon C, Hines DK, Yednock TA, Fritz LC, Horner HC. A monoclonal antibody to a4 integrin suppresses and reverses active experimental autoimmune encephalomyelitis. *J Neuroimm* 1995;58:1-10.
41. Zhang J, Li Y, Chen J, Cui Y, Lu M, Elias SB, Mitchell JB, Hammill L, Vanguri P, Chopp M. Human bone marrow stromal cell treatment improves neurological functional recovery in EAE mice. *Exp Neurol* 2005;195:16-26.
42. Brundula V, Rewcastle NB, Metz LM, Bernard CC, Yong VW. Targeting Leukocyte MMPs and Transmigration: Minocycline as a Potential Therapy for Multiple Sclerosis. *Brain* 2002;125:1297-1308.
43. Fazekas F, Barkhof F, Filippi M, Grossman RI, Li DK, McDonald WI, McFarland HF, Paty DW, Simon JH, Wolinsky JS, Miller DH. The contribution of MRI to the diagnosis of MS. *Neurology* 1999; 53:448-456.
44. Filippi M, Inglese M. Overview of diffusion-weighted magnetic resonance studies in multiple sclerosis. *J Neurol Sci* 2001; 186:S37-S43.
45. Rudick RA, Ransohoff RM, Lee JC, Peppler R, Yu M, Mathisen P, Tuohy VK. In vivo effects of interferon beta-1a on immunosuppressive cytokines in multiple sclerosis. *Neurology* 1998;50:1294-1300.
46. Sorensen PS, Wanscher B, Jensen CV, Shreiber K, Blinkenberg M, Ravnborg M, Kirsmeier H, Larson VA, Lee M, Cstat ML. Intravenous immunoglobulin G reduces MRI activity in relapsing multiple sclerosis. *Neurlogy* 1998; 50:1273-81.
47. Capello E, Saccardi R, Murialdo A, Gualandi F, Pagliai F, Bacigalupo A, Marmont A, Uccelli A, Inglese M, Bruzzi P, Sormani MP, Cocco E, Meucci G, Massacesi L, Bertolotto A, Lugaresi A, Merelli E, Solari A, Filippi M, Mancardi GL, and the Italian GITMO-Neuro Intergroup on ASCT for Multiple sclerosis intense immunosuppression followed by autologous stem

cell transplantation in severe multiple sclerosis. *Neurol Sci* 2005; 26:S200–S203.
48. Wehrli FW, McGowan JC. The basis of MR contrast in magnetic resonance imaging of the brain and spine. Philadelphia: Lippincott-Raven;1996. p29-47.
49. Bruck W, Schmied M, Suchanek G, Bruck Y, Breitschopf H, Poser S, Piddlesden S, Lassmann H. Oligodendrocytes in the early course of multiple sclerosis. *Ann Neurol* 1994; 44:635-641.
50. Zivadinov R, Bakshi R. Role of MRI in multiple sclerosis I: inflammation and lesions. *Front Biosci* 2004; 9:665-683
51. van Walderveen MA, Kamphorst W, Scheltens P, van Waesberghe JH, Ravid R, Valk J, Polman CH, Barkhof F. Histopathologic correlate of hypointense lesions on $T_1$-weighted spin-echo MRI in multiple sclerosis. *Neurology* 1998; 50:1282-8.
52. MacFarland HF, Frank JA, Albert PS, Smith ME, Martin R, Harris JO, Patronas N, Maloni H, McFarlin DE. Using gadolinium-enhanced magnetic resonance imaging lesions to monitor disease activity in multiple sclerosis. *Ann Neurol* 1992; 32:758-766.
53. Katz D, Taubenberger JK, Cannella B, McFarlin DE, Raine CS, McFarland HF. Correlation between magnetic resonance imaging findings and lesion development in chronic, active multiple sclerosis. *Neurol* 1993; 34:661-9.
54. Nesbit GM, Forbes GS, Scheithauer BW, Okazaki H, Rodriguez M. Multiple sclerosis: histopathologic and MR and/or CT correlation in 37 cases at biopsy and three cases at autopsy. *Radiology* 1991; 180:467-74.
55. Hawkins CP, Munro PM, MacKenzie F, Kesselring J, Tofts PS, du Boulay EP, Landon DN, McDonald WI. Duration and selectivity of blood-brain barrier breakdown in chronic relapsing experimental allergic encephalomyelitis studied by gadolinium-DTPA and protein markers. *Brain* 1990; 113:365-78.
56. Fredrikson S and Link H. Advances in Multiple Sclerosis. 1999. Martin Dunitz Publishers. A textbook for medical professionals.
57. Inglese M, Benedetti B, Filippi M. The relation between MRI measures of inflammation and neurodegeneration in multiple sclerosis. *J Neurol Sci* 2005; 233:15-19
58. Berger C, Hiestand P, Kindler-Baumann D, Rudin M, Rausch M. Analysis of lesion development during acute inflammation and remission in a rat model of experimental autoimmune encephalomyelitis by visualization of macrophage infiltration, demyelination and blood-brain barrier damage. *NMR Biomed* 2006; 19:101-7.
59. Floris S, Blezer EL, Schreibelt G, Dopp E, van der Pol SM, Schadee-Eestermans IL, Nicolay K, Dijkstra CD, de Vries HE. Blood-brain barrier permeability and monocyte infiltration in experimental allergic encephalomyelitis: a quantitative MRI study. *Brain* 2004; 127:616-27
60. Steinbrecher A, Weber T, Neuberger T, Mueller AM, Pedre X, Giegerich G, Bogdahn U, Jakob P, Haase A, Faber C. Experimental autoimmune encephalomyelitis in the rat spinal cord: lesion detection with high-resolution MR microscopy at 17.6 T. *Am J Neuroradiol* 2005; 26:19-25.

61. Robitaille PM, Abduljalil AM, Kangarlu A, Zhang X, Yu Y, Burgess R, Bair S, Noa P, Yang L, Zhu H, Palmer B, Jiang Z, Chakeres DM, Spigos D. Human magnetic resonance imaging at 8 T. *NMR Biomed* 1998; 11:263-5.
62. Foster-Gareau P, Heyn C, Alejski A, Rutt BK. Imaging single mammalian cells with a 1.5T clinical MRI scanner. *Magn Reson Med* 2003; 49:968-71.
63. Heyn C, Ronald JA, Mackenzie LT, MacDonald IC, Chambers AF, Rutt BK, Foster PJ. In vivo magnetic resonance imaging of single cells in mouse brain with optical validation. *Magn Reson Med* 2006; 55:23-9.
64. Stark DD, Weissleder R, Elizondo G, Hahn PF, Saini S, Todd LE, Wittenberg J, Ferrucci JT. Superparamagnetic iron oxide: clinical application as a contrast agent for MR imaging of the liver. *Radiology* 1988; 168:297-301.
65. Weissleder R, Hahn PF, Stark DD, Elizondo G, Saini S, Todd LE, Wittenberg J, Ferrucci JT. Superparamagnetic iron oxide: enhanced detection of focal splenic tumors with MR imaging. *Radiology* 1988; 169:399-403.
66. Weissleder R, Elizondo G, Wittenberg J, Rabito CA, Bengele HH, Josephson L. Ultrasmall superparamagnetic iron oxide: characterization of a new class of contrast agents for MR imaging. *Radiology* 1990; 175:489-93.
67. Weissleder R, Elizondo G, Wittenberg J, Lee AS, Josephson L, Brady TJ. Ultrasmall superparamagnetic iron oxide: an intravenous contrast agent for assessing lymph nodes with MR imaging. *Radiology* 1990; 175:494-8.
68. Bush CH, Mladinich CR, Montgomery WJ. Evaluation of an ultrasmall superparamagnetic iron oxide in MRI in a bone tumor model in rabbits. *J Magn Reson Imag* 1997; 7:579-84.
69. Enochs WS, Harsh G, Hochberg F, Weissleder R. Improved delineation of human brain tumors on MR images using a long-circulating, superparamagnetic iron oxide agent. *J Magn Reson Imag* 1999; 9:228-32.
70. Anzai Y, Prince MR, Chenevert TL, Maki JH, Londy F, London M, McLachlan SJ. MR angiography with an ultrasmall superparamagnetic iron oxide blood pool agent. *J Magn Reson Imag* 1997; 7:209-14.
71. Van Furth R. Origin and kinetics of monocytes and macrophages. *Seminars in Hematology* 1970; 7:125-141.
72. Dunn EA, Weaver LC, Dekaban GA, Foster PJ. Cellular imaging of inflammation after experimental spinal cord injury. *Mol Imag* 2005; 4:53-62.
73. Beckmann N, Cannet C, Fringeli-Tanner M, Baumann D, Pally C, Bruns C, Zerwes HG, Andriambeloson E, Bigaud M. Macrophage labeling by SPIO as an early marker of allograft chronic rejection in a rat model of kidney transplantation. *Magn Reson Med* 2003; 49:459-67.
74. Kleinschnitz C, Bendszus M, Frank M, Solymosi L, Toyka KV, Stoll G. In vivo monitoring of macrophage infiltration in experimental ischemic brain lesions by magnetic resonance imaging. *J Cereb Blood Flow Metab* 2003; 23:1356-61.
75. Schmitz SA, Coupland SE, Gust R, Winterhalter S, Wagner S, Kresse M, Semmler W, Wolf KJ. Superparamagnetic iron oxide-enhanced MRI of atherosclerotic plaques in Watanabe hereditable hyperlipidemic rabbits. *Invest Radiol* 2000. 35:460-71.

76. Wadghiri YZ, Sigurdsson EM, Sadowski M, ElliottJI, Li Y, Scholtzova H, Tang CY, Aguinaldo G, Pappolla M, Duff K, Wisniewski T, Turnbull DH. Detection of Alzheimer's amyloid in transgenic mice using magnetic resonance microimaging. *Magn Reson Med* 2003; 50:293-302.
77. Engberink RDO, vad der Pol SM, Dopp E, de Vries HE, Blezer EL. Comparison of SPIO and USPIO for in vitro labeling of human monocytes with respect to MR detection and cellular activation status. *ISMRM Proc* 2006.
78. Metz S, Bonaterra G, Rudelius M, Settles M, Rummeny EJ, Daldrup HE. Capacity of human monocytes to phagocytose approved iron oxide MR contrast agents in vitro. *Euro Radiol* 2004; 14:1851-8.
79. Xu S, Jordan EK, Brocke S, Bulte JWM, Quigley L, Tresser N, Ostuni JL, Yang Y, McFarland HF, Frank JA. Study of relapsing remitting experimental allergic encephalomyelitis in the SJL mouse model using MION-46L enhanced in vivo MRI: Early histopathological correlation. *J Neuro Res* 1998; 52:549-58.
80. Dousset V, Delalande C, Ballarino L, Quesson B, Seilhan D, Coussemacq M, Thiaudiere E, Brochet B, Canioni P, Caille JM. In vivo macrophage activity imaging in the central nervous system detected by magnetic resonance. *Magn Reson Med* 1999; 41:329-33.
81. Dousset V, Gomez C, Petry KG, Delalande C, Caille JM. Dose and scanning delay using USPIO for central nervous system macrophage imaging. *MAGMA* 1999; 5:135-9.
82. Dousset V, Ballarino L, Delalande C, Coussemacq M, Canioni P, Petry KG, Caille JM. Comparison of ultrasmall particles of iron oxide (USPIO)-enhanced $T_2$-weighted, conventional $T_2$-weighted, and gadolinium-enhanced $T_1$-weighted MR images in rats with experimental autoimmune encephalomyelitis. *Am J Neuroradiol* 1999; 20:223-7.
83. Rausch M, Hiestand P, Baumann D, Cannet C, Rudin M. MRI-based monitoring of inflammation and tissue damage in acute and chronic relapsing EAE. *Magn Reson Med* 2003; 50:309-14.
84. Floris S, Blezer ELA, Schreibelt G, Dopp E, van der Pol SMA, Schadee-Eestermans IL, NicolayK, Dijkstra CD, de Vries HE. Blood brain barrier permeability and monocyte infiltration in experimental allergic encephalomyelitis: A quantitative MRI study. *Brain* 2004; 127:616-627
85. Brochet B, Deloire MSA, Touil T, Anne O, Caille´ JM, Dousset V, Petry KG. Early macrophage MRI of inflammatory lesions predicts lesion severity and disease development in relapsing EAE. *Neuroimage* 2006; 32:266-74.
86. Dousset V, Brochet B, Deloire MSA, Lagoarde L, Barroso B, Caille JM, Petry KG. MR Imaging of Relapsing Multiple Sclerosis Patients Using Ultra-Small-Particle Iron Oxide and Compared with Gadolinium. *Amer J Neuro Rad* 2006; 27:1000-5.
87. Bloembergen N, Purcell EM, Pound RV. Relaxation effects in nuclear magnetic resonance absorption. *Phys Rev* 1948; 73:679-710.

88. Oweida AJ, Dunn EA and Foster PJ. Cellular imaging at 1.5T: detecting cells in neuroinflammation using active labeling with superparamagnetic iron oxide. *Mol Imag* 2004; 3:85-95.
89. Shapiro EM, Sharer K, Skrtic S, Koretsky AP. In Vivo Detection of Single Cells by MRI. *Magn Reson Med* 2006; 55:242-49.
90. Shpairo EM, Skrtic S, Koretsky AP. Sizing it up: Cellular MRI using micron-sized iron oxide particles. *Magn Reson Med* 2005; 53:329-38.
91. Bulte JWM, Douglas T, Witwer B, Zhang SC, Strable E, Lewis BK, Zywicke H, Miller B, Gelderen P, Moskowitz BM, Duncan I, Frank JA. Magnetodendrimers allow endosomal magnetic labeling and i*n vivo t*racking of stem cells. *Nature* 2001; 19:1141-47.
92. Rodriguez O, Fricke S, Chien C, Dettin L, VanMeter J, Shapiro E, Dai HN, Casimiro M, Ileva L, Dagata J, Johnson MD, Lisanti MP, Koretsky A, Albanese C. Contrast-enhanced in vivo imaging of breast and prostate cancer cells by MRI. *Cell Cycle* 2006; 5:113-9.
93. Modo M, Hoehn M, Bulte JWM. Cellular MR Imaging. *Mol Imag* 2005; 4:143-64.

# Chapter 2

# Cellular Imaging of Macrophages in a Novel EAE Mouse Model [1]

## *2.1 Introduction*

Multiple sclerosis (MS) is an inflammatory, demyelinating disease of the central nervous system (CNS) (1). The major pathological hallmark of MS is the presence of sclerotic plaques in the brain and spinal cord (2). The pathologic picture of many MS plaques is consistent with immune cell-mediated damage to the myelin sheath (3). Experimental allergic encephalomyelitis (EAE) is an animal model for immune-inflammatory diseases of the CNS in general, and for MS in particular. EAE can be induced in various laboratory animals, including the mouse, rat, guinea pig and primates (4,5). Ongoing pathogenesis in MS and EAE is due to an active inflammatory process and is associated with blood-brain-barrier (BBB) damage (6). The inflammatory infiltrates in acute EAE and MS include a diverse accumulation of lymphocytes and macrophages, primarily in white matter regions of brain tissue (7). The importance of T cells in EAE has been extensively documented, particularly the ability to initiate the disease and the autoimmune specificity for myelin provided by these cells (8). Other immune cell types, specifically the macrophages, are also implicated in the pathogenesis of EAE (9,10).

---

[1] Chapter 2 submitted for publication to *Journal of Magnetic Resonance Imaging*, May 27, 2006.

Within the CNS of rats with EAE different types of macrophages can be distinguished: (i) macrophages which are bone marrow derived, including the hematogenous monocytes/macrophages that infiltrate the CNS, and (ii) macrophages derived from activated microglia. The hematogenous macrophages have been shown to play multiple roles in EAE. They secrete numerous products that are involved in BBB breakdown, the activation and recruitment of immunocompetent cells into the CNS and the degradation of myelin (11). Furthermore, infiltrating hematogenous macrophages have been shown to be important for the generation of neurological deficits in EAE (12-14). For example, Kent *et al* showed that blocking T cell and monocyte/macrophage infiltration using antibodies against the $\alpha 4\beta 1$-integrin caused a sustained reversal of disease pathology in chronic EAE (14).

Besides the T cells and infiltrating, hematogenous macrophages, the resident macrophages of the CNS have also been implicated in the pathogenesis of EAE. These resident cells include perivascular macrophages and microglia. The perivascular macrophages form a distinct population of cells. They are also bone-marrow derived, are phagocytic and are thought to exist in an activated state (15). As a component of the BBB they form a first line of defense once the endothelial integrity of the barrier is breached or damaged (16). As the primary immune effector cells of the CNS, microglia respond by migrating to the site of inflammation, where they proliferate, differentiate and become phagocytic (17). Like other tissue macrophages they release pro-inflammatory cytokines that

amplify the inflammatory response by recruiting additional immune cells to the site of injury.

A key issue for understanding the pathogenesis of MS is the reliable identification of the macrophages that are capable of degrading myelin and presenting autoantigen to T cells. Knowledge of which specific cells are participating in MS lesion formation, their spatial distribution and the timing of their infiltration or activation are important questions in MS research. Currently the most common methods for assessing macrophage involvement in EAE involve histopathological or immunohistochemical evaluations of multiple tissue sections. However, there are certain limitations with the use of these methods for investigating inflammation in EAE. Traditional histological techniques are laborious, destructive and provide only one measurement point per experimental animal at a defined point in time. In addition, there is currently no unique histological marker that allows for the differentiation between hematogenous macrophages and microglia.

Cellular MRI is a newly emerging field of imaging research that combines the ability to generate high resolution in vivo MRI data with contrast agents for labeling cells (18,19). The use of iron oxide nanoparticles for cell-specific imaging by MRI has now been demonstrated in a number of different disease models (20-24). Cells are either pre-labeled with iron nanoparticles prior to their injection or transplantation (25,26), or free iron nanoparticles are administered by

intravenous (iv) injection and taken up by cells in vivo. The latter approach has been termed "active" or "in vivo labeling" of cells. Some of the first MR studies to use this active labeling approach were in animal models of EAE (27-31). The presence of intracellular iron oxide is typically indicated by signal hypointensities in $T_2$ or $T_2$* weighted images (32). We have previously shown that individual perivascular cuffs can be visualized in images of EAE rat brain using the steady state free precession imaging sequence (3DFIESTA) after intravenous administration of Feridex® (33). Recently, Dousset *et al* demonstrated the application of USPIO to imaging immune cells in MS patients (34).

It is clear that cellular MRI techniques can be used to detect iron labeled cells in EAE brain tissue. However, little is known about the identity of the cells that are responsible for the signal loss in MR images. Several studies have compared MRI findings with immunohistochemical analyses with ED1, a marker for activated macrophages in rats, and shown that regions of signal loss in MR images correspond to cells in EAE lesions that are ED1 positive. However, all phagocytosing macrophages (hematogenous macrophages and microglia) in the rat are recognized by the monoclonal antibody (mAb) ED1. Furthermore, all of the macrophage subsets that have been implicated in the pathogenesis of EAE are naturally phagocytic and have the potential to internalize iron nanoparticles. In this study we use cellular MRI, and a novel transgenic mouse model of EAE to differentiate between macrophage subsets and to investigate the degree to which hematogenous macrophages contribute to the regions of signal loss detected in

MR images of EAE brain. This mouse expresses the enhanced green fluorescent protein (EGFP) in the myelomonocytic lineage of hematopoietic cells (35); as a result hematogenous macrophages fluoresce green while microglia do not.

## *2.2 Methods*

### 2.2.1 Transgenic Mouse

These studies used the lysozyme M-EGFP-*ki* (*lys*-EGFP-*ki*) transgenic mouse created by Faust *et al* (35). The *lys*-EGFP-*ki* model was created using EGFP knocked into the C57Bl/6 genome replacing the lysozyme M (*lys*-M) gene. The *lys*-M promoter drives the expression of EGFP specifically in mature myelomonocytic cells, which include monocytes, macrophages and neutrophils (but not microglia). The wild type C57Bl/6 mouse, which is the genetic background of the *lys*-EGFP-ki mouse, has been used by many investigators for various models of EAE (36,37).

### 2.2.2 EAE Induction

EAE was induced in 6 week old female lys-EGFP-ki transgenic mice by a subcutaneous injection of a mixture of 100 ug synthetic myelin oligodendrocyte glycoprotein peptide 35-55 ($MOG_{35-55}$), 0.050 ml complete Freund's adjuvant (CFA) containing 500ug irradiated mycobacterium tuberculosis. 0.1 ml was injected in the flank while the mice were under general anesthesia. Pertussis toxin (500ng) was administered i.p. on days 0 and 2 post-disease immunization. A booster injection was given 8 days after the initial inoculation, in which

incomplete Freund's adjuvant replaced CFA. All protocols used for this experiment were approved by the University of Western Ontario Animal Care Committee and were conducted in accordance with the policies and guidelines of the Canadian Council on Animal Care.

### 2.2.3 Clinical assessment

Animals were weighed and scored daily for the clinical features of EAE according to the following scale: 0 = normal healthy animal, 0.5 = partial loss of tail tonus, 1 = loss of tail tonus, 2 = hind limb weakness, 3 = complete hindlimb paralysis, 4 = hindlimb and forelimb weakness, 5 = complete paralysis, incontinence, and moribund conditions. Scoring began the day after immunization. Day 0 was considered the day of immunization.

### 2.2.4 *In vivo* Cellular MR Imaging

Fourteen EAE mice were administered Feridex® (Advanced Magnetic Industries) i.v. via tail vein injection (2mMol/kg) on day 16-22 post immunization. Control groups included EAE mice administered saline iv (n=4) and normal healthy mice administered Feridex® (n=7) or saline (n=7) on day 19. Animals were imaged in vivo 24 hours after the injection of Feridex® or saline. In addition, two EAE animals were imaged repeatedly, at three time-points (24, 48 and 72 hours) after a single iv injection of Feridex®.

Mice were imaged at 1.5 Tesla on a clinical MR system (GE EXCITE) equipped with a custom-built, high performance gradient coil insert, designed and constructed in our lab. The coil had the following characteristics: inner diameter 11cm, peak slew rate 2000 T/m/s and maximum gradient strength 1200mT/m. Mice were anesthetized using the gas anesthetic isoflurane (1% in oxygen) and positioned within a custom-built mouse head solenoidal radio-frequency coil which was placed within the gradient insert. To maintain normal body temperature during imaging, warm water was circulated around the RF coil compartment. In vivo brain images were acquired using a steady state free precession imaging sequence (3DFIESTA, GE Medical Systems, Milwaukee, WI), which was previously optimized in our lab for imaging SPIO labeled cells (38,39). The FIESTA imaging sequence parameters were as follows: TR/TE 7.7/3.6 ms, flip angle 30°, 21 kHz bandwidth, 20 signal averages, 2 cm field of view, 200x200 matrix, and a slice thickness of 0.2 mm. The resulting spatial resolution was 100x100x200 $\mu$m. Scan time was approximately 1 hour per animal.

### 2.2.5 Histopathology and Fluorescence Imaging

After imaging, euthanasia was performed with an overdose of pentobarbitol and mice were perfusion-fixed with 3.75 % neutral buffered formalin (Sigma Chemical, Oakville, ON). The mouse brains were excised and stored in 10% formalin for 24 hours. The specimens were then placed in increasing concentrations of sucrose solution (10%, 20%, 30%) over 3 days to prepare the

tissue for cryosectioning. Tissue was serially sectioned at a thickness of 16μm, in the axial plane and thaw-mounted on gelatin-coated slides. The MR images were used to guide the choice of which brain region to section. Between 10-60 tissue sections were cut for each mouse brain.

To distinguish the EGFP positive hematogenous macrophages from resident microglia, sections were double-labeled with Alexa Fluora ® 488 conjugated with rabbit anti-GFP antibody (Molecular Probes, Burlington, ON, Canada) and then with either biotinylated tomato lectin for macrophages and blood vessels (Vector Laboratories, Burlington, ON), or with the macrophage marker, biotinylated F4/80 antibody (Cedarlane, Hornby, ON, Canada). Because the detergent Triton X-100 needed for F4/80 and lectin staining quenches EGFP fluorescence, the anti-EGFP antibody was used to label EGFP positive cells. After three 10-minute washes in Tris PBS plus 0.1% Triton X-100 (TPBS-X), sections were blocked with 10% normal horse serum (NHS) plus 10% normal rat serum (NRS) in TPBS-X for 1 hour at room temperature. Sections were then incubated at room temperature for 48 hours with the mAb F4/80 (1:400 dilution) and anti-GFP-alexa fluor 488 (1:2000 dilution). Following a wash with TPBS-X containing 1% each of NMS and NHS, sections were incubated with HRP-Streptavadin (1:1000 dilution) in 1% each of NHS and NRS for 1 hour. Signal was amplified using the Tyramide Signal Amplification system according to the manufacturer's instructions (Perkin Elmer, Boston, MA, USA). Rhodamine Red-X conjugated to streptavidin (1:200 dilution) was applied for 30 minutes to bind with the

biotinlyated F4/80 mAb. 4'-6-Diamidino-2-phenylindole (DAPI) solution was applied to the sections for 5 minutes, rinsed with TPBS, distilled water, and cover slipped using Vectashield (Vector Laboratories, Burlington, ON Canada). Alternatively sections were first stained with biotinylated tomato lectin according to the manufacturers' instructions with strepavidin Alexa 594 then stained with the Alexa 488 anti-GFP antibody as described above in order to provide the same level of sensitivity of detection. Visualization of all stained sections was performed via fluorescence microscopy using an Olympus IX50 microscope.

Following the acquisition of fluorescence images the cover slips were carefully removed and the sections were re-stained with diaminobenzidine-enhanced Perls prussian blue (DAB-PPB) and counterstained with Nuclear Fast Red to demonstrate iron uptake and localization in the tissue. Histological and MR images were compared by locating corresponding anatomical landmarks. Regions of signal loss in the 3D MR image data sets were counted and compared with the numbers and locations of GFP positive and PPB positive regions in the tissue sections.

## *2.3 Results*

### 2.3.1 EAE clinical course

A reproducible, relapsing-remitting form of EAE was produced in the lys-EGFP-ki transgenic mice. Figure 2.1A shows the clinical course of the disease until day 19 after EAE induction. The animals began to develop clinical symptoms on day 12 post-EAE inoculation. By day 16, all EAE-induced animals had clinical symptoms ranging from a score of 1-4. The mean day of onset was 16.

Two animals were monitored until day 70 post-disease induction. These animals entered into three relapse phases evident by recovery followed by recurring clinical symptoms of the disease (Figure 2.1B).

### 2.3.2 *In Vivo* Cellular Imaging

Discrete areas of signal loss were observed in the *in vivo* FIESTA images of all EAE animals administered Feridex® (Figure 2.2). The regions of signal loss were observed throughout the brain, often in periventricular locations, and spanned several contiguous 200um MR image slices. Figure 2.2 shows representative MR images from three different EAE animals administered Feridex® (2.2 A-C) and one non-EAE animal administered Feridex® (2.2 D). No regions of signal loss were observed in any of the control animals.

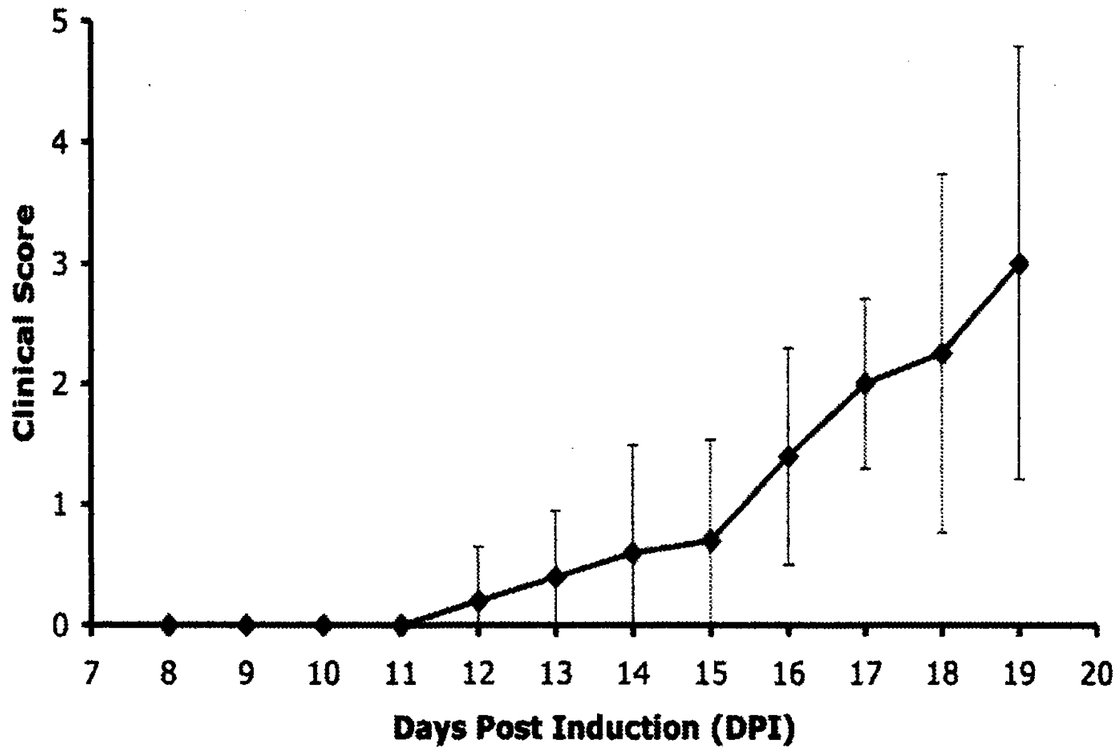


**Figure 2.1A:**
Graphical representation of the acute EAE disease course over a period of 19 days in Lys-EGFP-ki transgenic mice (N = 6).

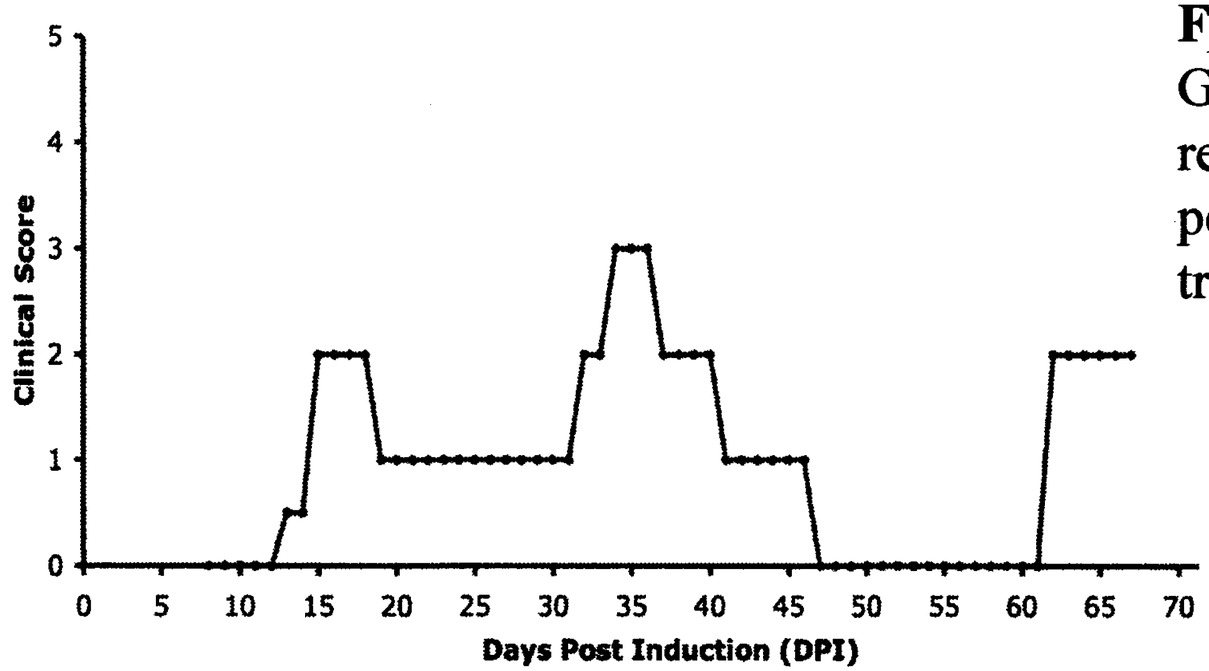


**Figure 2.1B:**
Graphical representation of the relapsing-remitting EAE disease course over a period of 67 days in a Lys-EGFP-ki transgenic mouse (N = 1).

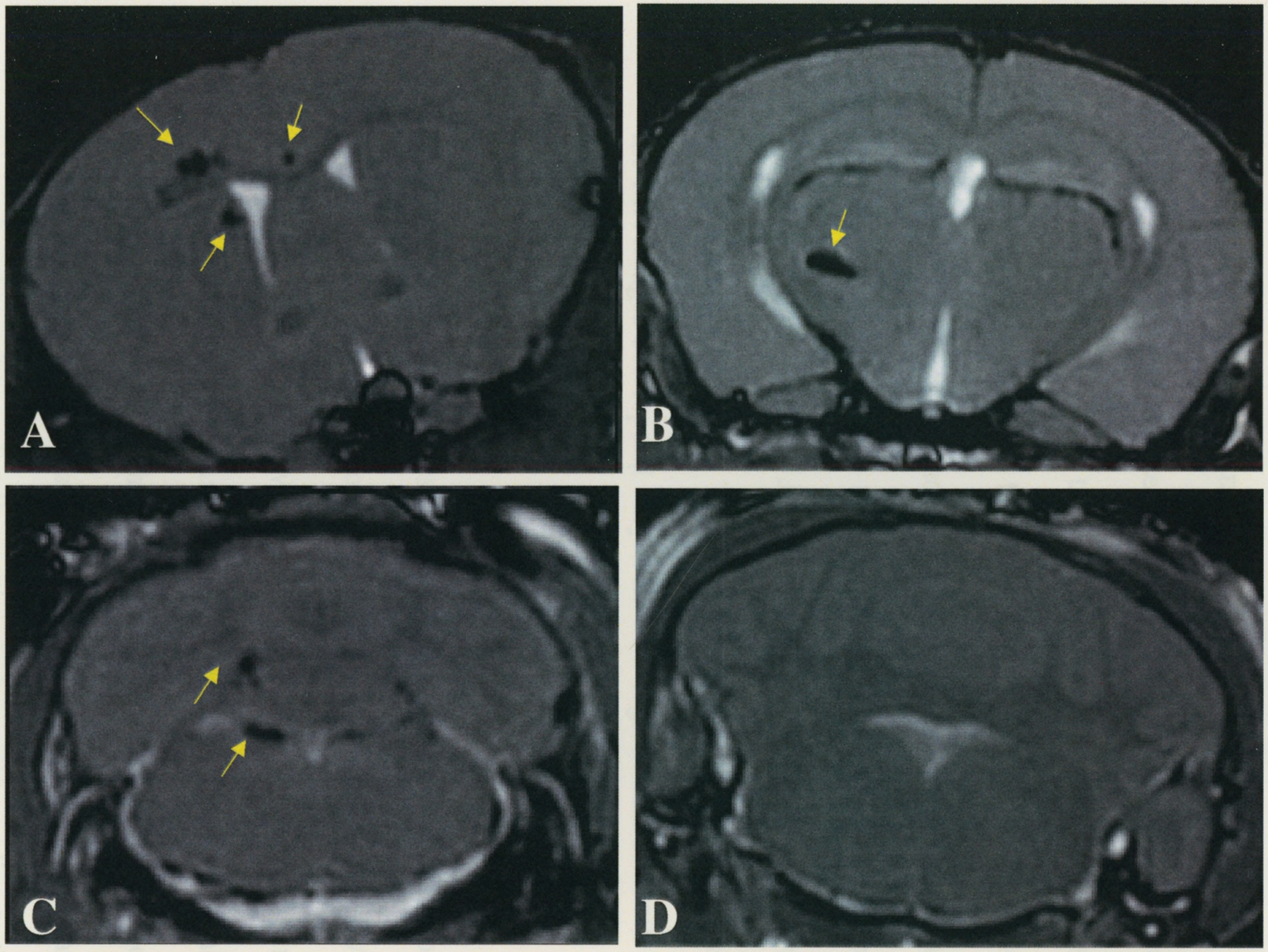


**Figure 2.2:** *In vivo* MR brain images of four Lys-EGFP-ki transgenic mice. (A-C) show brain images of animals induced with EAE and scanned 24 hours post Feridex injection. Arrows indicate regions of signal loss observed through the cerebrum (A), mid-brain (B) and cerebellum (C); (D) shows an MR image of a control non-EAE animal imaged 24 hours post Feridex injection.

Regions of signal loss were observed in the brains of EAE animals imaged over time, at 24, 48 and 72 hours post Feridex®. The appearance of the regions of signal loss was stable over the three imaging days (Figure 2.3).

### 2.3.3 Histopathology and Fluorescence Microscopy

Figure 2.4 shows representative FIESTA images from two EAE animals administered Feridex®, at the level of the midbrain (A) and the cerebellum (B). Regions of signal loss are highlighted in the yellow boxes and shown at higher magnification in 2.4 C and F. Tissue sections were sequentially stained. First sections were stained with the anti-GFP antibody and fluorescence images were collected (Figure 2.4 E,H,J,L). Subsequently, the same sections were stained with PPB (Figure 2.4 D,G,I,K). These results demonstrate that regions of signal loss in the MR images correspond very well with regions that are both PPB positive and GFP positive.

Regions of signal loss observed in MR images were also compared with the presence and distribution of macrophages, examined using F4/80 and anti-GFP antibodies. A representative FIESTA image of a mouse brain, from an EAE animal administered Feridex®, is shown in Figure 2.5A. A focal, peri-ventricular region of signal loss is highlighted in the yellow box and enlarged in 2.5B. Anti-F4/80 reactivity (2.5C) was observed throughout the brain parenchyma (white arrows) and in a denser distribution in an area corresponding to the location of the region of signal loss in the MR image (yellow arrow). Anti-GFP staining (2.5D)

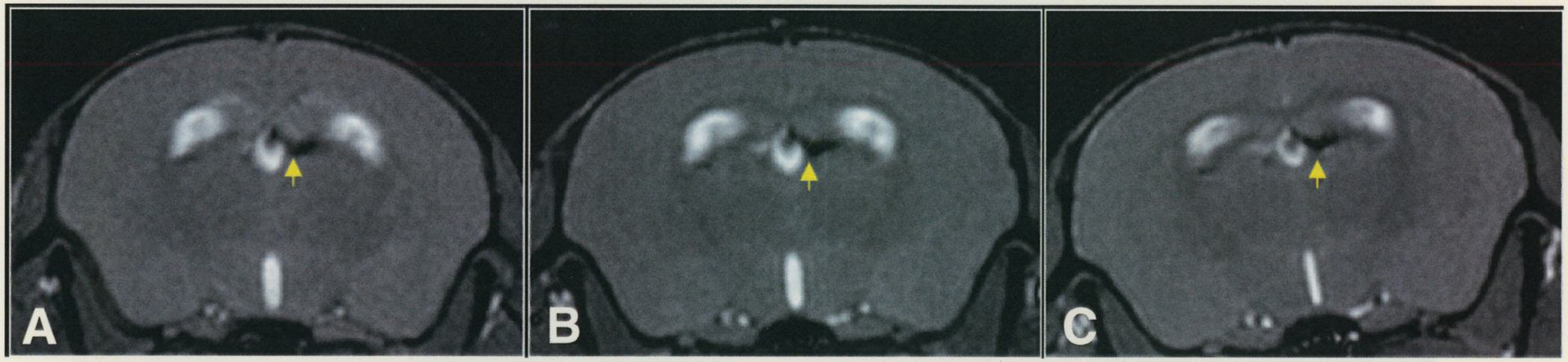


**Figure 2.3**: MR images of the cerebrum region of the brain in an EAE animal scanned at 24 hours (A), 48 hours (B) and 72 hours (C) post Feridex injection. Arrows point to the region of signal loss in the images.

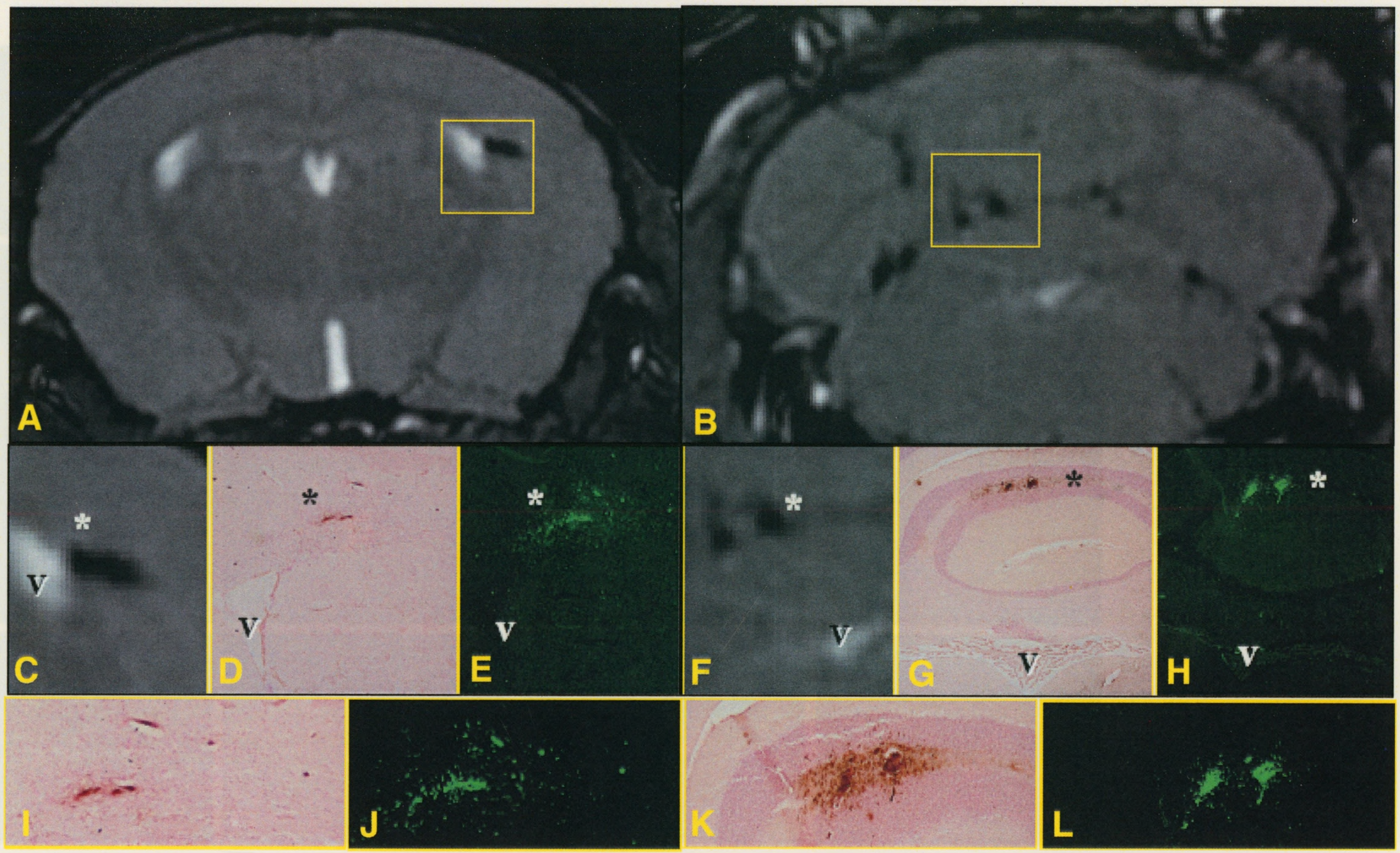


**Figure 2.4:** Correlation of signal loss on MR images to PPB positive and GFP positive histology. Two representative MR images of EAE mouse brains (A,B) show discrete regions of signal loss in the mid-brain and cerebellum. Regions of signal loss are highlighted in the yellow boxes in A and B. The three images below show the region of signal loss (enlarged) alongside the corresponding PPB and GFP stained tissue sections (C,D,E and F,G,H). V= ventricle, * indicates region of inflammation. A higher magnification (x40) of the tissue sections is shown for each example in (I,J) and (K,L) demonstrating excellent correspondence with regions of signal loss.

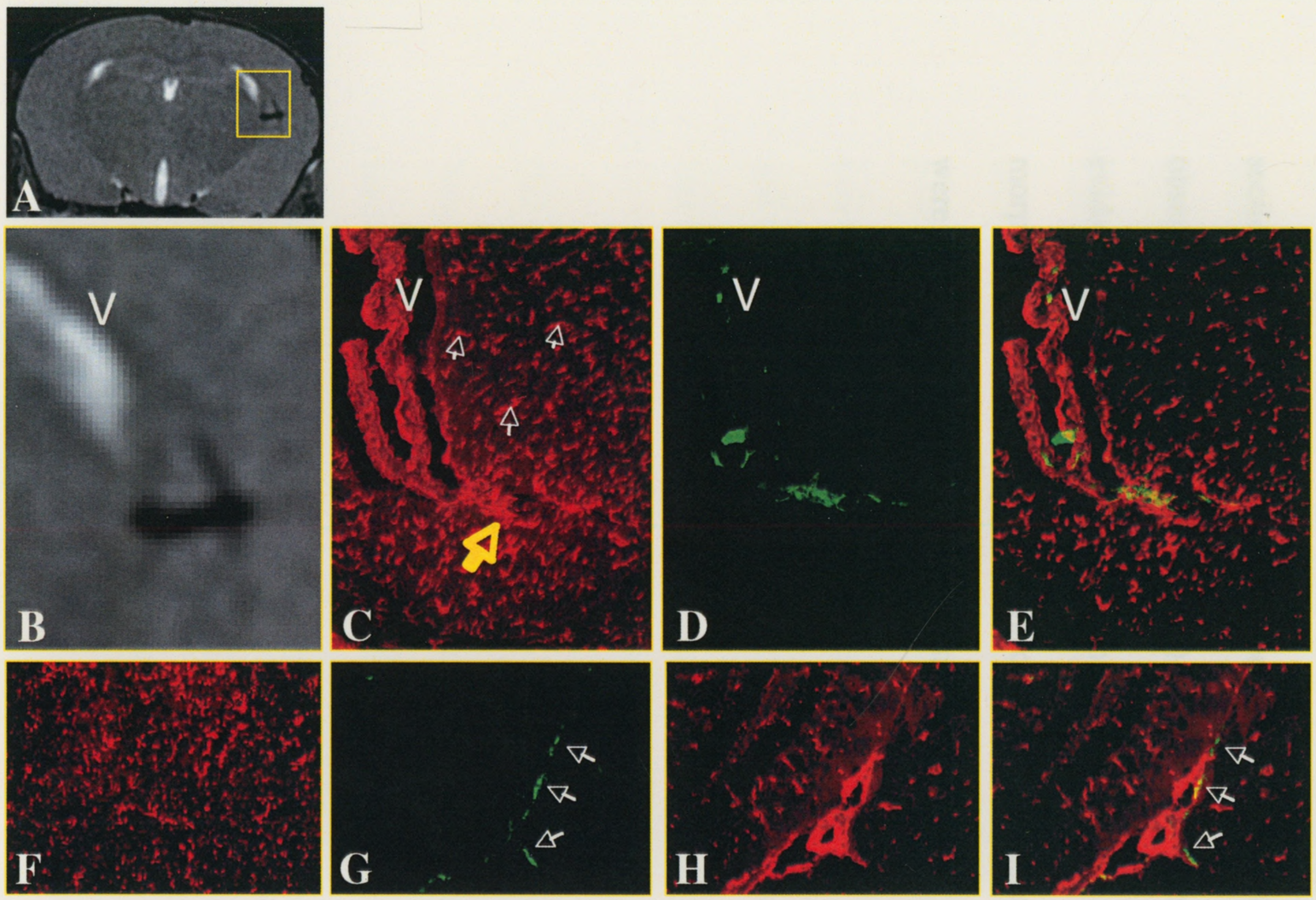


**Figure 2.5**: Correlation of signal loss on MR images with macrophage positive and GFP positive histology. MR Fiesta image (A) shows a peri-ventricular region of signal loss. Corresponding histology section shows macrophage accumulation with F4/80 staining (B) and GFP expression with anti-GFP staining (C). White arrows point to microglia and yellow arrow points to macrophage accumulation in (C). Ventricles are indicated with the letter V. An overlay image shows the overlap of GFP signal with macrophage-positive staining (E). Control sections from non-EAE animals injected with Feridex show microglia positive staining (F) that does not correspond to GFP positive regions. When GFP positive regions are detected (Arrows in G) they are within blood vessels as evident by tomato lectin staining (H,I).

was observed in the same location as the intense anti-F4/80 reactivity as evident by the image overlay in 2.5E, indicating the presence of hematogenous macrophages.

Panels 2.5F-G are control sections. Typical F4/80 reactivity was observed in control mouse brains; speckled pattern corresponding to normal microglia distribution. Regions of more intense F4/80 reactivity were not observed in sections from non-EAE animals injected with Feridex® (2.5F). GFP positive cells observed in non-EAE brains (2.5G) were clearly located along blood vessels as evident by the co-localization using tomato lectin staining (2.5 H,I) and had morphology consistent with perivascular macrophages. No GFP positive regions were observed within the brain parenchyma.

## *2.4 Discussion*

In cellular MRI studies of EAE and other models of neuroinflammation, signal loss has been attributed to the accumulation of infiltrating iron-labeled macrophages. This is because active labeling is based on the assumption that phagocytic cells in the blood during an immune response can be targeted with an i.v. injection of (U)SPIO, and these cells will migrate to the site of inflammation carrying the magnetic label with them. In this paper, we provide the first direct evidence that SPIO-labeled hematogenous macrophages can be identified in the brain after iv administration of Feridex® and that these cells contribute to the regions of signal loss observed in MR images of EAE brain. This was achieved using a novel EAE mouse model in which hematogenous macrophages are GFP positive and microglia are GFP negative. With this unique mouse model we show excellent correspondence between areas in the EAE brain that are PPB positive and GFP positive and we show that these areas can be related to regions of signal loss observed in FIESTA MR images of EAE mouse brains.

Our results do not provide direct evidence that hematogenous macrophages are being labeled in the blood after Feridex® is administered iv; only that macrophages that originate in the periphery are iron-labeled and exist in the CNS lesions in EAE. In EAE, the integrity of the BBB is compromised and it has been suggested that nonspecific SPIO uptake may occur through a leaky BBB. Thus, it is conceivable that cells already present in the CNS at the time of Feridex® administration are being labeled in the CNS by iron particles crossing the BBB

passively. There is however some indirect evidence to support the notion that Feridex® nanoparticles are being taken up by hematogenous macrophages in the blood during inflammation and are not labeled nonspecifically. Muldoon *et al* showed that after BBB disruption by mannitol Feridex® particles passed the capillary endothelial cells but did not cross beyond the basement membrane (40). This finding was in contrast to their finding that smaller USPIO (MION particles) were found intracellularly and extracellularly in the neuropil. Therefore in this study it is unlikely that hematogenous macrophages (or other cells beyond the basement membrane) are labeled by passively diffusing Feridex®.

There is still some question of whether other cells in addition to the hematogenous macrophages are labelled with Feridex® and contribute to the signal loss in the MR images. It is possible that endothelial cells are also iron labelled. Our histology showed that a small number of MR signal voids were observed, that corresponded to PPB positive regions, but could not be matched to GFP positive regions on corresponding fluorescent images; these MR signal voids might represent other GFP-negative cell types that are iron labelled. Alternatively, the lack of perfect correspondence might be attributed to the challenges of correlative imaging including the fact that not every contiguous tissue slice is sectioned and stained and that there is a discrepancy between the slice thickness (MRI = 200 μm, histology = 16 μm).

In conclusion this study demonstrates that regions of signal loss observed in the brains of EAE animals after iv SPIO result from the accumulation of iron labelled hematogenous macrophages in inflammatory lesions. This unique mouse model for EAE will allow us to continue to investigate the role of the hematogenous macrophages in BBB breakdown, lesion formation and disease progression in MS.

## *2.5 References*


1. Ewing C, Bernard CC. Insights into the etiology and pathogenesis of multiple sclerosis. *Immunol Cell Biol* 1998:76: 47-54.
2. Morales Y, Parisi JE, Lucchinetti CF. The pathology of multiple sclerosis: evidence for heterogeneity. *Adv Neurol* 2006:98:27-45.
3. Smith E. Phagocytosis of myelin in demyelinative disease: a review. Neurochem Res 1999:24: 261-268.
4. Petry KG, Boullerne AI, Pousset F, Brochet B, Caille JM, Dousset V. Experimental allergic encephalomyelitis animal models for analyzing features of multiple sclerosis. *Pathol Biol* 2000:48:47-53.
5. Gold R, Hartung HP, Toyka KV. Animal models for autoimmune demyelinating disorders of the nervous system. *Mol Med Today* 2000:6:88-91.
6. Minagar A and Alexander JS. Blood-brain barrier disruption in MS. *Mult Scler* 2003:9: 540-549.
7. Tanaka R, Iwasaki Y and Koprowski H. Ultrastructural studies of perivascular cuffing cells in multiple sclerosis brain. *Am J Pathol* 1975:81:467-478.
8. Bernard CCA, Leydon J, Mackay IR. T cell necessity in the pathogenesis of experimental autoimmune encephalomyelitis in mice. *Eur J Immunol* 1976: 6:655-660.
9. Bruck W, Sommermeier N, Bergmann M, Zettl U, Goebel HH, Kretzschmar HA, Lassmann H. Macrophages in multiple sclerosis. *Immunobiology* 1996:195:588-600.
10. Benveniste EN. Role of macrophages/microglia in MS and EAE. *J Mol Med* 1997:75:165-173.
11. Eng LF, Ghirnikar RS, Lee YL. Inflammation in EAE: role of chemokine/cytokine expression by resident and infiltrating cells. *Neurochem Res* 1996:21: 511-525.
12. Piraino PS, Yednock TA, Freedman SB, Messersmith EK, Pleiss MA, Karlik SJ. Prolonged reversal of chronic experimental allergic encephalomyelitis using a small molecule inhibitor of alpha4 integrin. *J Neuroimmunol* 2002:131:147-59.
13. Huitinga I, van Rooijen N, de Groot CJA, Uitdehaag BMJ, Dijkstra CD. Suppression of experimental allergic encephalomyelitis in lewis rats after elimination of macrophages. *J Exp Med* 1990:172:1025-1033.
14. Kent SJ, Karlik SJ, Cannon C, Hines DK, Yednock TA, Fritz LC, Horner HC. A monoclonal antibody to alpha 4 integrin suppresses and reverses active experimental allergic encephalomyelitis. *J Neuroimmunol* 1995:58:1-10.
15. Polfliet MM, van de Veerdonk F, Dopp EA, van Kesteren-Hendrikx EM, van Rooijen N, Dijkstra CD, van den Berg TK. The role of perivascular and meningeal macrophages in EAE. *J Neuroimmunol* 2002:22:1-8.
16. Hickey WF, Kimura H. Perivascular microglial cells of the CNS are bone marrow derived and present antigen *in vivo*. *Science* 1988:239: 290-292.

17. Smith M. Phagocytic properties of microglia in vitro: implications for a role in MS. *Microsc Res Tach* 2001:54:81-94.
18. Weissleder R, Cheng H-C, Bogdanov A, Bogdanov Jr. A. Magnetically labeled cells can be detected by MR imaging. *J Magn Reson Imag* 1997:7:258-263.
19. Modo M, Hoeh M and Bulte JWM, Cellular MR imaging. *Mol Imag* 2005:4(3):143-164.
20. Pirko I, Ciric B, Johnson AJ, Gamez J, Rodriguez M and Macura S. MRI of immune cells in inflammation of central nervous system. *Croat Med J* 2003:44:463-468.
21. Moore A, Marecos E, Bogdanov A Jr. and Weissleder R. Tumoral distribution of long circulating dextran coated iron oxide nanoparticles in a rodent model. *Radiology* 2000:214: 568-574.
22. Kanno S, Wu YJ, Lee PC, Dodd SJ, Williams M, Griffith BP, Ho C. Macrophage accumulation associated with rat cardiac allograft rejection detected by MRI with USPIO. *Circulation* 2001:104: 934-938.
23. Wadghiri YZ, Sigurdsson EM, Sadowski M, Elliott JI, Li Y, Scholtzova H, Tang CY, Aguinaldo G, Pappolla M, Duff K, Wisniewski T, Turnbull DH. Detection of Alzheimer's amyloid in transgenic mice using magnetic resonance microimaging. *Magn Reson Med* 2003:50:293-302.
24. Dunn EA, Dekaban GA, Weaver LC and Foster PJ. Cellular imaging of inflammation after spinal cord injury. *Mol Imag* 2005:4:1-10.
25. Heyn C, Ronald JA, Mackenzie LT, MacDonald IC, Chambers AF, Rutt BK and Foster PJ. In vivo MRI of single cells in mouse brain with optical validation. *Magn Reson Med* 2006:55:23-29.
26. Lee IH, Bulte JW, Schweinhardt P, Douglas T, Trifunovski A, Hofstetter C, Olson L, Spenger C. *In vivo* magnetic resonance tracking of olfactory ensheathing glia grafted into the rat spinal cord. *Exp Neurol* 2004:187:509-16.
27. Dousset V, Gomez C, Petry KG, Delalande C and Caille JM. Dose and scanning delay using USPIO for central nervous system macrophage imaging. *MAGMA* 1999:8:185-189.
28. Dousset V, Delalande C, Ballarino L, Quesson B, Seilhan D, Coussemacq M, Thiaudiere E, Brochet B, Canioni P, Caille JM. *In vivo* macrophage activity imaging in the central nervous system detected by magnetic resonance. *Magn Reson Med* 1999:41: 329-333.
29. Anderson SA, Shukaliak-Quandt J, Jordan EK, Arbab AS, Martin R, McFarland H, Frank JA. MRI of labeled T-cells in a mouse model of multiple sclerosis. *Ann Neurol* 2004:55:654-659.
30. Rausch M, Hiestad P, Baumann D, Cannet C and Rudin M. MRI-based monitoring of inflammation and tissue damage in acute and chronic relapsing EAE. *Magn Reson Med* 2003:50:309-314.
31. Xu S, Jordan EK, Brocke S, Bulte JW, Quigley L, Tresser N, Ostuni JL, Yang Y, McFarland HF, Frank JA. Study of relapsing remitting experimental allergic encephalomyelitis SJL mouse model using MION-

46L enhanced in vivo MRI: early histopathological correlation. *J Neurosci Res* 1998:52:549-558.

32. Wang YXJ, Hussain SM, Krestin GP. Superparamagnetic iron oxide contrast agents: physicochemical characteristics and applications in MR imaging. *Eur Radiol* 2001:11:2319-2331.
33. Oweida AJ, Dunn EA and Foster PJ. Cellular imaging at 1.5T: detecting cells in neuroinflammation using active labeling with superparamagnetic iron oxide. *Mol Imag* 2004:3:85-95.
34. Dousset V, Brochet B, Deloire MSA, Lagoarde L, Barroso B, Caille J-M, Petry KG. MR imaging of relapsing multiple sclerosis patients using ultra-small-particle iron oxide and compared with Gadolinium. *Am J Neuroradiol* 2006:27:1000-5.
35. Faust N, Varas F, Kelly LM, Heck S, Graf T. Insertion of enhanced green fluorescent protein into the lysozyme gene creates mice with green fluorescent granulocytes and macrophages. *Blood* 2000:96:719-26.
36. Costa O, Divoux D, Ischenko A, Tron F, Fontaine M. Optimization of an animal model of experimental autoimmune encephalomyelitis achieved with a multiple MOG35-55 peptide in C57BL6/J strain of mice. *J Autoimmunity* 2003:20:51-61.
37. Tran EH, Kuziel WA, Owens T. Induction of experimental autoimmune encephalomyelitis in C57BL/6 mice deficient in either the chemokine macrophage inflammatory protein-1a or its CCR5 receptor. *Eur J Immunol* 2000:30:1410-1415.
38. Foster-Gareau PJ, Heyn C, Alejski A and Rutt BK. Imaging single mammalian cells with a 1.5T clinical MRI scanner. *Magn Reson Med* 2003:49:968-971.
39. Heyn C, Bowen CV, Rutt BK and Foster PJ. Detection threshold for single SPIO labeled cells with FIESTA. *Magn Reson Med* 2005:53:312-20.
40. Muldoon LL, Pagel MA, Kroll RA, Roman-Goldstein S, Jones RS, Neuwalt EA. A physiological barrier distal to the anatomical blood-brain-barrier in a model of transvascular delivery. *Am J Neuroradiol* 1999:20: 217-222.

# Chapter 3

# Cellular Imaging of Neuroinflammation in Macrophage-Depleted EAE Animals

## *3.1 Introduction*

Macrophages play an important role in the clinical manifestation of EAE. The ability to track macrophages *in vivo* will allow for better assessment of the inflammatory phase in multiple sclerosis and better evaluation of therapies directed at blocking macrophage infiltration into the CNS. Cellular MRI with SPIO has shown considerable potential as a marker of macrophages in inflammatory disease. In previous work shown in chapter 1, I demonstrated the ability to detect inflammatory regions on MR images in the CNS of rats induced with acute EAE. The inflammatory regions were detected as areas of ED1 positive staining, which stains for hematogenous macrophages and microglia (Appendix I). In chapter 2, experiments were performed on a novel transgenic mouse in which the hematogenous macrophages express GFP and the microglia do not. The results of chapter 2 demonstrated that regions of signal loss on MRI due to SPIO are largely attributed to the hematogenous macrophage population. Another method of addressing the involvement of hematogenous macrophages in the uptake of SPIO is to deplete the hematogenous macrophage population and study the changes in signal loss in the brains of macrophage-depleted animals after SPIO injection.

Clodronate liposomes (CL) contain the drug dichloromethylene diphosphonate ($CL_2MDP$), which is commonly used to eliminate macrophages (1). $CL_2MDP$-containing liposomes are ingested by macrophages, and high concentrations of intracellularly released $CL_2MDP$ kill the cell (1). When injected systemically, CL eliminates almost all phagocytosing macrophages in the spleen and liver (2). The method has multiple applications and has been used to study: lymphocyte migration in the spleen in the absence of macrophages (3), macrophage subset repopulation in the spleen or rats and mice (4,5), functions of lung macrophages (6), and the role of macrophages infiltrating into inflammatory tissue (7). CL also effectively eliminates circulating hematogenous macrophage populations (9) and has been used to study the inflammatory response in EAE in the absence of circulating hematogenous macrophages (10).

The work described in this chapter is from a pilot study designed to provide additional information about the cells involved in SPIO uptake in EAE and their contribution to the MR signal loss. In this study I used the acute EAE rat model (previously studied, paper in Appendix I) and a method for depleting hematogenous macrophages. The hypothesis for this experiment was: if hematogenous macrophages are depleted then regions of signal loss in MR images would be decreased.

## *3.2 Methods*

### 3.2.1 EAE Induction

EAE was induced in 8-week old female Lewis rats by a single injection of whole Hartley guinea pig CNS homogenate in complete Freund's adjuvant (CFA) and inactivated H37Ra MTB. Immunization was performed by intradermal inoculation of 0.1 ml in the footpad of each hind leg under general anesthesia. All animals were kept in individual cages with standard conditions of light and free access to water and food.

The clinical signs of EAE began approximately 12 days post immunization. Animals were weighed and scored daily for the clinical features of EAE according to the following scale: 0 = normal healthy animal, 0.5 = two consecutive days of weight loss (>20g), 1 = loss of tail tonus, 2 = hind limb weakness, 3 = complete hind limb paralysis, 4 = complete paralysis, incontinence, and moribund conditions. Scoring began the day after immunization. Day 0 was considered the day on which inoculation of EAE occurred.

### 3.2.2 Clodronate Liposome Treatment Experiment

EAE was induced in two groups of animals: CL-treated group (group I, n=9) and saline treated group (group II, n=9). Control animals consisted of non-EAE animals administered CL (n=4) or saline (n=4). At 8 and 10 days post immunization (dpi) rats in Group I were administered clodronate loaded liposomes iv, (0.25g/ml) (VU Medical Centre) and rats in Group II were

administered saline iv. Liposome encapsulated clodronate induces the selective apoptotic death of monocytes and macrophages. Depletion occurs rapidly and without directly affecting other peripheral leukocytes. A single iv injection of CL in rats results in the elimination of macrophages in bone marrow, spleen and liver within 2 days. This technique has been used previously by Huitinga *et al* who showed that effective macrophage depletion was attained 2 days after the first i.v. injection of CL (9).

### 3.2.3 Imaging

All rats were administered the SPIO, Feridex® (Advanced Magnetic Industries), (22.4 mg Fe/kg) i.v. when hindlimb weakness was observed, which occurred at 12-14 days post inoculation in all animals. Animals were sacrificed 24 hours after Feridex® administration and the brain, liver and spleen were removed and prepared for *ex vivo* imaging. Imaging was performed at 1.5T using a customized microimaging protocol, which consisted of a high-powered gradient coil insert as described in section 1.3.1 and a custom built solenoid RF coil. Images were obtained using 3DFIESTA with TR/TE 10/5ms, 30 flip angle, 21 kHz bandwidth, 100 micron in-plane spatial resolution, 200 micron slice thickness, 8 signal averages, 20 minute scan time. The imaging protocol was optimized previously in experiments performed during my 4$^{th}$ year thesis work (Appendix I).

### 3.2.4 Histopathological Analysis

#### 3.2.4.1 Brain Histology

After imaging, the specimens were prepared for histopathological analysis. Specimens were embedded in paraffin in such a manner that 8 $\mu$m sections could be cut from the block. Sections were stained with hematoxylin and eosin (H & E) to assess the cellular infiltrate. Contiguous sections were stained with DAB-enhanced Perl's Prussian Blue (PPB) counterstained with Nuclear Fast Red to demonstrate iron uptake and immunolabeled with mouse anti-rat ED1 (also known as anti-CD68). The monoclonal antibody (mAb) ED1 is widely used as a marker for rat macrophages. The ED1 antigen is expressed on lysosomal membranes, and weakly on the cell surface of myeloid cells. The ED1 antigen is expressed by the majority of tissue macrophages and weakly by peripheral blood granulocytes. ED1 (1:300) was applied to sections overnight in a humidified chamber at 40$^0$C after blocking with 5% normal goat serum (NGS), and 0.3% H2O2 in PBS. Sections were rinsed with PBS-Tween 20 (3x), after which a biotinylated goat anti-mouse (H+L) IgG secondary antibody was applied (1:500) for 2.5 hours at room temperature. Sections were washed again with PBS-Tween 20, treated with extravadin-peroxidase (1:500, 3 hours) (Sigma) and finally a DAB solution. Sections were counterstained with hematoxylin. Sections were dehydrated through ascending alcohols, cleared in xylene, and cover slipped with Cytoseal-60 (VWR International). Histopathological and MR images were matched by locating corresponding landmarks.

### 3.2.4.2 Liver and Spleen Histology

Liver and spleen sections were cut and stained for iron using PPB and macrophages using the monoclonal ED1 antibody. The PPB staining protocol was the same as that implemented for the brain sections (see above). The ED1 protocol was similar with the following exceptions: Peroxide block was comprised of 1%$H_2O_2$ in 1x PBS (1X=1%) for 1 hr 35 minutes and the protein block was comprised of 6% NGS (normal goat serum) in 1x PBS with 0.3%Triton X (detergent) for 2 hours.

## 3.2.5 Flow Cytometry Experiment

In a separate experiment, flow-assisted cytometry (FACS) was performed to assess the degree of depletion of hMac in the blood circulation. First, 0.2ml blood samples were obtained through the tail vein of each animal. For all staining protocols, cells were stained in 5ml polystyrene round-bottom tubes (BD Falcon). All samples were blocked by incubating in PBS containing 10.8 mg/ml mouse IgG for 15 minutes on ice. Samples were stained with the following primary or isotype control antibodies (BD Pharmingen): PE-conjugated RP-1 mouse anti-rat granulocytes mAb, R-PE-conjugated mouse $IgG_{2a,k}$ isotype control, FITC-conjugated anti-rat CD11b (integrin $\alpha_M$ chain, Mac-1 $\alpha$ chain) mAb, FITC-conjugated mouse IgA isotype control, PE-Cy5-conjugated mouse anti-rat CD45 (leukocyte common antigen) mAb, PE-Cy5-conjugated mouse $IgG_1$ isotype control. Peripheral blood monocytes were isolated by lysis of red blood cells using ammonium chloride lysing reagent (BD Pharmingen). Tubes were mixed

and placed on ice for 5 min. Samples were centrifuged at 500g for 5 min. Cells were pelleted and the supernatants removed by an inverted flick of the tube. Samples were kept on ice until reading. All FACS analysis was performed using a BD Calibur with 488nm laser and Flowjo software. The side-scatter plot and CD45 stain were used to select for leucocytes. Macrophages were selected from the CD45-positive population based on positive expression for CD11b and negative expression for RP-1.

Animals were divided into saline-treated and CL-treated groups with 6 animals in each group. Blood samples were collected from all animals on day 7 post-immunization and FACS analysis was performed to obtain the baseline level of macrophages prior to injection of CL or saline. CL or saline was injected iv on days 8 and 10 post immunization. Blood samples for FACS analysis were obtained from the saline-treated group on day 12 and from the CL-treated group on day 13. After obtaining the blood samples, the animals were injected with Feridex® i.v. and sacrificed 24 hours later. The brain, liver and spleen were excised for imaging and histological analysis. FACS was performed on the blood samples to obtain a measure of the number of macrophages after treatment.

## *3.3 Results*

In both the saline-treated EAE group and the CL-treated EAE group all animals developed clinical signs of EAE ranging in score from 0.5-3.5. The onset of clinical signs occurred between days 12-14 post-immunization in both groups. Table 3.1 summarizes the data for each group of animals. The mean score for CL-treated EAE animals was 1.56 (SD=1.33) and for saline-treated EAE animals 1.94 (SD=0.98). No statistically significant difference was found between the saline-treated EAE group and the CL-treated EAE group ($P = 0.05$, t-test).

### 3.3.1 MRI

The imaging results from this experiment were unexpected. Depletion of blood-derived macrophages, prior to the administration of the cellular imaging label Feridex®, did not inhibit the observation of signal loss as hypothesized. In fact, the extent of signal loss observed in CL treated rats was considerably greater than for saline treated rat (figure 3.1). The signal loss observed in the brains of saline treated EAE rats was very similar to that observed in our earlier cellular MRI studies (8); signal loss was sparse and only observed in the brainstem and medulla (figure 3.1 C,D) with minimal or no signal loss observed in the cerebrum or the midbrain (figure 3.1 A,B). In brains from CL-treated EAE rats, prominent regions of signal loss were observed throughout the brain in various locations including the cerebrum, midbrain, brainstem, medulla and cerebellum (figure 3.1 E,F,G,H).

**Table 3.1:** Comparison of clinical scores in saline-treated and CL-treated EAE animals. No significant difference could be established between the two groups using the t-test ($P = 0.05$).

| CL-Treated EAE | | Saline-Treated EAE | |
|---|---|---|---|
| **Animal** | **Score** | **Animal** | **Score** |
| 1 | 0.50 | 1 | 3.00 |
| 2 | 0.50 | 2 | 3.00 |
| 3 | 0.50 | 3 | 2.00 |
| 4 | 0.50 | 4 | 2.00 |
| 5 | 3.50 | 5 | 3.00 |
| 6 | 0.50 | 6 | 2.00 |
| 7 | 2.50 | 7 | 1.50 |
| 8 | 3.50 | 8 | 0.50 |
| 9 | 2.00 | 9 | 0.50 |

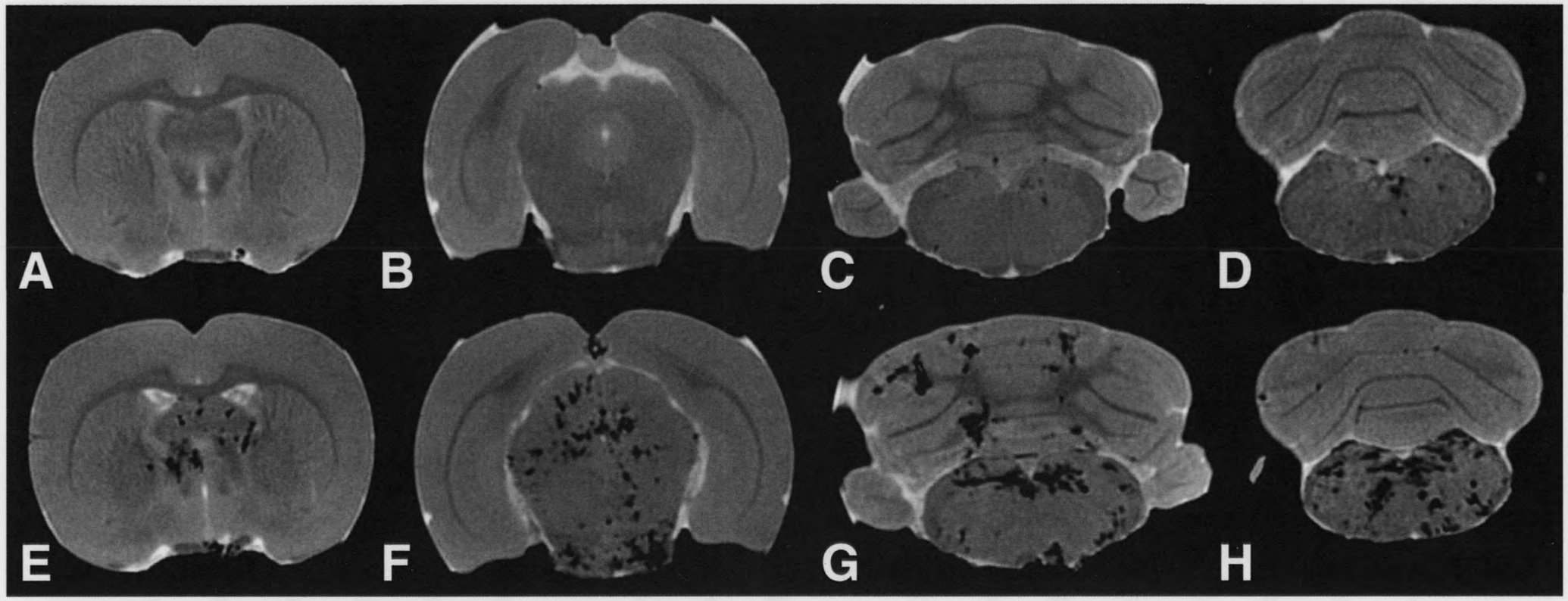


**Figure 3.1:** 3DFIESTA images of EAE rat brain (100x100x200 microns), 24 hrs after *in vivo* iv administration of Feridex. **Top row:** control EAE rat brain showing discrete regions of signal loss mainly in the brainstem region of the hind brain (C,D); No regions of signal loss could be observed in the cerebrum (A) or the midbrain (B). **Bottom row:** brain images of EAE rat brain treated with CL to deplete hematogenous macrophages; Regions of signal loss are observed throughout the brain including the cerebrum (A), midbrain (B) and hindbrain (G,H).

### 3.3.2 Extent of Depletion

FACS analysis showed that the administration of CL reduced the macrophage populations in the circulation prior to Feridex® administration in all animals. Figure 3.2 shows the mean number of macrophage populations for all animals before and after CL treatment. Table 3.2 shows the population level of macrophages prior-to and after the injection of saline or CL. In the CL-treated EAE group a drastic reduction in the macrophage population is observed in the animals after treatment with CL. The degree of depletion varied from 45% to 99%. No relationship could be established between the degree of depletion and the expression of clinical symptoms or the extent of signal loss in MR images. In the saline-treated EAE group, similar macrophage populations were observed to those in the CL-treated group prior to treatment. However, macrophage populations in the saline-treated EAE group increased slightly after administration of saline due to a natural increase in the number of immune cells throughout the EAE disease course. Figure 3.3 shows the flow cytometry profile in a dot plot for one representative EAE animal before and after CL treatment. In the RP1+/CD11b+ quadrant the population of neutrophils detected is affected by the CL treatment. Prior to CL administration the neutrophil population is RP1+/CD11b+, however after CL treatment the neutrophil population is RP1+/CD11b-. In the RP1-/CD11b+ quadrant, the macrophage population is largely eliminated after CL treatment.

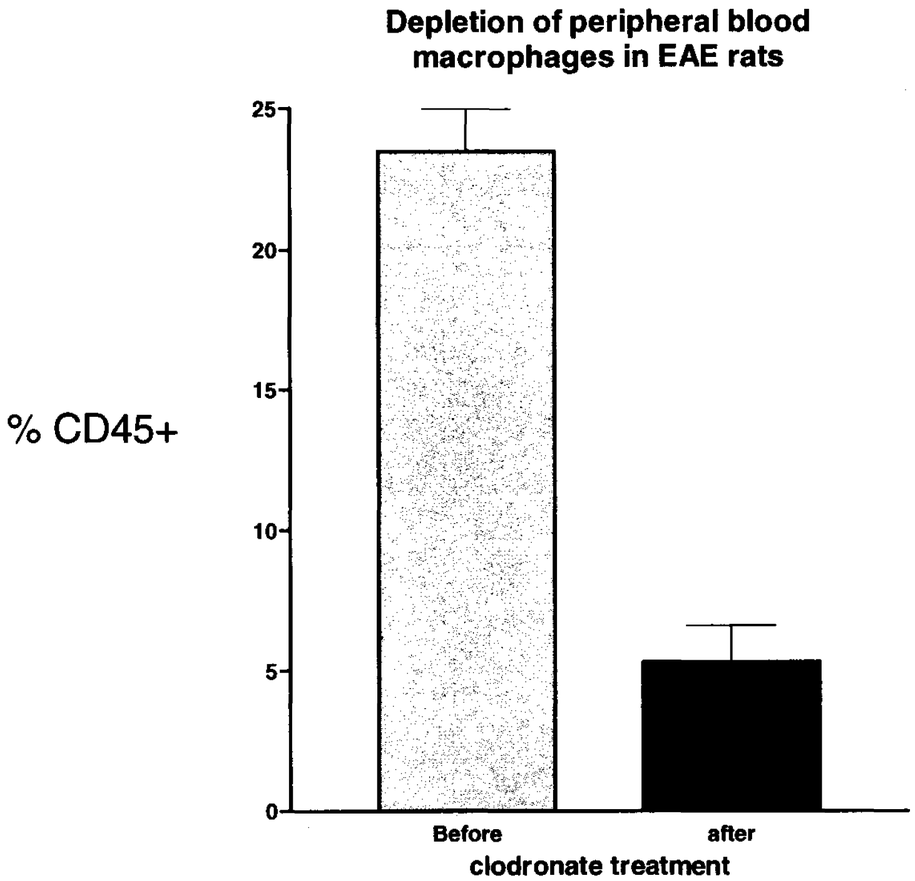


**Figure 3.2:** Comparison of the mean macrophage populations (% of CD45+ cells) before and after CL treatment in EAE rats. CL treatment dramatically reduces the percent of CD45+ cells, which are identified as macrophages (N = 7).

**Table 3.2:** Comparison of macrophage levels (% of CD45+) between EAE animals treated with CL and EAE animals treated with saline.

| CL-treated | | | |
|---|---|---|---|
| **Animal** | **Pre** | **Post** | **% Change** |
| 1 | 21.22 | 5.83 | -72.53 |
| 2 | 28.53 | 10.06 | -64.74 |
| 3 | 11.67 | 5.34 | -54.24 |
| 4 | 24.91 | 2.98 | -88.04 |
| 5 | 19.30 | 10.45 | -45.85 |
| 6 | 24.83 | 0.20 | -99.19 |

| Saline-treated | | | |
|---|---|---|---|
| **Animal** | **Pre** | **Post** | **% Change** |
| 1 | 20.96 | 25.64 | 22.33 |
| 2 | 37.97 | 47.95 | 26.28 |
| 3 | 33.01 | 43.85 | 32.84 |
| 4 | 53.00 | 59.00 | 11.32 |
| 5 | 27.52 | 47.59 | 72.93 |
| 6 | 24.38 | 27.42 | 12.47 |

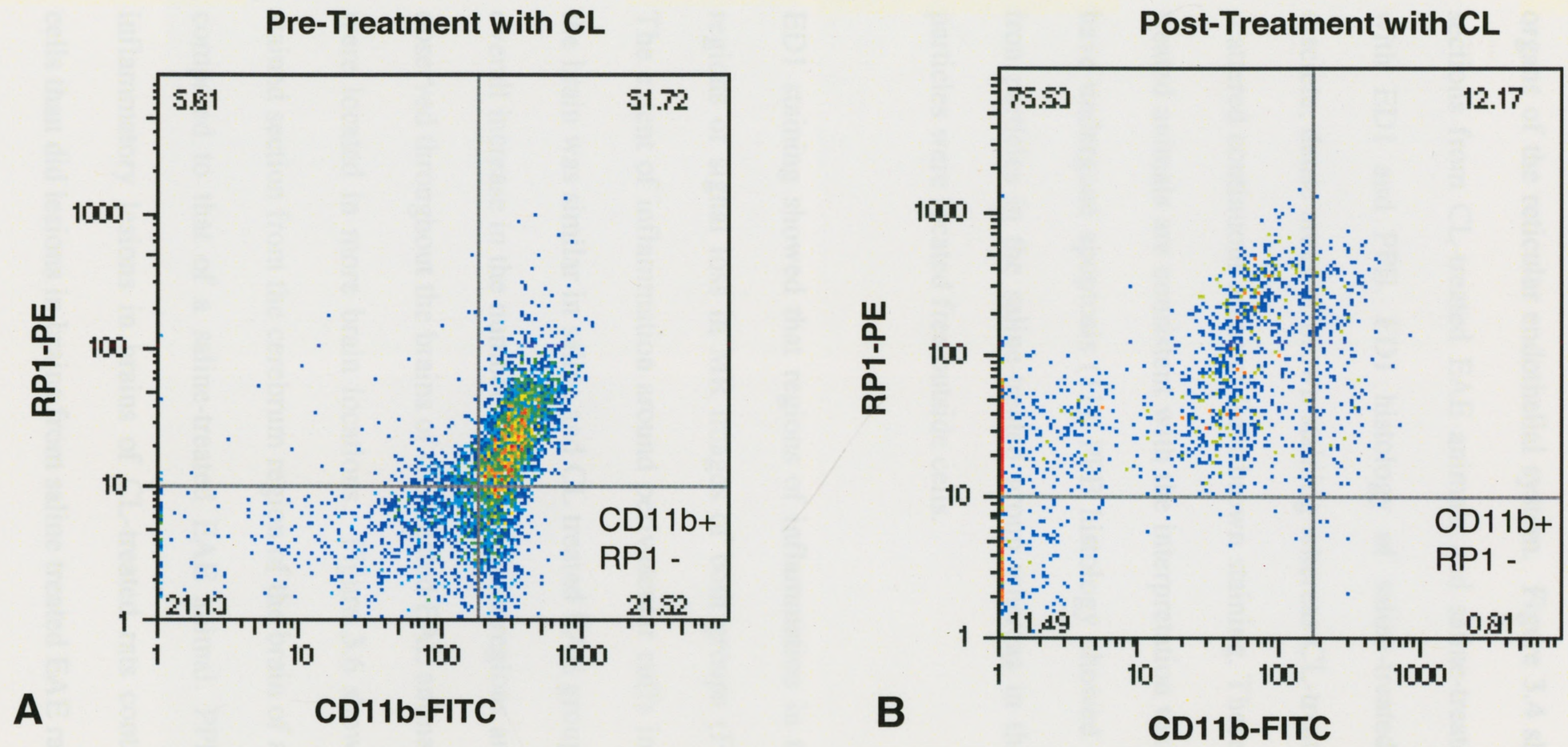


**Figure 3.3:** Flow cytometry data for a representative EAE animal prior to (A) and after (B) treatment with CL. All cells were gated for CD45. Quadrants were set according to staining with isotype-matched control mAbs. The bottom right quadrant represents the population of cells expressing CD11b, but not RP1. A drastic reduction of cells in the bottom right quadrant indicates effective elimination of macrophages after CL treatment.

### 3.3.3 Histology

Liver and spleen histology confirmed the depletion of macrophage populations in organs of the reticular endothelial system. Figure 3.4 shows representative liver sections from CL-treated EAE animals and saline-treated EAE animals stained with ED1 and PPB. ED1 histology of saline-treated EAE animals showed discrete, dense areas of brown staining whereas CL-treated EAE animals showed scattered continuous areas of light brown staining. These observations in the CL-treated animals are consistent with the interpretation that they are dead cells that have undergone apoptosis (11). PPB histology showed compartmentalization of iron particles in the saline-treated group whereas in the CL-treated group iron particles were located free outside cells.

ED1 staining showed that regions of inflammation in the brain correlated with regions of signal loss in MR images of both groups (Figure 3.5 A,B and E,F). The extent of inflammation around perivascular cuffs in the brainstem region of the brain was similar in saline and CL treated EAE groups (Figure 3.5 C, G). An overall increase in the number of ED1 positive regions and perivascular cuffs was observed throughout the brains of CL-treated EAE animals. ED1 positive regions were located in more brain locations. Figure 3.6 shows a representative ED1-stained section from the cerebrum region of the brain of a CL-treated EAE animal compared to that of a saline-treated EAE animal. PPB staining revealed that inflammatory lesions in brains of CL-treated rats contained more iron labeled cells than did lesions in brains from saline treated EAE rats (Figure 3.5 D,H).

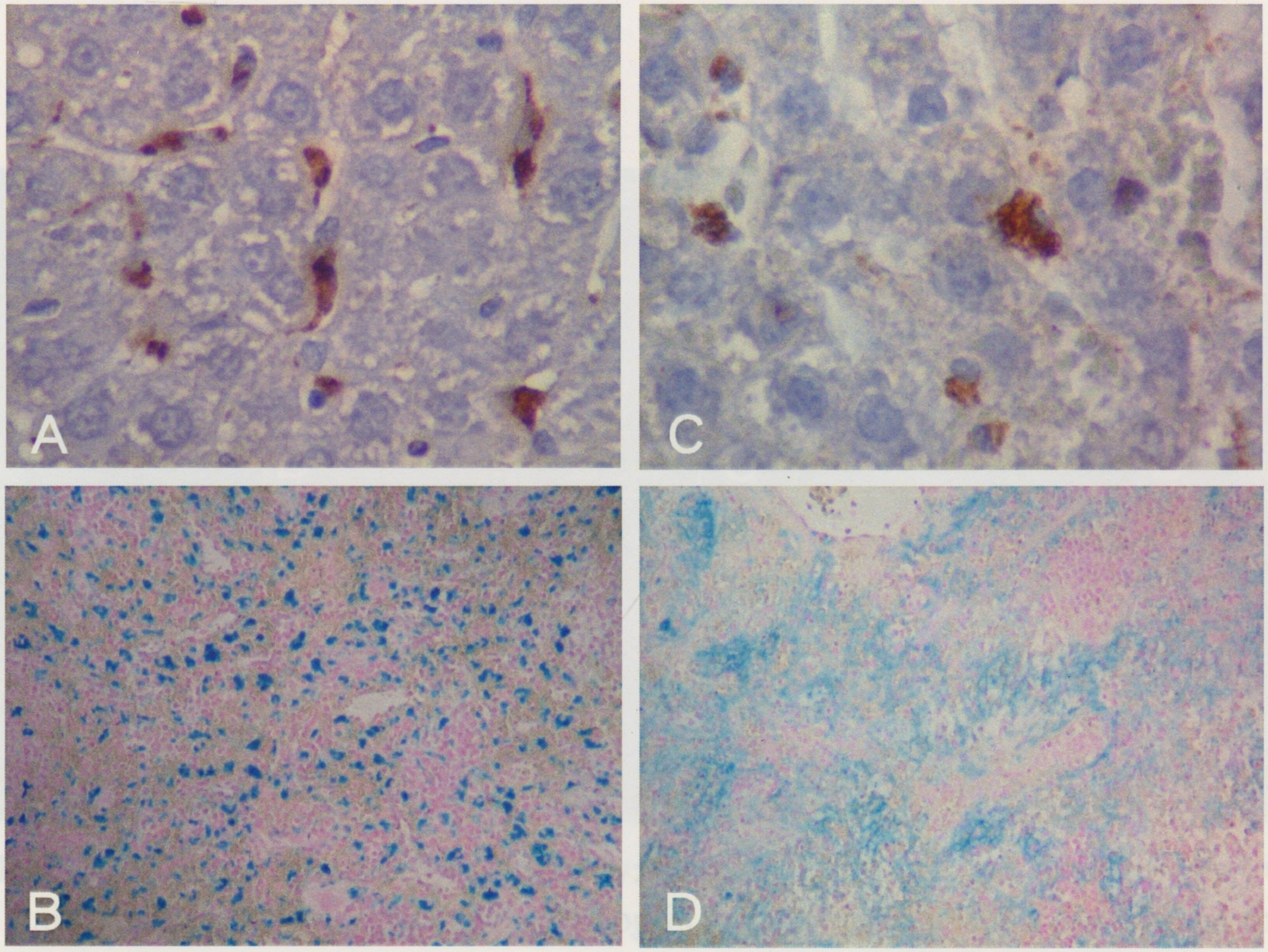


**Figure 3.4:** Representative liver sections from saline-treated EAE animals (A,B) and EAE animals treated with CL (C,D). ED1 staining (A) and PPB staining (B) is intracellular and localized in saline-treated EAE animals and is sparse and extracellular in CL treated EAE animals (C,D). Magnification x40 in (A,C) and x10 in (B,D).

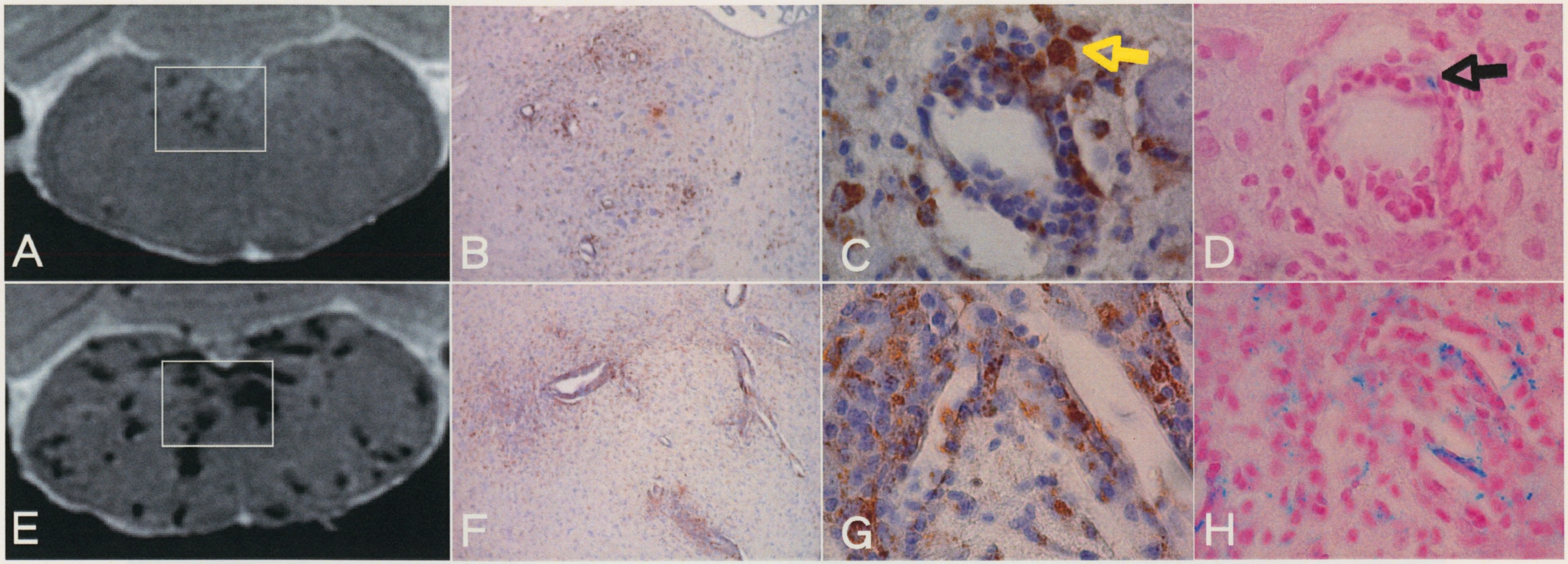


**Figure 3.5:** MR and histology comparison. Top row: control EAE rat brain. Bottom row: CL-treated EAE rat brain. ED1 stains monocytes/macrophages/microglia (yellow arrow in C) and shows that the degree of inflammation in both groups is similar (B,F) magnification x10 and (C,G) magnification x100. PPB stains iron (black arrow in D). Many more ED1+ cells are also PPB+ in CL-treated EAE rat brains (H) relative to saline-treated EAE rat brains (D) magnification x100. PPB+ cells are mainly perivascular. Stained tissue sections are 8 microns; MR is 200 microns slice thickness.

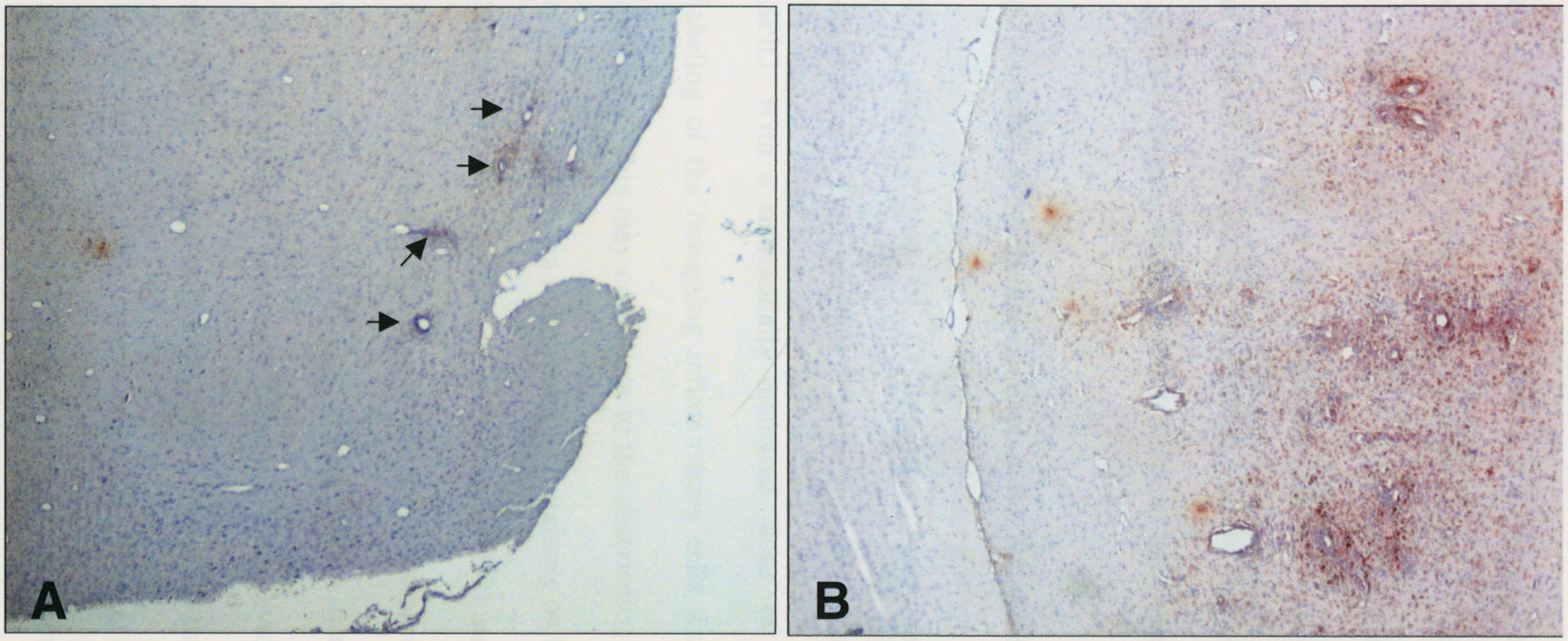


**Figure 3.6:** Histological brain section of a saline-treated (A) and CL-treated (B) EAE rat using the macrophage marker ED1. Only few macrophage intense regions (brown) are observed in saline-treated EAE animals (black arrows in A). Many more macrophages are found in CL-treated EAE animals (brown staining in B). Sections are taken from similar locations in the cerebrum region of the brain. Magnification x10.

## *3.4 Discussion*

Depletion of hematogenous macrophages in EAE-induced Lewis rats using CL prior to iv injection of Feridex® did not eliminate nor reduce the appearance of regions of signal loss on MR images. On the contrary, a drastic increase in the number and distribution of the regions of signal loss was observed. The increase in signal loss on MR images corresponded to an increase in inflammation, as evident by ED1 staining, in the brains of macrophage depleted EAE animals.

There are a number of points that can explain our unexpected findings:

1. The administration of CL depletes macrophages of the reticular endothelial system, which will cause an increase in the circulating level of SPIO. With a substantially increased 'dose' of Feridex®, the *in vivo* labeling of the remaining inflammatory cells would be expected to be enhanced. This may contribute to the observation of an increased degree of signal loss in brain images and PPB staining on histology.
2. The degree of inflammation, as evident by ED1 staining, was increased in CL treated animals. This may contribute to the observation of an increased degree and spatial extent of signal loss in brain images.
3. The observation of increased inflammation, as evident by ED1 staining, is difficult to understand, especially in view of the fact that the clinical symptoms of EAE were not substantially different in the CL treated versus saline treated animals. There is one report of macrophage depletion using

mannoyslated-CL in EAE mice which suggests that other immune cells may be upregulated in response to depletion (10).

4. It is possible that since the degree of depletion varies from animal to animal and since the time period between CL injection and Feridex® injection may have allowed for repopulation of monocytes from the bone marrow, hematogenous macrophages/monocytes have the potential to take up large amounts of SPIO and infiltrate the CNS carrying the label with them.
5. Other cell populations maybe involved in the uptake of SPIO. For example, endothelial cells lining blood vessels can become activated during an inflammatory response and have the potential to take up SPIO through various mechanisms. Weissleder *et al* demonstrated that USPIOs transmigrate the capillary wall by means of vesicular transport and through interendothelial junctions (11).

The results of this pilot experiment are interesting and have stimulated a number of new, important research questions. These new directions and additional possibilities for future work in this area are described next in Chapter 4.

## *3.5 References*


1. Van Rooijen N. The Liposome-mediated macrophage suicide technique. *J Immunol Methods*. 1989; 124:1-7.
2. Van Rooijen N, Niewuwmegen RV. Elimination of phagocytic cells in the spleen after intravenous injection of liposome-encapsulated dichloromethylene diphosphonate: An enzyme-histochemical study. *Cell Tissue Res*. 1984;238:355-8.
3. Kraal G, Rodriques H, Hoeben K, Van Rooijen N. Lymphocyte migration in the spleen: The effect of macrophage elimination. *Immunology*. 1989; 68:227-32.
4. Van Rooijen N, Kors N, Raal G. Macrophage subset repopulation in the spleen: differential kinetics after liposome-mediated elimination. J *Leukocyte Biol*. 1989; 45:97-
5. Van Rooijen N, Kors N, Ende MVD, Dijkstra CD. Depletion and repopulation of macrophages in spleen and liver of rat after intravenous treatment with liposome-encapsulated dichloromethylene diphosphonate. *Cell Tissue Res*. 1990; 260:215-22
6. Thepen T, Van Rooijen N, Kraal G. Alveolar macrophage elimination *in vivo* is associated with an increase in pulmonary immune response in mice. *J Exp Med*. 1989; 170:499-509.
7. Huitinga I, van Rooijen N, de Groot CJA, Uitdehaag BMJ, Dijkstra CD. Suppression of experimental allergic encephalomyelitis in Lewis rats after elimination of macrophages. *J Exp Med*. 1990; 172, 1025–1033.
8. Oweida AJ, Dunn E, Foster PJ. Cellular imaging at 1.5T: Detecting cells in neuroinflammation using active labeling with superparamagnetic iron oxide. *Molecular Imaging*. 2004; 3(2):85-95
9. Huitinga, I, Damoiseaux JGMC, van Rooijen N, Do¨pp EA, Dijkstra CD. Liposome mediated affection of monocytes. *Immunobiology*. 1992;185:11-19.
10. Tran EH, Hoekstra K, van Rooijen N, Dijkstra CD, Owens T. Immune invasion of the central nervous system parenchyma and experimental allergic encephalomyelitis, but not leukocyte extravasation from blood, are prevented in macrophage-depleted mice. *The J Immunol*. 1998; 161:3767-75.
11. Weissleder R, Elizondo G, Wittenberg J, Rabito CA, Bengele HH, Josephson L. Ultrasmall superparamagnetic iron oxide: Characterization of a new class of contrast agents for MR imaging. *Radiology*. 1990; 175: 489–493.

# Chapter 4

# Conclusion and Future Work

## *4.1 Future Work*

### 4.1.1 *In vivo* longitudinal monitoring of EAE using cellular MRI

Currently, Gad-enhanced MRI is the most common tool for diagnosis and monitoring of MS lesions and assessing brain inflammation. However, the simple movement of Gad across a transiently broken BBB does not provide insight on the cellular components of inflammation (1). In chapter 2 it was shown that SPIO-MRI can be used to label macrophages *in vivo* during active inflammation and to detect the label in the CNS using MRI. In previous work, I demonstrated that regions of signal loss on MRI correspond to regions of inflammation on histology as evident by ED1 staining for macrophages (Appendix I). The next logical step is to use SPIO-cellular MRI to follow the course of EAE over time and to observe pathological changes that may occur with and without the use of targeted treatments. Such study will have to compare how the dynamics of the regions of signal loss on MRI change over time after a single iv injection of SPIO and after multiple injections. Determining whether a region of signal loss changes over the course of EAE and whether multiple SPIO injections allow for increased detection of regions of signal loss are all important questions to consider when performing a longitudinal study using SPIO-cellular MRI.

### 4.1.2 Macrophage Depletion

To address some of the unexplained results shown in chapter 3 of this thesis a number of studies can be performed. First, a study that will determine the blood-half life of Feridex® in CL-treated animals is needed to verify that indeed macrophages are being exposed to SPIO for a longer period of time than the saline-treated EAE animals and therefore the labeling efficiency of SPIO is greater in CL-treated EAE animals. This may help to explain the increase in regions of signal loss on MR images from CL-treated EAE animals. To determine the cell type involved in SPIO uptake a number of histopathological stains can be used. First, staining for perivascular and meningeal macrophages using the monoclonal antibody ED2 (2) will provide insight on whether this macrophage population is increased after CL treatment and whether it is preferentially expressed in other regions of the brain, such as the cerebrum. Staining for endothelial cell activity and correlating the images to PPB staining will provide insight on the involvement of endothelial cells in SPIO uptake. Electron microscopy can also be performed to determine whether endothelial cells contain iron oxide particles.

## *4.2 Summary and Conclusions*

Cellular MRI has the potential to revolutionize diagnostic measures for multiple sclerosis and other CNS inflammatory diseases. SPIO-enhanced MRI will improve our understanding of the evolution of the MS lesion and how the lesion(s) changes with the use of treatments that target inflammation.

In the work presented in this thesis I have demonstrated the feasibility of performing high-resolution cellular MRI on a clinical 1.5T scanner with specialized MR hardware. This strategy produces images which are of high spatial resolution, have high SNR and which have very high sensitivity to signal loss generated by the presence of iron oxide nanoparticles in cells. I have used this novel MRI technique to address an important, yet unresolved problem in the field of cellular imaging. Namely, the identification of the cell that is responsible for signal loss on MR images after the injection of SPIO contrast agents.

Using a novel transgenic mouse, whereby the hematogenous macrophages express the GFP signal and the resident CNS microglia do not, I demonstrated, for the first time, direct evidence that the hematogenous macrophage is the major contributor to regions of signal loss on MRI. These results have significant implications on the utility of cellular imaging as a tool to study the inflammatory response *in vivo* in various animal models and to test the efficacy of disease-modifying drugs that are directed against preventing macrophage infiltration into the CNS.

## *4.3 References*

1. Filippi M, Falini A, Arnold DL, Fazekas F, Gonen O, Simon JH, Dousset V, Savoiardo M, Wolinsky JS. Magnetic resonance techniques for the in vivo assessment of multiple sclerosis pathology: Consensus report of the white matter study group. *J Magn Reso Imag*. 2005; 21:669-75.

2. Dijkstra CD, Dopp EA, Joling P, Kraal G. The heterogeneity of mononuclear phagocytes in lymphoid organs: distinct macrophage sub- populations in the rat recognized by monoclonal antibodies ED1, ED2 and ED3. *Immunology*. 1985; 54: 589 – 99.

# APPENDIX I: *PREVIOUS WORK*

RESEARCH ARTICLE

Molecular Imaging • Vol. 3, No. 2, April 2004, pp. 1–11 1

## Cellular Imaging at 1.5 T: Detecting Cells in Neuroinflammation Using Active Labeling with Superparamagnetic Iron Oxide

*Ayman J. Oweida, Elizabeth Dunn, and Paula J. Foster*

Robarts Research Institute

### Abstract

**The ability to visualize cell infiltration in experimental autoimmune encephalomyelitis (EAE), a well-known animal model for multiple sclerosis in humans, was investigated using a clinical 1.5-T magnetic resonance imaging (MRI) scanner, a custom-built, high-strength gradient coil insert, a 3-D fast imaging employing steady-state acquisition (FIESTA) imaging sequence and a superparamagnetic iron oxide (SPIO) contrast agent. An "active labeling" approach was used with SPIO administered intravenously during inflammation in EAE. Our results show that small, discrete regions of signal void corresponding to iron accumulation in EAE brain can be detected using FIESTA at 1.5 T. This work provides early evidence that cellular abnormalities that are the basis of diseases can be probed using cellular MRI and supports our earlier work which indicates that tracking of iron-labeled cells will be possible using clinical MR scanners.** *Mol Imaging* (2004) **3,** 1–11.

**Keywords:** EAE, multiple sclerosis, superparamagnetic iron oxide, inflammation, MRI.

### Introduction

Multiple sclerosis (MS) is an autoimmune demyelinating disease of the central nervous system (CNS). The symptoms of MS vary depending on the pathological nature and the location of lesions within the CNS [1]. Experimental autoimmune encephalomyelitis (EAE) encompasses a group of CNS inflammatory/autoimmune diseases in various laboratory animals, including the mouse, rat, guinea pig, primate and marmoset [2–4]. Ongoing disease activity, in MS and EAE, is due to an active inflammatory process and is associated with blood–brain barrier (BBB) damage. Most evidence indicates that inflammatory cell infiltration, through the disrupted BBB, is an early event in the development of the MS lesion [5]. The prime inflammatory process is around blood vessels; in histological images, this process is recognized as perivascular cuffs of infiltrating inflammatory cells [6].

The importance of T cells in EAE has been extensively documented, particularly the ability to initiate the disease and the autoimmune specificity for myelin provided by these cells [7]. However, other cell types, specifically the infiltrating macrophages and endogenous microglia, likely provide the actual effector mechanisms leading to inflammation and demyelination. The macrophage is involved in different phases of disease in EAE and MS and plays an important role in the process of demyelination [8,9]. Macrophages emigrating from blood vessels digest myelin either as a response to inflammatory damage to the myelin or as a response to activation signals produced in either the perivascular region or the lesion. This inappropriate macrophage activation leads to patchy demyelination and axonal damage. Some evidence suggests that the degree of macrophage infiltration associated with certain MS lesions is very closely related to the likelihood of progressing to demyelination [10]. Several studies have correlated the presence of certain macrophage populations with different phases of the disease and this has led to new classification schemes that are based on the macrophage populations associated with lesions [11]. Clearly, there are important and unresolved questions related to how the degree of macrophage involvement, the role of distinct populations of macrophages and their spatial distribution contribute to lesion development and disease progression in MS and EAE.

The most common method for assessing the extent of macrophage involvement, or the effectiveness of various therapeutic strategies that inhibit inflammation, involves a histopathological evaluation of multiple tissue sections. Pathologic grading systems are frequently used to estimate the extent of perivascular cuffing using a cellular stain such as hemotoxylin and eosin (H&E). These techniques are often only semi-quantitative, laborious, and destructive. Methods that would permit the nondestructive or noninvasive definition of macrophage involvement in neuroinflammation, over the time course of the disease, would have a tremendous advantage over

Corresponding author: Paula J. Foster, Robarts Research Institute, Imaging Research Laboratories, 100 Perth Drive, London, Ontario, Canada, N6A 5K8; e-mail: pfoster@imaging.robarts.ca.

Received 22 January 2004; Accepted 20 April 2004.

conventional histological techniques, and may represent important markers for early events in MS.

Magnetic resonance microscopy (MRM) is well suited to study cellular events in neuroinflammation [12–15]. Individual perivascular cuffs have been visualized in EAE guinea pig brain tissue by MRM at 9.4 T with high-resolution 3-D T1 stains [16]. Cellular imaging is a newly emerging field that combines the ability to obtain high-resolution MRM data with novel contrast agent strategies for labeling specific cells, thereby enhancing their detectability. The use of iron oxide based contrast agents for cell-specific imaging by MRI has now been demonstrated in a number of different disease applications [17–24]. The detection of brain lesions in EAE models was one of the early applications of this imaging approach [19,20]. Intravenously administered iron oxides, taken up by macrophages in the brains of EAE animals, could be visualized with MRI. This approach has been termed "active labeling" of cells. The presence of iron oxide is indicated by hyperintense regions in T1W images or abnormal signal hypointensities in T2- or T2*-weighted images, depending on the magnetic field strength and the concentration of iron. The large magnetic susceptibility of these particles can affect an area much larger than the actual size of the particles; this effect is known as a "blooming artifact" and leads to an exaggeration of the region occupied by iron oxide. The particle size, dose, and delay before scanning have all been shown to be important factors to consider for optimal detection of macrophages in EAE [25–27]. Several other factors also influence the visualization of iron-labeled cells in tissues, including the main magnetic field strength, the pulse sequence and timing parameters, and the spatial resolution.

The purpose of this work was to determine whether active labeling strategies could be used together with new tools and concepts for cellular and microimaging at low field, developed in our laboratory [28], to enable the visualization of perivascular cuffing in EAE using a clinical 1.5 T scanner. Our results show that small, discrete regions of signal void (RSVs) corresponding to iron accumulation in EAE brain can be detected using FIESTA at 1.5 T. This work provides early evidence that cellular abnormalities that are the basis of disease can be probed and supports our earlier work that indicates that tracking iron-labeled cells will be possible using clinical MR scanners.

## Materials and Methods

### *Animal Model*

EAE was induced in 8-week-old female Lewis rats by a single injection of whole CNS homogenate in complete Freund's adjuvant (CFA) with inactivated *Mycobacterium tuberculosis*. Immunization was performed by intradermal inoculation of 0.1 mL in the footpad of each hind leg under general anesthesia. The dose per rat was calculated to be the following: 0.1 g of Hartley guinea pig CNS, 0.01 mL CFA, 0.75 mg additional irradiated mycobacteria tuberculosis H37Ra. All animals were kept in individual cages with standard conditions of light and free access to water and food.

The clinical signs of EAE begin approximately 6 days postimmunization. Animals were weighed and scored daily for the clinical features of EAE according to the following scale: 0 = normal healthy animal, 1 = loss of tail tonus, 2 = hind limb weakness, 3 = complete hind limb paralysis, 4 = complete paralysis, incontinence, and moribund conditions. Scoring began the day after immunization. Day 0 was considered the day on which inoculation of EAE occurred.

### *In Vivo Imaging: Gadolinium Enhancement Studies*

Imaging was performed at 1.5 T using a CVi/MR GE clinical scanner. Gadolinium enhancement in T1-weighted images was assessed in the brains of EAE rats ($n$ = 15). Animals were anesthetized for imaging using an intraperitoneal injection of ketamine/xylazine (100/10 mg/kg) and positioned inside a custom-built quadrature surface RF coil. A T1W multislice spin-echo image (TR/TE 600/20 msec) was acquired before and immediately following a single intravenous injection of gadolinium-DTPA (Magnevist, 100 mmol/kg) into the tail vein. Five animals were imaged on each of four consecutive days, beginning when the first clinical signs were apparent. Five animals were imaged once, when the clinical score was 2, and five others were imaged once, when the clinical score was 3. Information about the leakiness of the BBB was used to guide the choice of timing for the intravenous injection of iron oxide contrast agent in subsequent EAE animal imaging experiments.

### *Ex Vivo Cellular Imaging Studies*

Rat brain specimens were imaged using a custom-built gradient insert coil, designed and constructed in our laboratory. The coil was designed using a Constrained Current Minimum Inductance design algorithm [29]. The resulting coil had the following characteristics: inner diameter 11 cm, peak slew rate 2000 T/m/sec and maximum gradient strength 1200 mT/m. The entire set-up procedure required approximately 15 min to complete.

Seven EAE rats were administered Feridex (Berlex). A catheter (24 gauge) was inserted into the rat tail vein then heparin diluted in saline was injected (0.5 mL) followed by Feridex (22.4 mg Fe/kg) diluted in saline

(1 mL total volume). Control animals consisted of normal healthy animals administered Feridex ($n$ = 4) or saline ($n$ = 4), and EAE animals administered saline ($n$ = 4). Twenty-four hours after the injection euthanasia was performed and the rats were perfusion-fixed with 3.75% neutral-buffered formalin (Sigma). Rat brains were excised and stored in 10% formalin until imaging. Just prior to imaging, brain specimens were placed in 1-cm diameter plastic tubes and immersed in Fluorinert (3M, Ontario, Canada) then positioned in a custom-built solenoidal RF coil within the gradient insert.

Rat brain specimens were imaged using a 3-D fully refocused gradient-echo sequence (3DFIESTA, GE Medical Systems, Milwaukee, WI), which was previously optimized for cellular imaging [28]. The parameter values used for rat brain imaging with FIESTA were as follows: TR/TE 7.7/3.6 msec, flip angle 30°, 21 kHz bandwidth, spatial resolution was either 100 or 200 μm isotropic using a 2-cm FOV, 200 × 200 or 400 × 400 matrix, and a slice thickness of 0.1 or 0.2 mm. 3DFIESTA images were compared with 2-D T2-weighted fast spin-echo (2DFSE) and 3-D spoiled gradient-echo (3DSPGR) images. SPGR images were acquired with the imaging parameters closely matched to those as of FIESTA. For 2DFSE, the scan parameters were as follows: BW 16 kHz, TR/TE 3000/80 msec, 256 × 128 matrix, slice thickness 0.2 mm. For 3DSPGR, the scan parameters were as follows: BW 21 kHz, TR/TE = 9/4 msec, 200 × 200 matrix, slice thickness 0.1 or 0.2 mm and 30° flip angle (FA). To investigate the influence of SNR and spatial resolution on the ability to detect iron-labeled cells in brain tissue, the number of signal averages, bandwidth, matrix size, and/or slice thickness were varied. SNR was defined as the mean SI in a region of interest (ROI) drawn in brain GM and WM, divided by the standard deviation of noise SI from an ROI selected in background air. An average value for SNR was determined from three SI measurements taken in various parts of the brain images. CNR was calculated as the difference between mean SI in brain tissue versus the mean SI in regions of iron oxide induced signal void (RSV), divided by the standard deviation of noise SI measured in background air.

*Correlative Histopathology*

After imaging, the specimens were prepared for histopathological analysis. Specimens were embedded in paraffin in such a manner that 8-μm sections could be cut from the block. Sections were stained with H&E to assess cellular infiltrate. Contiguous sections were stained with Perl's Prussian Blue (PPB) counterstained with Nuclear Fast Red to demonstrate iron uptake and immunolabeled with mouse anti-rat ED1 (also known as anti-CD68). The monoclonal antibody (mAb) ED1 is widely used as a marker for rat macrophages. The ED1 antigen is expressed on lysosomal membranes, and weakly on the cell surface of myeloid cells. This antigen is expressed by the majority of tissue macrophages and weakly by peripheral blood granulocytes. ED1 (1:300) was applied to sections overnight in a humidified chamber at 4°C after blocking with 5% normal goat serum (NGS), and 0.3% $H_2O_2$ in PBS. Sections were rinsed with PBS-Tween 20 (3 ×), after which a biotinylated goat anti-mouse (H + L) IgG secondary antibody was applied (1:500) for 2.5 hr at room temperature. Sections were washed again with PBS-Tween 20, treated with extravadin–peroxidase (1:500, 3 hr) (Sigma), and finally, a DAB solution. Sections were counterstained with hematoxylin. Sections were dehydrated through ascending alcohols, cleared in xylene, and coverslipped with Cytoseal-60 (VWR International). Histopathological and MRM images were matched by locating corresponding landmarks.

## Results

*In Vivo Gadolinium Enhancement Study*

Gadolinium enhancement observed in post Gad T1W SE images was a useful indication of BBB permeability in EAE rats. Of the 15 EAE rats imaged, Gad enhancement was observed in 13 animals. In all 13 rats, enhancement was observed when the animal's clinical score was either 2 or 3. This time point varied between Days 9 and 12 postimmunization. Based on these findings, the clinical score, and not the day postimmunization, was used to plan iron oxide administration. Feridex was administered to seven EAE rats, five of these animals had a clinical score of 3 and two animals had a clinical score of 2.

*Ex Vivo Brain Specimen Scanning*

The FIESTA imaging sequence has proven to be highly sensitive to the superparamagnetic effects of iron oxide. Small, localized RSVs were visualized in the brains of all EAE rats that were injected with SPIO. In non-EAE animals injected with SPIO, and in EAE animals that were injected with saline, RSVs were not observed. Multiple brain regions were affected. Figure 1 shows representative brain images, from control animals and four different EAE animals.

In Figure 2, FIESTA images are compared to the more commonly used T2W FSE. For FIESTA images, the spatial resolution is either 200 μm isotropic (B) or 100 μm isotropic (C). When comparing T2W FSE and FIESTA images, it is clear that the area of signal loss is

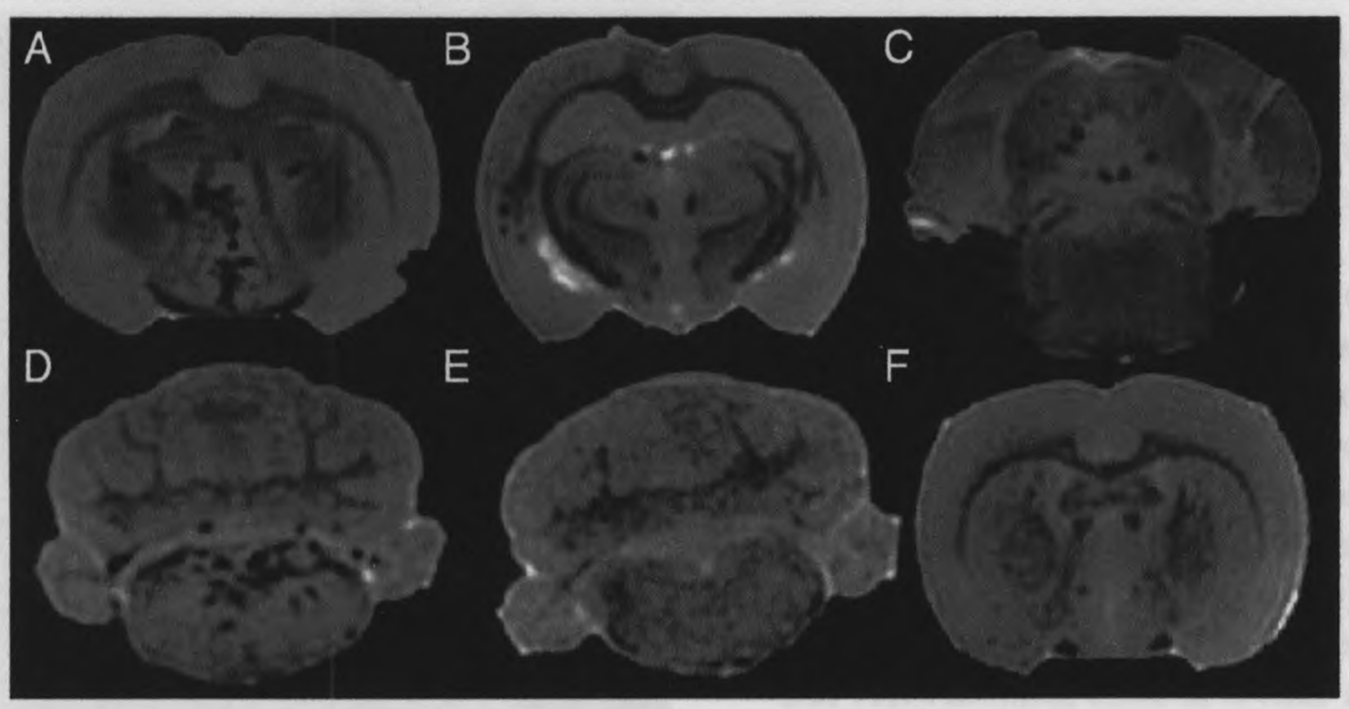


**Figure 1.** *Representative FIESTA images (100 μm isotropic spatial resolution) of rat brain demonstrating the detection of localized RSVs in EAE animals administered Feridex intravenously during the course of neuroinflammation. (A–D) Images from four different EAE animals with areas of signal loss observed throughout the brain; (E) Brain image from normal rat injected with Feridex; (F) Brain image from EAE rat injected with saline.*

more exaggerated in the FSE image. In FSE images with lower SNR, small discrete areas of signal void observed in FIESTA images went undetected. The RSVs are more distinct in the higher-resolution FIESTA image (C). This is likely due to partial voluming in the 200-μm-thick image slice of Figure 2B. Tissue contrast is similar in T2W FSE and FIESTA images.

Figure 3 compares FIESTA and SPGR images. Table 1 lists the SNR and CNR for the RSVs 1 and 2. Images (A) and (B) are FIESTA images matched for resolution (100 μm isotropic) and TR/TE (7.7/3.6 msec) with increasing SNR due to signal averaging. The parameters are: (A) 1 nex, 3-min scan time, SNR = 10; (B) 16 nex, 55-min scan time, SNR = 38. The ability to detect the small discrete RSVs is clearly enhanced with increased SNR and CNR. CNR was measured for the RSVs indicated by numbers 1 and 2 in Figure 3B. CNRs were 8.3 and 5.9 in (A), and 31 and 28 in (B), for RSVs 1 and 2, respectively.

While the SNR contributes to the CNR, it is not the only factor influencing the ability to detect these small regions of signal loss. As shown in Figure 2, lower spatial resolution (increased voxel size), which increases SNR, interferes with the ability to localize small areas of signal loss due to partial voluming effects (Figure 2, B vs. C). In Figure 3, the FIESTA image in (C) has higher spatial resolution (50 × 50 × 100 μm) relative to that in (A), but the SNR is matched (SNR = 10) through signal averaging (6 nex). The CNRs for RSV1 and RSV2 are higher in (C) than in (A), at 10 and 9.5, indicating an enhanced ability to detect the RSVs. In this case, detectability is likely improved by both higher spatial resolution (50 × 50 × 100 μm) and longer TR/TE (12.7/6.3 msec). The CNRs for RSV1 are consistently higher than those for RSV2 in the FIESTA images. In addition, the signal loss extended through more image slices for RSV1 than for RSV2. These observations may indicate either the presence of a higher concentration of iron or the distribution of iron over a greater spatial extent.

The SPGR image in (D) is also matched to the FIESTA image in (A) for SNR [10] as well as resolution (100 μm isotropic) and TR/TE (7.7/3.6 msec). However, the con-

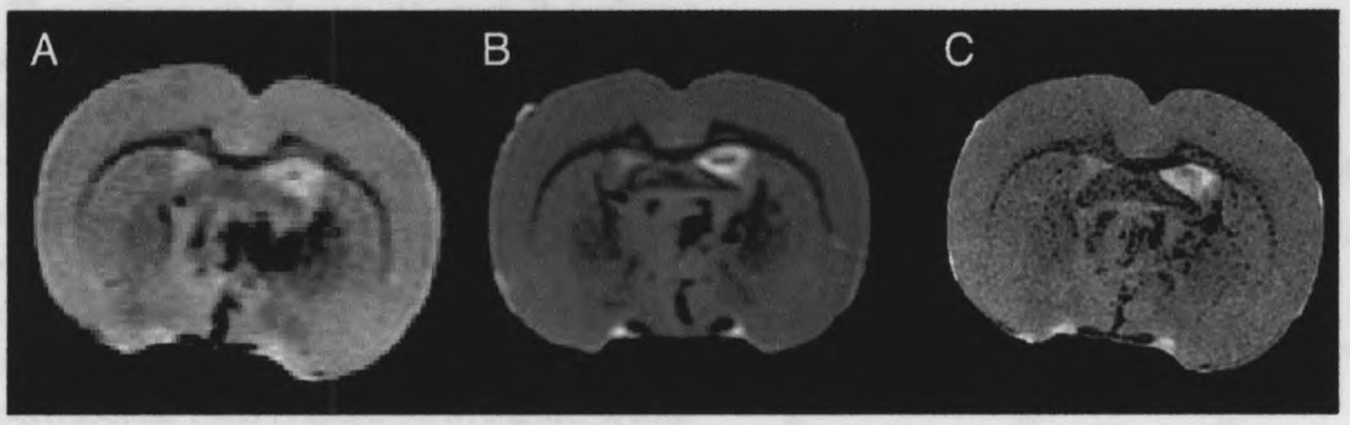


**Figure 2.** *Comparing the FIESTA and T2-weighted FSE imaging sequences for detecting susceptibility induced contrast from iron oxide accumulation in rat brain tissue at 1.5 T. (A) 2-D T2W FSE; (B) FIESTA 200 μm isotropic spatial resolution; and (C) FIESTA 100 μm isotropic spatial resolution.*

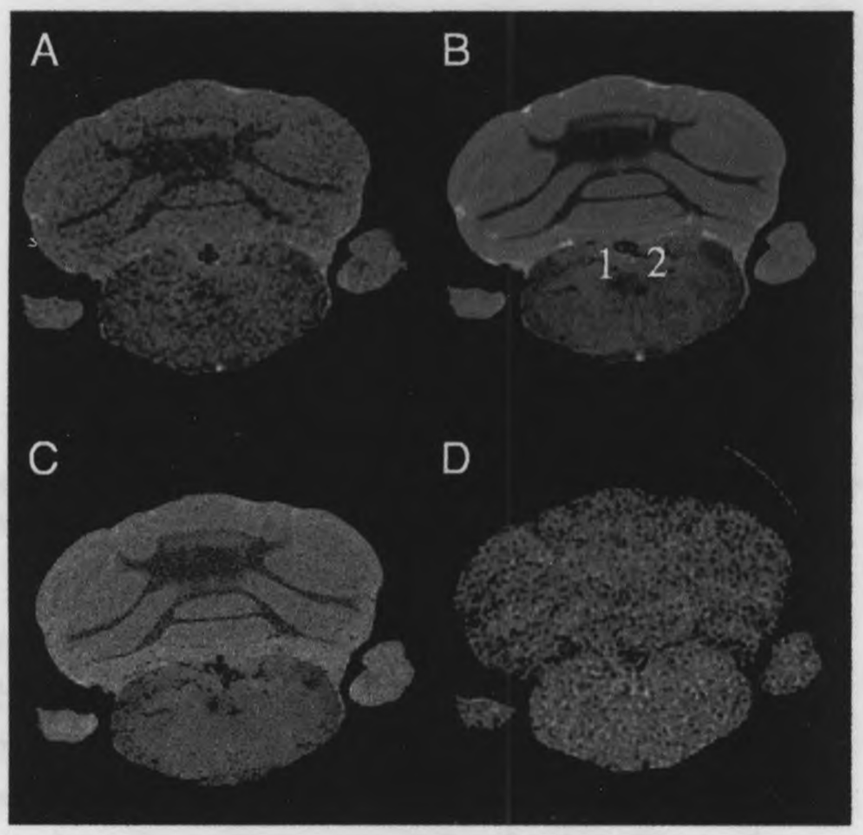


**Figure 3.** *Comparing the FIESTA and SPGR images. Two RSVs, visible in the medulla of this EAE rat brain, are labeled 1 and 2. (A–C) FIESTA images; (A) 100 μm isotropic resolution, no averaging, TR/TE = 7.7/3.6 msec, SNR = 10, 3 min; (B) 100 μm isotropic resolution, 16 nex, TR/TE = 7.7/3.6 msec, SNR = 38, 55 min; (C) 50 × 50 × 100 μm, 6 nex, TR/TE = 12.7/6.3 msec, SNR = 10, 1 hr, (D) 3DSPGR 100 μm isotropic resolution, 16 nex, TR/TE = 7.4/3.1 msec, SNR = 10, 50 min.*

trast due to the presence of iron oxide is very low in these SPGR images, and does not permit the visual discrimination of small regions of signal loss from background, and so precludes a measurement of CNR. With higher CNR, due to increased SNR or larger regions of signal loss associated with higher concentrations of iron, SPGR may permit the visualization of small RSVs. However, the scan time required to obtain equivalent CNR through increased SNR, by signal averaging, would be prohibitive.

*Histology*

Our histological analysis showed that patterns of signal loss in the FIESTA images of EAE rat brain matched patterns of perivascular cuffing that were identified in the corresponding H&E stained sections (Figure 4). The arrows in Figure 4A and B indicate where the RSVs in the MR image and the perivascular cuffs in the H&E image correlate. Exact correspondence is not achievable since the MR image slice is 100 μm thick and the histological image is only 8 μm thick. PPB staining showed the presence of SPIO particles in cells. The discrete areas of signal loss correspond to individual clusters of iron-labeled cells associated with cell infiltration in perivascular cuffs (Figure 5). In Figure 5, four individual RSVs are indicated in the FIESTA images (A and B). In the PPB-stained histological image (Figure 5C), four individual perivascular cuffs are shown which correspond to these RSVs. In Figure 5B and C, these are numbered 1 through 4. In Figure 5D, a single cuff is shown which corresponds to area.

In EAE brains, clusters of ED1 positive cells were found throughout the brain (Figure 6). The ED1 positive cells were predominantly located around blood vessels (Figure 6B and C). In Figure 6C and D, higher magnification of an individual perivascular cuff is shown. While many ED1 positive cells surround the vessel in Figure 6C, only a few of these cells (arrows) have been labeled with iron as indicated by the PPB stain (D). This figure reveals some of the concerns with the active labeling strategy and Perl's staining. First, as is clear in Figure 6D, not all of the cells in a single cuff are iron labeled. This was a common observation. Another second point to note is that only a small percentage of the many perivascular cuffs in the EAE brains contain any cells that are iron labeled. This results in a percentage of the cuffs going undetected with any MRI pulse sequence. Finally, it was often necessary to analyze multiple contiguous PPB-stained histological slices to account for the iron-labeled cells in a single perivascular cuff which contribute to the RSV observed in the FIESTA image. Because it is practically impossible to obtain evenly sliced contiguous slices through an entire brain specimen, iron-labeled cells will go unaccounted for.

## Discussion

We have developed methods for cellular imaging at 1.5 T, using a clinical whole-body scanner, for an alternative approach to microimaging. To accomplish this, new tools and concepts were applied and tested which included a custom-built, insertable, high-powered imaging gradient set, customized radio-frequency (RF) coils and optimized pulse sequence technology. This strategy, together with active cell labeling with the use of superparamagnetic iron oxide nanoparticles, has allowed us to visualize small clusters of inflammatory cells in EAE brain.

**Table 1.** CNR and SNR for RSVs in the Medulla of the EAE Rat Brain in Figure 3

| | *RSV1* | | RSV2 | |
|---|---|---|---|---|
| *Image* | SNR | CNR | SNR | CNR |
| A | 10 | 8.3 | 10 | 5.9 |
| B | 38 | 31 | 38 | 28 |
| C | 10 | 10 | 10 | 9.5 |
| D | 10 | – | 10 | – |

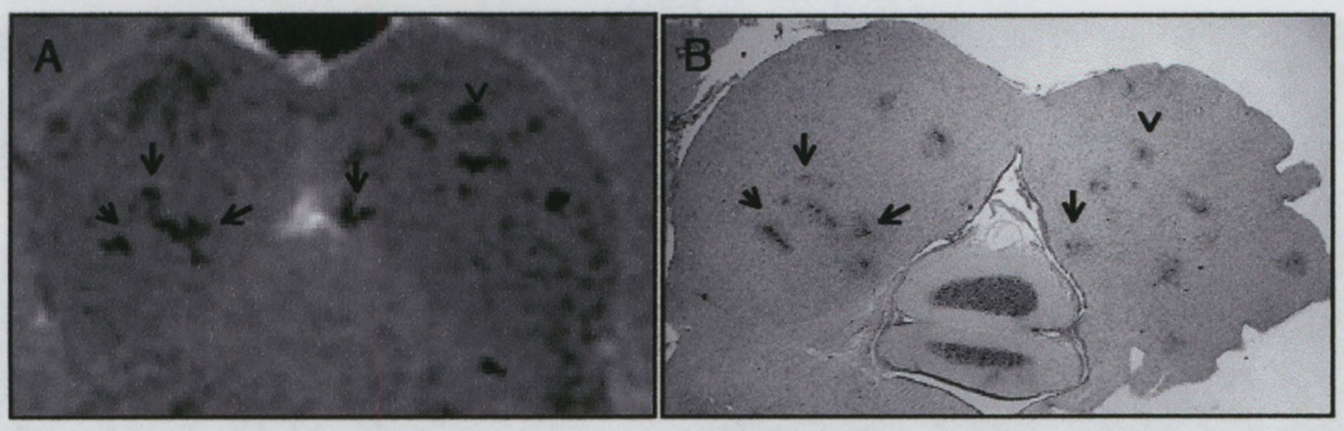


**Figure 4.** *Correspondence between perivascular cuffing in EAE brain identified with (A) FIESTA imaging and (B) H&E stained histology. Arrows indicate where the RSVs in the MR image and the perivascular cuffs in the H&E image correlate.*

*MR Detection*

The large magnetic susceptibility of SPIO particles produces magnetic field inhomogeneities that are known to affect regions in MR images over a far greater extent than the actual particle distribution. This effect, on the microscopic scale, permits the visualization of single cells in vitro [28,30]. On the macroscopic scale, however, large collections of SPIO-labeled cells can influence MR signal intensity many pixels away, and produce an effect typically described as blooming artifact. The size of the blooming artifact is sequence and echo time dependent. To visualize this effect, most

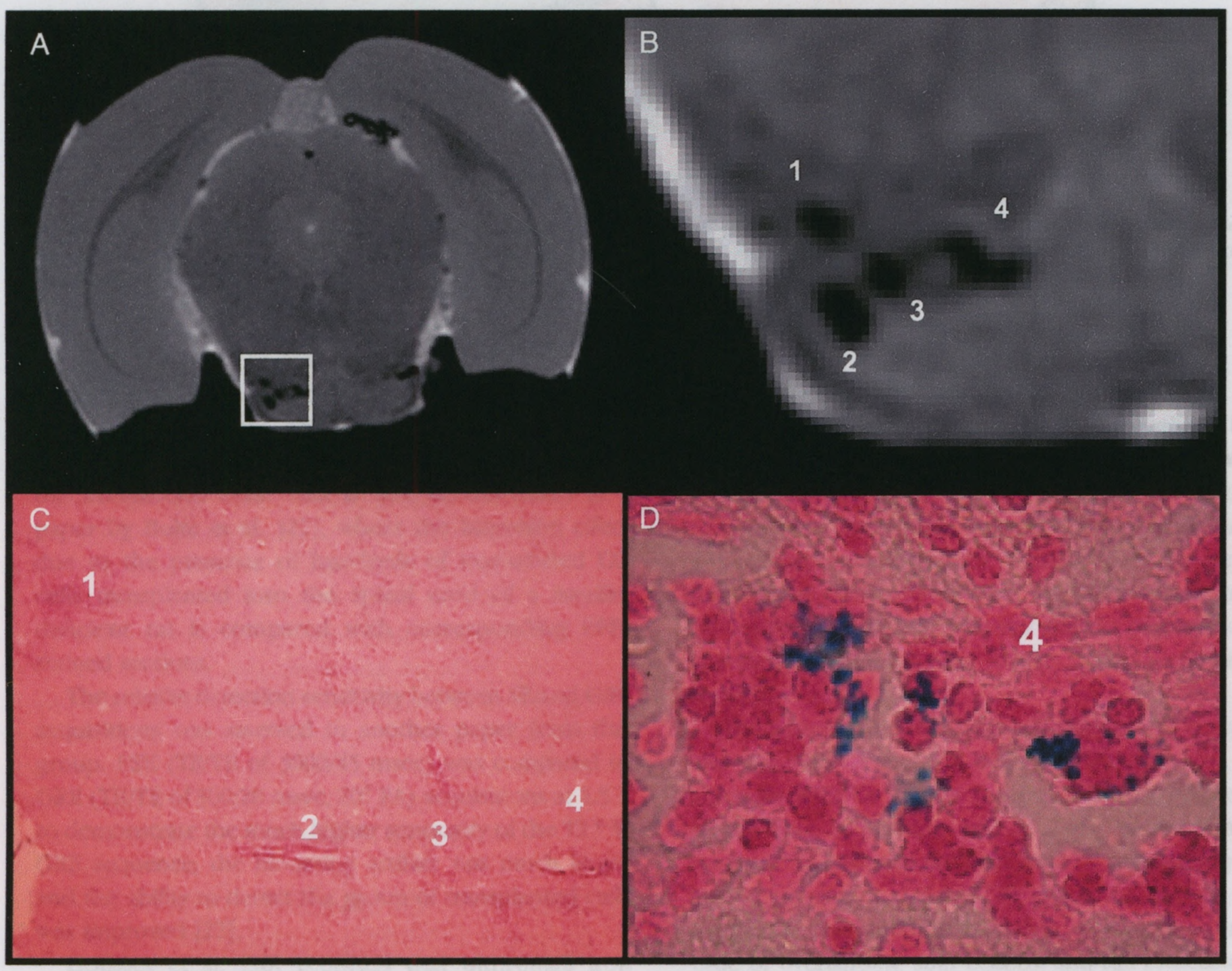


**Figure 5.** *Correspondence between iron-loaded cells detected in FIESTA images of EAE brain and PPB-stained histology. High-resolution FIESTA images provide details on the number, size, and shape of perivascular cuffs in EAE brain tissue. (A) FIESTA image slice; (B) Magnified view of ROI indicated in A; (C) Corresponding PPB-stained histology at ×4 magnification and (D) at ×40 magnification. In (D), the stained cells correspond to area 4 of (B) and (C).*

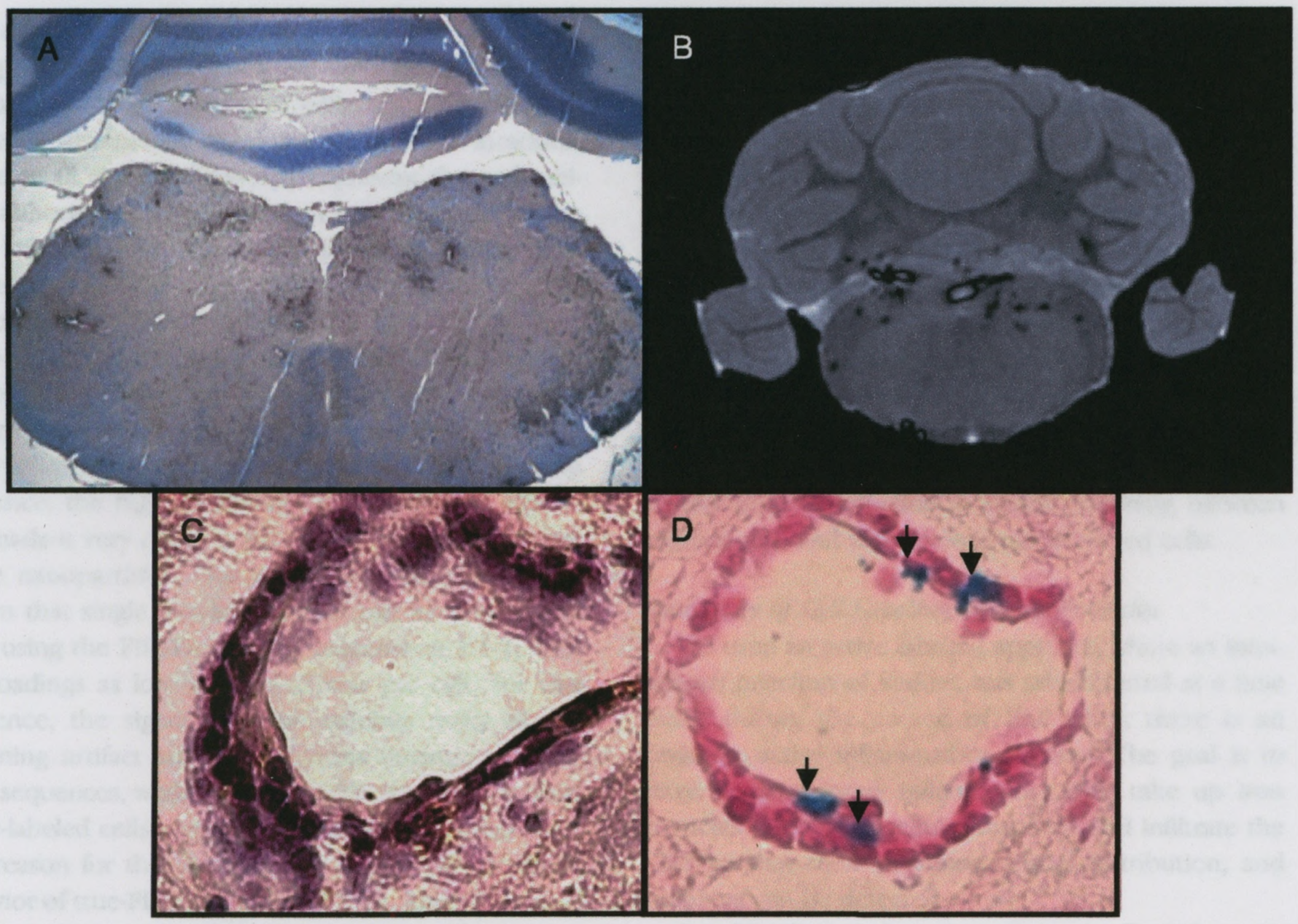


**Figure 6.** *ED1 positive cells (brown product) are visible throughout the medulla in the EAE brain (A). RSVs are also commonly observed in the medulla as shown in this 100 μm isotropic FIESTA image (B). At the level of an individual perivascular cuff, ED1 positive cells are found primarily surrounding the blood vessel (C). Iron-positive cells (arrows) identified in the Perl's stained section are fewer in number than ED1 positive cells.*

imaging studies have used T2- or T2*-weighted SE and GRE pulse sequences. The RSV in these MR images is consequentially larger than the actual area occupied by the iron-labeled cells. This is well demonstrated in a paper by Bulte et al. [21], where the blooming effect due to the presence of hundreds of iron-labeled CG cells transplanted into the spinal cord of a myelin-deficient rat is compared with corresponding PPB-stained sections.

The relative detection sensitivity between SE and GRE acquisitions was assessed in another paper from this group. FSE (TR/TE of 3000/45 msec) was compared to GRE (TR/TE of 300/20 msec, 20° FA) acquisitions at 1.5 T to demonstrate the much higher sensitivity of the T2 * W GRE sequence; the blooming artifact was much larger and the ability to detect the group of transplanted cells was improved [22].

Dousset et al. [20] reported that ultra-small iron oxide nanoparticles (USPIOs) administered intravenously, and in vivo T2-weighted SE imaging provided 100% sensitivity for lesion detection in EAE rats; RSVs were observed in all EAE animals. In this and other EAE studies, large regions of signal loss, resulting from blooming artifact are typically observed in the brainstem and cerebellum. Many studies have used iron oxide nanoparticles and similar imaging techniques in various applications to successfully visualize the presence of iron-labeled cells in tissues [18–24]. The relative trade-off between detection sensitivity and the degradation of specificity from blooming artifact is still problematic though.

The images obtained with our microimaging system and the FIESTA imaging sequence are different. The acronym FIESTA stands for fast imaging employing steady-state acquisition and is also described in the literature as balanced fast field echo or fast imaging with steady precession (true-FISP) sequence [31,32]. The technique uses multiple RF pulses to generate a multitude of overlapping spin echoes, and full refocusing of transverse magnetization. The FIESTA images we have presented show very small, discrete regions of signal loss in numerous brain regions. Our histological data indi-

cate that the number of iron-labeled cells associated with perivascular cuffing in these EAE brains is small, on the order of ones to tens of cells, and that they are scattered throughout the brain in multiple locations. These small abnormalities may represent the early cellular abnormalities and events in lesion formation that have not been visualized previously in similar EAE studies which used T2W SE and FSE or T2*W GRE sequences.

The FIESTA imaging sequence has a number of advantageous features, over other imaging sequences, for certain cellular imaging applications. What was originally considered a negative aspect of this imaging sequence, the high sensitivity to off-resonance effects, has made it very effective for cellular imaging with iron oxide nanoparticles. Our previous studies [28] have shown that single iron-loaded cells can be detected in vitro using the FIESTA imaging sequence at 1.5 T, with cell loadings as low as 6 pg of iron per cell. For this sequence, the signal response exhibits many of the blooming artifact suppression traits intrinsic to spin-echo sequences, while maintaining the sensitivity to iron oxide-labeled cells intrinsic to gradient-echo sequences. The reason for this lies with the unique off-resonance behavior of true-FISP sequences [32,33]. The NMR signal at the readout time (TR/2) for true-FISP sequences is well described as a spin echo, with the refocusing axis of the spin echo along either the $+y'$ or $-y'$ axis of the rotating frame. The specific axis along which the spin echo forms depends upon the local off-resonance frequency of the NMR signal, and alternates direction for off-resonance bands having full width defined by 1/TR. Therefore, macroscopic field inhomogeneities responsible for blooming, as produced by imperfect shimming or proximity to large clusters of iron oxide cells, are refocused as a spin echo. However, since the off-resonance produced, by even a single cell with 6 pg of iron, can span several thousand Hertz locally, pixels containing such cells involve spin-echo signal formation along two opposing axis, producing signal cancellation comparable to that observed with gradient-echo sequences. It is this unique response to off-resonance, which produces both the blooming artifact suppression and cellular detection sensitivity, which results in FIESTA acquisitions being so well suited to imaging iron oxide-labeled cells.

In addition, the FIESTA sequence provides substantially enhanced SNR, relative to GRE and SE sequences, as a result of the multiple signal refocusing paths available for tissues with T2 much greater than TR. This significant improvement in SNR efficiency allowed for microimaging at lower field strengths than is typically possible, and for the acquisition of images at high spatial resolution with reasonable scan times. These two factors were key to our ability to visualize small numbers of iron-labeled cells. Imaging at 1.5 T with FIESTA is an advantage since at higher magnetic field strengths, more typically used for microimaging, off-resonance banding artifacts that result from imperfect shimming, are more pronounced. The gradient coil insert was key to obtaining fast, high-resolution images with FIESTA. The benefits of which were illustrated by an observed 40% average increase in the CNR for regions of signal loss (Figure 3) as the voxel size were reduced. The increased CNR results from a reduction in partial voluming between regions with and without iron oxide-labeled cells.

*Specificity of Cell Labeling by SPIO Particles*

We used an active labeling approach where an intravenous injection of Feridex was administered at a time point during the course of EAE when there is an ongoing, active inflammatory reaction. The goal is to have hematogenous inflammatory cells take up iron particles during the cellular response and infiltrate the CNS so that their presence, spatial distribution, and numbers can be detected.

Our histological data show that not all of the perivascular cuffs in EAE brains contain iron-labeled cells. In addition, not all of the infiltrated cells contained in an MR-visible perivascular cuff contain iron oxide particles. However, not all of the cells in an individual cuff need to be iron labeled to allow the visualization of that cuff in the FIESTA image. Our studies have shown that even a few iron-labeled cells will allow the identification of a perivascular cuff in high-resolution FIESTA images. It is likely that in previous studies which have used more conventional T2-weighted SE or T2*-weighted GRE imaging sequences, or lower resolution imaging, lesions with only a small number of iron-labeled cells were not detected.

The low efficiency of cell labeling with intravenous iron oxide administration is not unique to these studies. It is well known that in vivo targeted cell labeling with iron oxide depends on the physical characteristics of the particles and their uptake by cells of the reticuloendothelial system (RES) (liver, spleen, and lymph). A large fraction of the iron oxide particles administered intravenously will be taken up by the RES. Larger particles are, in fact, taken up by the RES more efficiently [34] and this has led to the preferential use of USPIOs, which consequentially have a longer blood half life than SPIO, for most imaging studies of neuroinflammation [35–37].

Even with long-circulating USPIOs, only a small fraction of cells are labeled. Still, many studies have demonstrated that this approach does in fact result in sufficient numbers of cells being labeled with iron in the bloodstream and transported to the site of inflammation to allow their detection with MRI. For our studies, we chose to use Feridex, an SPIO, despite its shorter circulation time, because of its greater susceptibility [38] and because free Feridex is not likely to cross the basement membrane of capillaries, as smaller iron oxide agents do [39]. At a sufficiently high dose, the RES is saturated [40] and iron oxide particles are captured in the bloodstream by phagocytic cells of the immune system. More efficient in vivo cell labeling may come with the advent of new agents that have improved uptake and internalization into cells, surface modifications that allow the resistance to protein adsorption and recognition by cells of the RES, or are capable of targeted uptake by specific cells [41–43].

The concept of identifying only a portion of the infiltrated cells in active inflammation may at first seem futile. However, clinically, there is tremendous value in noninvasive markers that can demonstrate changes in the degree of inflammation, during disease progression, or in response to anti-inflammatory therapies or treatments. Macrophages are involved in every stage of disease progression in MS. Their presence has been noted during inflammation, in removal of myelin debris, and even in myelin repair [44].

Our results suggest that the RSVs in the FIESTA images represent the locations of iron-labeled cells in the EAE brain. In most cases, the patterns of signal loss and correlative histology suggest a perivascular location. However, the location does not establish the "source" of these cells. Within the CNS of rats with EAE, there are at least three different subpopulations of macrophages that might occupy these locations [45]. These include: (i) blood-borne macrophages infiltrating the perivascular lesions in the CNS; (ii) "resident" perivascular macrophages; and (iii) "resident" reactive microglial cells. It has also been suggested that iron oxide phagocytosed by CNS endothelial cells may be the cause of the signal loss in some cases [46]. All of these phagocytic cell types are known to take up iron oxide particles in vitro, either by endocytosis or phagocytosis depending on the particle size, and with different efficiencies depending on the cell type. The considerable functional and immunophenotypic heterogeneity of these cell types makes it unclear whether and how in vivo factors will influence cell-specific iron oxide uptake.

In order to determine what types of cells are in the tissue, it is common to use histological or immunohistochemical analysis to visualize the morphology (size and shape) or the response to markers (antibodies). There are currently, however, no unique histochemical markers that can distinguish resting or activated microglia from monocytes/macrophages in the circulation, or from macrophages which have invaded the brain. A multitude of stains would be required to get a limited appreciation of the true source of cells in the CNS. Alternatively, the source of the cells can be addressed indirectly by cell manipulation or inflammation modulation experiments; these types of studies are underway in our labs.

Using histological stains to identify the presence of iron in cells, and to correlate the location of iron-labeled cells in brain tissue with RSVs detected in the MR images, is also very challenging. The staining technique we used to stain iron in cells or tissue is known as Perl's Prussian Blue [47]. Staining iron oxide-labeled cells is trivial when you have hundreds or thousands of cells in a location but is much more difficult when there are only a few cells to locate. New 3-D optical imaging methods may permit a more realistic representation of cells in tissues [48,49].

Despite the various challenges for histological verification of the presence of iron in cells, and the source of cells, a body of indirect evidence is growing which supports the notion that, with active labeling techniques, the signal loss in MR images depicts the actual migration of iron-laden macrophages from the circulation into the brain. Dousset et al. demonstrated that the scanning delay is critical for performing macrophage activity imaging. Their studies suggest that images should be acquired approximately 24 hr after intravenous injection of iron oxides, which is 5–10 times the blood half life of USPIO or SPIO in the rat, While free iron oxide particles may cross the BBB during this window, an active cellular uptake of iron oxide particles is necessary for the particles still to be present in the parenchyma after 5–10 blood half lives. In studies of EAE, MS, and ischemia [35–37,50], which compare Gad-enhanced T1W images and SPIO-induced signal loss in T2 or T2*W images, breakdown of the BBB and macrophage infiltration appear to be unrelated events. The results of these studies counter the idea that passive diffusion of particles is occurring through a leaky BBB with subsequent uptake by local resident macrophages.

Our imaging approach has shown that even very small numbers of iron-labeled cells can be detected in

neuroinflammation. This work provides early evidence that cellular abnormalities that are the basis of disease can be probed and supports our earlier work which indicates that tracking of iron-labeled cells will be possible using clinical MR scanners. In vivo imaging of EAE rat brain is the next step and will present the next challenges.

## Acknowledgments

This work was supported by the Canadian Institutes of Health Research. We thank Dr. Brian Rutt and Andrew Alejski for pulse sequence and gradient coil insert development. Dr. Chris Bowen is gratefully acknowledged for assistance in reviewing the manuscript.

## References

[1] Adams CW, Poston RN, Buk SJ (1989). Pathology, histochemistry and immunocytochemistry of lesions in acute multiple sclerosis. *Neurol Sci.* **92**:291–306.

[2] Gold R, Hartung HP, Toyka KV (2000). Animal models for autoimmune demyelinating disorders of the nervous system. *Mol Med Today.* **6**:88–91.

[3] Petry KG, Boullerne AI, Pousset F, Brochet B, Caille JM, Dousset V (2000). Experimental allergic encephalomyelitis animal models for analyzing features of multiple sclerosis. *Pathol Biol.* **48**:47–53.

[4] 't Hart BA, Amor S (2003). The use of animal models to investigate the pathogenesis of neuroinflammatory disorders of the central nervous system. *Curr Opin Neurol.* **16**:375–383.

[5] Tonra JR, Reiseter BS, Kolbeck R, Nagashima K, Robertson R, Keyt B, Lindsay RM (2001). Comparison of the timing of acute blood-brain barrier breakdown to rabbit immunoglobulin G in the cerebellum and spinal cord of mice with experimental autoimmune encephalomyelitis. *Comp Neurol.* **430**:131–144.

[6] Tanaka R, Iwasaki Y, Koprowski H (1975). Ultrastructural studies of perivascular cuffing cells in multiple sclerosis brain. *Am J Pathol.* **81**:467–478.

[7] Raine CS, Cannella B, Hauser SL, Genain CP (1999). Demyelination in primate autoimmune encephalomyelitis and acute multiple sclerosis lesions: A case for antigen-specific antibody mediation. *Ann Neurol.* **46**:144–160.

[8] Bruck W, Sommermeier N, Bergmann M, Zettl U, Goebel HH, Kretzschmar HA, Lassmann H (1996). Macrophages in multiple sclerosis. *Immunobiology.* **195**:588–600.

[9] Bruck W, Porada P, Poser S, Rieckmann P, Hanefeld F, Kretzschmar HA, Lassmann H (1995). Monocyte/macrophage differentiation in early multiple sclerosis lesions. *Ann Neurol.* **38**:788–796.

[10] Li H, Newcombe J, Groome NP, Cuzner ML (1993). Characterization and distribution of phagocytic macrophages in multiple sclerosis plaques. *Neuropathol Appl Neurobiol.* **19**:214–223.

[11] Lucchinetti CF, Bruck W, Rodriguez M, Lassmann H (1996). Distinct patterns of multiple sclerosis pathology indicates heterogeneity on pathogenesis. *Brain Pathol.* **6**:259–274.

[12] Johnson GA, Benveniste H, Black RD, Hedlund LW, Maronpot RR, Smith BR (1993). Histology by magnetic resonance microscopy. *Magnetic Reson Q.* **9**:1–30.

[13] Morrisey SP, Stodal H, Zettl U, Simonis C, Jung S, Keifer R (1996). In vivo MRI and its histological correlates in acute adoptive transfer experimental allergic encephalomyelitis: Quantification of inflammation and edema. *Brain.* **119**:239–248.

[14] Wadghiri YZ, Sigurdsson EM, Sadowski M, Elliott JI, Li Y, Scholtzova H, Tang CY, Aguinaldo G, Pappolla M, Duff K, Wisniewski T, Turnbull DH (2003). Detection of Alzheimer's amyloid in transgenic mice using magnetic resonance microimaging. *Magn Reson Med.* **50**:293–302.

[15] Pirko I, Ciric B, Johnson AJ, Gamez J, Rodriguez M, Macura S (2003). Magnetic resonance imaging of immune cells in inflammation of central nervous system. *Croat Med J.* **44**:463–468.

[16] Gareau PJ, Wymore AC, Cofer GP, Johnson GA (2002). Imaging inflammation: Direct visualization of perivascular cuffing in EAE by magnetic resonance microscopy. *J Magn Reson Imaging.* **16**:28–36.

[17] Weissleder R, Cheng H-C, Bogdanov A, Bogdanov A Jr. (1997). Magnetically labeled cells can be detected by MR imaging. *J Magn Reson Imaging.* **7**:258–263.

[18] Moore A, Weissleder R, Bogdanov Jr. A (1997). Uptake of dextran-coated monocrystalline iron oxides in tumor cells and macrophages. *J Magn Reson Imaging.* **7**:1140–1145.

[19] Xu S, Jordan EK, Brocke S, Bulte JW, Quigley L, Tresser N, Ostuni JL, Yang Y, McFarland HF, Frank JA (1998). Study of relapsing remitting experimental allergic encephalomyelitis SJL mouse model using MION-46L enhanced in vivo MRI: Early histopathological correlation. *J Neurosci Res.* **52**:549–58.

[20] Dousset V, Delalande C, Ballarino L, Quesson B, Seilhan D, Coussemacq M, Thiaudiere E, Brochet B, Canioni P, Caille JM (1999). In vivo macrophage activity imaging in the central nervous system detected by magnetic resonance. *Magn Reson Med.* **41**:329–333.

[21] Bulte JWM, Zhang S-C, van Gelderen P, Jordan EK, Duncan ID, Frank JA (1999). Neurotransplantation of magnetically labeled oligodendrocyte progenitors: Magnetic resonance tracking of cell migration and myelination. *Proc Natl Acad Sci.* **96**: 15256–15261.

[22] Bulte JWM, Douglas T, Witwer B, Zhang SC, Strable E, Lewis BK, Zywicke H, Miller B, van Gelderen P, Moskowitz BM, Duncan ID, Frank JA (2001). Magnetodendrimers allow endosomal magnetic labeling and in vivo tracking of stem cells. *Nat Biotechnol.* **19**: 1141–1147.

[23] Kaim AH, Wischer T, O'Reilly T, Jundt G, Frohilch J, Schulthess GK, Allegrini PR (2002). MR imaging with ultra-small superparamagnetic iron oxide particles in experimental soft tissue infections in rats. *Radiology.* **225**:808–814.

[24] Ahrens ET, Feili-Hariri M, Xu H, Genove G, Morel PA (2003). Receptor-mediated endocytosis of iron-oxide particles provides efficient labeling of dendritic cells for in vivo MR imaging. *Magn Reson Med.* **49**:1006–1013.

[25] Dousset V, Gomez C, Petry KG, Delaande C, Caille JM (1999). Dose and scanning delay using USPIO for central nervous system macrophage imaging. *MAGMA.* **8**:185–189.

[26] Wang YXJ, Hussain SM, Krestin GP (2001). Superparamagnetic iron oxide contrast agents: Physicochemical characteristics and applications in MR imaging. *Eur Radiol.* **11**:2319–2331.

[27] Wilhelm C, Billotey C, Roger J, Pons JN, Bacri JC, Gazeau F (2003). Intracellular uptake of anionic superparamagnetic nanoparticles as a function of their surface coating. *Biomaterials.* **24**:1001–1011.

[28] Foster-Gareau PJ, Heyn C, Alejski A, Rutt BK (2003). Imaging single mammalian cells with a 1.5T clinical scanner. *Magn Reson Med.* **49**:968–971.

[29] Chronik BA, Rutt BK (1998). Constrained length minimum inductance gradient coil design. *Magn Reson Med.* **39**:270–278.

[30] Dodd SJ, Williams M, Suhan JP, Williams DS, Koretsky AP, Ho C (1999). Detection of single mammalian cells by high-resolution magnetic resonance imaging. *Biophys J.* **76**:103–109.

[31] Nitz WR. Fast and ultra-fast non-echo-planar MR imaging techniques (2002). *Eur Radiol.* **12**:2866–2882.

[32] Scheffler K, Hennig J (2003). Is TrueFISP a gradient-echo or a spin-echo sequence? *Magn Reson Med.* **49**:395–397.

[33] Freeman R, Hill HDW (1971). Phase and intensity anomalies in Fourier transform NMR. *J Magn Reson.* **4**:366–383.

[34] Majumdar S, Zoghbi SS, Gore JC (1990). Pharmacokinetics of superparamagnetic iron-oxide MR contrast agents in the rat. *Invest Radiol.* **25**:771–777.

[35] Dousset V, Ballarino L, Delalande C, Coussemacq M, Canioni P, Petry KG, Caille JM (1999). Comparison of ultrasmall particles of iron oxide (USPIO)-enhanced T2-weighted, conventional T2-weighted, and gadolinium-enhanced T1-weighted MR images in rats with experimental autoimmune encephalomyelitis. *Am J Neuroradiol.* **20**:223–227.

[36] Rausch M, Hiestand P, Baumann D, Cannet C, Rudin M (2003) MRI-based monitoring of inflammation and tissue damage in acute and chronic relapsing EAE. *Magn Med Reson.* **50**:309–314.

[37] Kleinschnitz C, Bendszus M, Frank M, Solymosi L, Toyka KV, Stoll G (2003). In vivo monitoring of macrophage infiltration in experimental ischemic brain lesions by magnetic resonance imaging. *J Cereb Flo Metab.* **23**:1356–1361.

[38] Kalish H, Arbab AS, Miller BR, Lewis BK, Zywicke HA, Bulte JWM, Bryant LH Jr, Frank JA (2003). Combination of transfection agents and magnetic resonance contrast agents for cellular imaging: Relationship between relaxivities, electrostatic forces, and chemical composition. *Magn Reson Med.* **50**:275–282.

[39] Muldoon LL, Pagel MA, Kroll RA, Ranan-Goldstein S, Jones RS, Neuwelt EA (1999). A physiological barrier distal to the anatomic blood–brain-barrier in a rat model of transvascular delivery. *Am J Neuroradiol.* **20**:217–222.

[40] Chouly C, Pouliquen D, Lucet I, Jeune JJ, Jallet P (1996). Development of superparamagnetic nanoparticles for MRI: Effect of particle size, charge and surface nature on biodistribution. *J Microencapsulation.* **13**:245–255.

[41] Frank JA, Zywicke H, Jordan EK, Mitchell J, Lewis BK, Miller B, Bryant LH Jr, Bulte JW (2002). Magnetic intracellular labeling of mammalian cells by combining (FDA-approved) superparamagnetic iron oxide MR contrast agents and commonly used transfection agents. *Acad Radiol.* **9**:S484–S487.

[42] Pouliquen D, Perdrisot R, Ermias A, Akoka S, Jallet P, Le Jeune JJ (1989). Superparamagnetic iron oxide nanoparticles as a liver MRI contrast agent: Contribution of microencapsulation to improved biodistribution. *Magn Reson Imaging.* **7**:619–627.

[43] Weissleder R, Lee AS, Khaw BA, Shen T, Brady TJ (1992). Anti-myosin labeled monocrystalline iron oxide allows detection of myocardial infarct: MR antibody imaging. *Radiology.* **182**: 381–385.

[44] Benveniste E (1997) Role of macrophages/microglia in multiple sclerosis and experimental allergic encephalomyelitis. *J Mol Med.* **75**:165–173.

[45] Dijkstra CD, Dopp EA, Joling P, Kraal, G (1985) The heterogeneity of mononuclear phagocytes in lymphoid organs: Distinct macrophage subpopulations in the rat recognized by monoclonal antibodies ED1, ED2, and ED3. *Immunology.* **54**:589–591.

[46] Bulte JW, Frank JA (2000). Imaging macrophage activity in the brain by using ultrasmall particles of iron oxide. *Am J Neuroradiol.* **21**:1767–1768.

[47] Perl DP, Good PF (1992). Comparative techniques for determining cellular iron distribution in brain tissues. *Ann Neurol.* **32**: S76–S81.

[48] Halbhuber KJ, Konig K (2003). Modern laser scanning microscopy in biology, biotechnology and medicine. *Ann Anat.* **185**: 1–20.

[49] Stephens DJ, Allan VJ (2003). Light microscopy techniques for live cell imaging. *Science.* **300**:82–86.

[50] Floris S, Blezer EL, Schreibelt G, Dopp E, Van Der Pol SM, Schadee-Eestermans IL, Nicolay K, Dijkstra CD, Vries HE (2004). Blood–brain barrier permeability and monocyte infiltration in experimental allergic encephalomyelitis. *Brain.*

# APPENDIX II: *ETHICS APPROVAL*

#2002-021-02

*The* UNIVERSITY *of* WESTERN ONTARIO

*University of Council on Animal Care*
*Animal Use Subcommittee*

**February 12, 2002**

***This is the Original Approval of this protocol***
***A Full Protocol submission will be required in 2006***

**Dear Dr. Gareau:**

**Your "Application to Use Animals for Research or Teaching" entitled:**

**" Investigation of Novel Magnetic Resonance Imaging (MRI) Techniques and Contrast Agents for Studying Experimental Allergic Encephalomyelitis (EAE) in Rats"**
**Funding Agency– CIHR**

**has been approved by the University Council on Animal Care.**

**This approval expires in one year on the last day of the month, but the protocol number will remain the same until a full protocol submission is required (2006). The new protocol number is #2002-021-02**

1. **This number must be indicated when ordering animals for this project.**
2. ***Animals for other projects may not be ordered under this number.***
3. **If no number appears please contact this office when grant approval is received.**
   **If the application for funding is not successful and you wish to proceed with the project, request that an internal scientific peer review be performed by the Animal Use Subcommittee office.**
4. **Purchases of animals other than through this system must be cleared through the ACVS office. Health certificates will be required.**

**ANIMALS APPROVED**

| | | | | | | |
|---|---|---|---|---|---|---|
| **Rats** | **-** | **Lewis** | **200-250 gm** | **F** | **-** | **58** |

**STANDARD OPERATING PROCEDURES**
**Procedures in this protocol should be carried out according to the following SOPs. Please contact the Animal Use Subcommittee office (661-2111 ext. 6770) in case of difficulties or if you require copies.**
**SOP's are also available at http://www.uwo.ca/animal/acvs**

- **# 310 Holding Period Post Admission**
- **# 320 Euthanasia**
- **# 321 Criteria for Early Euthanasia-Rodent**
- **# 331 Post-Operative/Post Anaesthetic Care - Level One**

**REQUIREMENTS/COMMENTS**
**Please ensure that individual(s) performing procedures on live animals, as described in this protocol, are familiar with the contents of this document.**

**1. Animals may need to monitored more frequently than twice a day. Monitoring must be performed frequently enough to prevent death or finding animals in extremis.**

**After hours emergency contact is: P. Gareau - 474-1997**

**c.c. Approved Protocol - P. Gareau, W. Lagerwerf**
**Approval Letter - W. Lagerwerf, K. Perry, L. Turner**

Feb 13/02

Western

May 2, 2006

***This is the Original Approval for this protocol***
*A Full Protocol submission will be required in 2010*

Dear Dr. Foster:

Your Animal Use Protocol form entitled:
Cellular Magnetic Resonance Imaging Studies of Immune Cells
Funding Agency Multiple Sclerosis Society of Canada

has been approved by the University Council on Animal Care. This approval is valid from **May 2, 2006** to **May 31, 2007**. The protocol number for this project is 2006-050-05 and replaces 2002-021-02.

1. This number must be indicated when ordering animals for this project.
2. Animals for other projects may not be ordered under this number.
3. If no number appears please contact this office when grant approval is received.
   If the application for funding is not successful and you wish to proceed with the project, request that an internal scientific peer review be performed by the Animal Use Subcommittee office.
4. Purchases of animals other than through this system must be cleared through the ACVS office. Health certificates will be required.

**ANIMALS APPROVED FOR 1 YR.**

| Species | Strain | Other Detail | Pain Level | Animal # Total for 1 Year |
|---|---|---|---|---|
| Mouse | C57BL/6J | 6-8 weeks M/F | E | 60 |

**STANDARD OPERATING PROCEDURES**
Procedures in this protocol should be carried out according to the following SOPs. Please contact the Animal Use Subcommittee office (661-2111 ext. 86770) in case of difficulties or if you require copies.
SOP's are also available at http://www.uwo.ca/animal/acvs
310 Holding Period Post-Admission
320 Euthanasia
330 Post-Operative Care/Rodent
343 Surgical Prep/Rodent/Recovery Surgery

**REQUIREMENTS/COMMENTS**
Please ensure that individual(s) performing procedures on live animals, as described in this protocol, are familiar with the contents of this document.

c.c. Approved Protocol - P. Foster, B. Dunn, W. Lagerwerf
Approval Letter - B. Dunn, W. Lagerwerf